EXPERIMENTAL AND SURFACE ANALYSES OF LASER DEPOSITED Al-Sn-Cu-Si COATINGS ON Ti-6Al-4V ALLOY

By

MARY-JANE CHINENYE OBIEGBU

A dissertation submitted to the Faculty of Engineering and the Built Environment in partial fulfilment of the requirements for the degree of

MAGISTER INGENERIAE

In

MECHANICAL ENGINEERING SCIENCE

at the

UNIVERSITY OF JOHANNESBURG

SUPERVISOR: PROF ESTHER T AKINLABI

CO-SUPERVISOR: DR OLAWALE S. FATOBA

NOVEMBER 2019

PLAGIARISM DECLARATION

I, Mary-Jane Chinenye Obiegbu, hereby declare that this dissertation is wholly my own work and has not been submitted anywhere else for academic credit either by myself of another person.

I understand what plagiarism implies and declares that this mini-dissertation is my own ideas, words, phrases, arguments, graphics, figures, results and organization except where reference is explicitly made to another's work.

I understand further that any unethical academic behaviour, which includes plagiarism, is seen in a serious light by the University of Johannesburg and is punishable by disciplinary action.

Signed..... ..... Date 26th November 2019

ACKNOWLEDGEMENT

This is to acknowledge everybody that has supported me in completing this masters'' program. I firstly want to appreciate Prof. Esther Akinlabi my great inspirational supervisor for accepting to run this program with diverse supports and funding provisions. Your strength, vigor and mental capacity as a leader has been distinguished and outstanding. Secondly, my appreciation goes to Dr. Olawale Fatoba, my workaholic co-supervisor for guiding and mentoring me each and every steps of this project.

I have great souls in the MAMS research groups that has stood by my side like Mr. Victor Aladesanmi, my nearest and quickest hand-on student assistance for the execution of most of the technical and laboratory work. I cannot fail to mention Mr. Micheal Abegunde, Mr. Baruwa Damilola, Mr Adedotun Adetula, Mr Oluwafemi Babarinde, Mr. Omolayo, Ikumapayi and many others.

This journey story cannot be complete without saluting Dr. George who motivated and inspire me to run this program. I also want to appreciate all the Ndigbo families and friends in Johannesburg, South Africa.

My esteemed greeting to my Husband, Mr. Romanus Chukwuma Obiegbu and children for believing and adding to my faith by your daily motivation.

This journey which had its challenges, ups and downs has thoroughly been fulfilling with its great output.

ABSTRACT

Modification of surfaces is very necessary in order to mitigate against catastrophic surface degradation of wear and corrosion. The one solution against this aforementioned degradation is to design coatings that can fight against this menace in order to retain the surface integrity. These fabricated coatings would bring innovative microstructures with exceptional properties and performance. The inability of conventional techniques to fabricate complex designs, shapes and enhanced microstructures have led to Additive Manufacturing (A.M) techniques in seeking for solution to this problem. The project sought to utilize laser cladding of Ti-6Al-4V alloy as a method of improving its surface properties therefore expanding the range of applications and lifespan of the material. This investigation also studied the effect of process parameters in the enhancement of microstructures, hardness, wear performance and mechanical properties of Al-Si-Sn-Cu/Ti-6Al-4V composite coatings

Al-Si-Sn-Cu/Ti6Al4V quaternary coatings were analysed using optical microscopy, scanning electron microscopy (SEM) with energy dispersive microscopy (EDS), indentation testing, x-ray diffraction (XRD) analysis. The hardness and wear resistance performances of the quaternary coatings were examined by high diamond dura scan microhardness tester and CERT UMT-2 reciprocating sliding machine.

From the results, the interfacial zone as a junction with high bond strength has various chemical reactions that ensue between the coatings and the substrate. Thus, as the result of an efficient metallurgical bonding, the mechanical property of the coating-substrate system was enhanced. Coarse dendrite structures were caused by low laser speed (16.7

mm/s) longer interaction of powders with a laser beam. An activated reduced rate of cooling emerges from the low scan speed that enables the longer interaction time, in turn forming granular dendrites. Refined grains occurred at higher scan speed (20.0 mm/s). The reduced grain sizes are actualized after solidification and result from the rapid nucleation created by this high cooling rate

Dilution effect from the base metal mixed with the reinforcement materials in melt pool during melting and solidification formed intermetallic Ti, Al_3Ti, Ti_3Al, CuTi, TiV, $AlSi_3Ti_2$, $Al_{0.25}Sn_{0.75}V_3$, Ti_2FeCu and $CuTi_2$. The confirmed presence of intermetallics are responsible for the enhanced hardness profiles of the cladded samples with increase in the wt. % composition Si and Cu at laser power of 1000 W. It is noteworthy that these intermetallic compounds have excellent match of properties viable for tailored applications in applications that require high temperature strength, good wear resistance, and microstructural integrity. Formation of β-Ti phase was as a result of atomic migration of copper during solidification in the Ti lattice. β-matrix crystallographic structure area more open by the migration of copper into the lattice of titanium.

Table of Contents

List of Figures

List of Tables

List of Publications

- **M.C. Obiegbu;** O.S. Fatoba; E.T. Akinlabi., S.A. Akinlabi (2019). Experimental Study on Characteristics of Laser Metal Deposited Al-Si-Sn-Cu/Ti-6Al-4V composite coatings. **Materials Express Research. Volume 6, number 4, 1-11.** https://doi.org/10.1088/2053-1591/aafe4d. **(Scopus)**

- **M.C. Obiegbu;** E.T. Akinlabi; O.S. Fatoba; S.A. Akinlabi (2019). The Effects of Silicon and Copper on the Microstructure and Wear Resistance Performance of Al-Si-Sn-Cu/Ti-6Al-4V Composite Coatings. 2019 IEEE 10th International Conference on Mechanical and Intelligent Manufacturing Technologies (ICMIMT 2019), Cape town, South Africa, pp. 20-25. doi: 10.1109/ICMIMT.2019.8712023. **(Scopus)**

- O.S. Fatoba; E.T. Akinlabi., S.A. Akinlabi; **M.C. Obiegbu** (2019). Data Related to Optimized Process Parameters Influence on Hardness, Microstructural Evolution and Wear Resistance Performance of Al-Si-Sn-Cu/Ti-6Al-4V Composite Coatings. **Data in Brief. Volume 6, number 4, 1-11.**https://doi.org/10.1016/j.dib.2019.103724. **(Scopus)**

- O.S. Fatoba; E.T. Akinlabi., S.A. Akinlabi; **M.C. Obiegbu** (2019). Effects of Silicon Carbide (SiC) Reinforcement on the Microstructure and Mechanical Properties of Laser Deposited Al-Sn-SiC/Ti-6Al-4V Composite Coatings. Key Engineering Materials, Vol. 796, pp. 53-61. doi.org/10.4028/www.scientific.net/KEM.796.53. **(Scopus).**

LIST OF SYMBOLS

Alphanumeric Symbols

T	Temperature [°C]
v	Scanning speed [m/s]
P	Power [W]
$\dot{m}$	Powder flow rate [kg/s]
R	Radius [m]
A	Area [m^2]
V	Volume [m^3]
k	Thermal Conductivity [$W/(m.K)$]
F	Force [N]
d	Diameter [m]
u	Velocity Field [m/s]
q	Heat Flux [W/m^3]

Greek symbols

ρ	Density [kg/m^3]

CHAPTER ONE: INTRODUCTION

1.1. Background/Motivation

The superiority of advanced materials due to their high temperature and corrosion resistance performance is noticeable in the various application in energy, aerospace, biomedical, defense and environmental. This has been one of the tasks of engineers all over the world. The wide applications of advanced materials have been due to technological innovation demands which can improve the performance of these materials in the aforementioned industries [1, 2]. Friction coefficient reduction, better hardness and wear performance enhancement have been linked to altering of microstructures which in turn lead to surface enhancement. [3]. Modification of surface is very necessary in order to mitigate against catastrophic surface degradation of wear and corrosion. The one solution against this aforementioned degradation is to design coatings that can fight against this menace in order to retain the surface integrity. These fabricated coatings will bring innovative microstructures with exceptional properties and performance. [4].

The inability of conventional techniques to fabricate complex designs, shapes and enhanced microstructures have led to Additive Manufacturing (A.M) techniques in seeking for solutions to this problem. Different surface modifications techniques had been published by researchers worldwide but these techniques still have limitations such as adhesion of reinforcement and base metal, pores, cracks, long processing time and not cost effective [5-9]. Additive Manufacturing processes had been the source that links

process parameters, materials and the properties of final product as a results of engineering design and analysis abilities.

Applications of Titanium alloy in aerospace due to its active strength-to-weight competency, immunity against corrosion and thermal steadiness could make titanium alloy an extremely alluring metal. Application of this metal can occur at higher temperature with an important temperature of roughly 600°C. Initially, aerospace application was the center of utilization of titanium alloy, however, its applications has surpassed aerospace and can also be found in sports, automotive, energy and medical where the exeptional characteristics of titanium alloys are being used. [10-12]. Varied components of aircraft in the aerospace industry has a touch of titanium where titanium alloy is chiefly and immensely employed such as the mechanical device blades, turbine and jet engines, and frame parts components. The extension of titanium applications to other sectors had been due to continual process and passion for new engineering components and industrial growth. For example, energy, medical and marine industries have thought about its application thanks to its wide range of most popular properties that symbolize outstanding corrosion resistance, unique mix of durability and high strength [13].

The base metal made of titanium alloy retains its characteristics while the surface is being improved. Despite the good properties exhibit by titanium alloy, drawbacks such as low hardness and poor wear property has necessitated improvements for better surface. Improvement of titanium surface can lead to enhanced properties and titanium alloys can be used in extended engineering applications [14-16]. Fatal accidents of engineering

components in service can be avoided through surface modification. These can be achieved by fabricating hard-coatings that can withstand corrosion and friction [17, 18]. These can lead to excellent microstructures and enhanced mechanical properties without changing the propoerties of the base metal [19-21]. Different surface modifications techniques had been published by researchers worldwide but these techniques still have limitations such as adhesion of reinforcement and base metal, pores, cracks, long processing time and not being cost effective [22-26].

Titanium is a hard, shiny, silver and strong metal and is the ninth most plentiful element on Earth. It is nearly occurring in all igneous rocks and is found in rutile, ilmenite, titanates and various iron ores. The first titanium mineral was discovered in 1791 in Cornwall but was only made into pure titanium metal in 1910 in the USA. Titanium and its compounds have a wide variety of applications. Compounds such as titanium dioxide, titanium trichloride, and titanium tetrachloride are used in smoke screens, white pigments, and production of polypropylene. It can be alloyed with other elements to produce the suitable alloys for applications such as mobile phones, jewellery, jet engines, medical implants and cars. The properties allowing these applications include its low density, high specific strength and superior corrosion resistance.

The most used titanium alloy in various industries is Ti-6Al-4V. The extent at which Ti-6Al-4V alloy is applied is limited due to its poor hardness, low wear resistance and ready oxidation at high temperature [27]. For these reasons, the material has to be replaced or repaired after it has failed; this implies more costs than anticipated. In light

of this, solutions need to be devised in order to minimize or eliminate material failure caused by the conditions and environment the material is exposed to. Surface modification is a viable technique that can be employed in the improvement of the properties of the material. This research aims to enhance the surface characteristics of Ti-6Al-4V when it is subjected to hostile environments where phenomena such as wear and corrosion occur. The project seeks to utilize laser cladding of Ti-6Al-4V as a method of improving its surface properties therefore expanding the range of application and lifespan of the material.

1.2. Problem Statement

Titanium alloys are used extensively in biomedical, chemical, aerospace and automobile industries because of their biocompatibility, high specific strength and low density. The application of these alloys is limited because of its low tribological performance and is susceptibility to galvanic corrosion as other elements are present in the alloy [28]

- Ti-6Al-4V alloy is considered the most used alloy in these applications. However, the uses of this alloy in severe environments, where the wear is the main failure mode, are limited due to its poor wear resistance [29].
- Titanium and its alloys exhibit attractive properties such as mechanical strength, biocompatibility and high temperature performance. However, the performance requirements and expectation under some service conditions that necessitates high hardness, wear and aggressive corrosion environment are not met adequately. Ti6Al4V alloy may fail after some time in a corrosive environment [30]

- The low hardness of Ti-6Al-4V limits its long-term performance in its application.

1.3. Aim of the Study

This study aims to study effect of process parameters in the enhancement of microstructures, hardness, electrochemical, and tribological characteristics of Al-Si-Sn-Cu/Ti-6Al-4V composite coatings.

1.4. Objectives of the Study

- To enhance the microstructure of Ti-6Al-4V by laser deposited with Al-Si-Sn-Cu coatings.
- To optimize laser process parameters during laser metal deposition of Al-Si-Sn-Cu/Ti6Al4V composite coatings and obtain crack free coating.
- Enhancing the wear behaviour of Al-Si-Sn-Cu/Ti-6Al-4V composite coating.
- Increasing the hardness property of the fabricated Al-Si-Sn-Cu/Ti-6Al-4V composite coating.

- To design a mathematical model simulating the relationship between laser parameters and final coating qualities

1.5. Hypothesis

It is hypothesized that

- The microstructure will exhibit grain refinement and the hardness and wear properties will be improved.
- Optimizing laser processing parameters will have an effect on the microstructure and eliminate residual stresses and cracks on the composite coatings surface.

- The wear behaviour of the composite coatings will be better than that of the Ti-6Al-4V substrate.

1.6. Significance of Research

The data obtained from the research will be used to determine the future application of Al-Si-Sn-Cu/Ti-6Al-4V composite coatings in aerospace industry. Developed properties will satisfy a greater scale of requirements for applications

The fabricated composite will improve the service life of titanium alloy.

Laser metal deposition technique will be further established as a technique that can target the specific problematic area rather than altering the whole component/structure.

Improvement in the wear behaviour of the coating will enable use in load bearing environment.

CHAPTER TWO: LITERATURE REVIEW

2.1. General remarks

This chapter covers the detailed literature review on laser metal deposition (LMD) technique with Al-Si-Sn-Cu coatings and titanium alloys and key areas where the LMD could be used in production and industry. The literature presents the general overview of the LMD processes and techniques, properties of the materials, different phenomena related to LMD, review on Ti-6Al-4V alloy with other reinforcements and the influence of reinforcements on the micro-hardness, corrosion and wear behaviour of laser metal deposited titanium alloys.

2.2. Additive manufacturing

Additive manufacturing (AM) is a new technology that can improve the existing supply chain capabilities for many productions in some industrial sectors and the creation of metallic parts. Recent studies have demonstrated that AM can be a sustainable alternative to traditional manufacturing processes. However, as it is a quite new and continuously developing technology, not all process failings involved have been effectively dealt with.

In spite of the fact that Laser additive manufacturing (AM) processes have a similar material additive manufacturing theory, each AM procedure has its particular features in terms of operational materials and applicable situations [31]. The capacity of acquiring great performance of metallic components with a controlled microstructural and mechanical properties that demonstrates a particular contrast for a variety of AM process. The beginning stage for the addictive manufacturing of a part is 3D CAD model that

demonstrates all the work-piece data in a readable digital form. For the development process, the 3D solids must be separated into singular layers thus reducing them to two dimensions [31]. These layer data will be characterized as a particular process in a computer numerical control (CNC) program.

The following manufacturing process is done on a numerically controlled machine that executes the information layer by layer thus generating a part. Figure 2-1 below shows how addictive manufacturing processes can be classified based on different mechanism of laser material interaction.

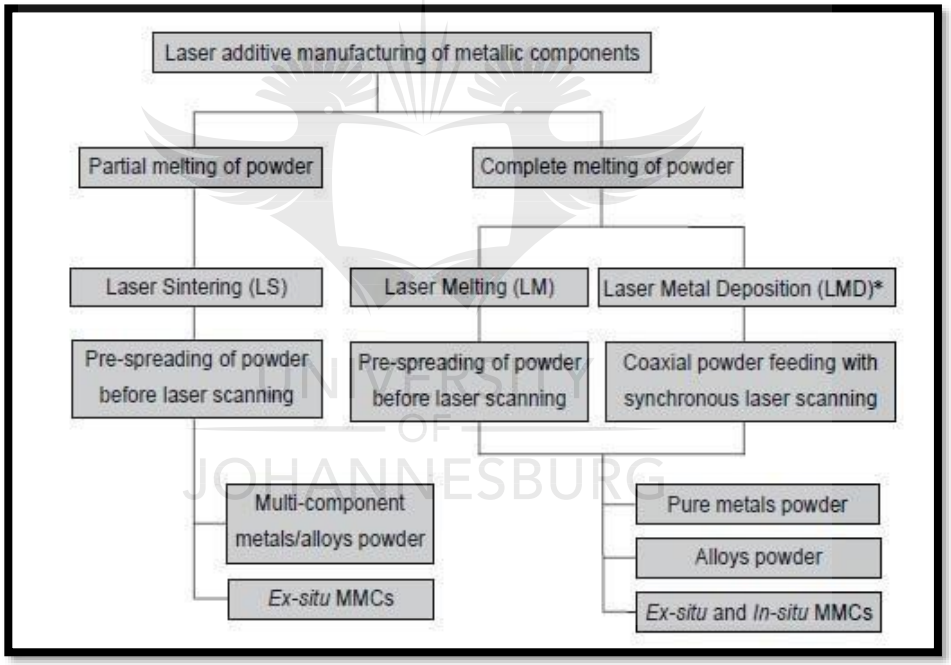

Figure 2-1: Classification of Laser AM processes focused on different mechanism of Laser-material [31]

2.3. Benefits of laser additive manufacturing

The key benefits of using rapid technology is that it conducts the additive processes to be faster than conventional methods. Conventional processes normally need tool making and will need big cost savings. For instance, laser cladding process can be utilized in rapid technologies which can be subdivided into three categories: rapid manufacturing, rapid prototyping and rapid tooling.

2.3.1. Rapid prototyping

Rapid technology is one of the fast innovations that are capable of generating speedy production of prototypes and test parts which are also cost-effective [32]. Moreover, these components normally have limited purposes. A design of the prototype must not have an optimization for series production. With rapid prototyping, it is also not important to utilize the costly material hence it will cover solely a little subset of additive applications [32].

2.3.2. Rapid tooling

Additive processes are utilized to make tools that molds and tools for the generation of prototypes, injection molds and arrangement parts. Generally, selective laser melting is utilized here permitting not solely rapid manufacture however as well as effective utilization of the shaping alternatives provided by rapid technologies [32].

2.3.3. Rapid manufacturing

It is the additive manufacturing of finished products for single part or sequences production. The parts are produced in the strong material focused on the design information and have all the characteristics of the final product [32]. Other than the

capacity to manufacture the party quickly, developing parts utilizing additive processes permits the formation of certain product design specifications which are not easy to be produced utilizing some conventional production techniques [32]. This implies that with this type technology it is probable to extend and master the numerous alternatives for the manufacture of new design components and to proceed onward specifically to the creation to the end products for single part or series production. Figure 2-2 below demonstrates an additive process that can be utilized economically anywhere during the creation of product process.

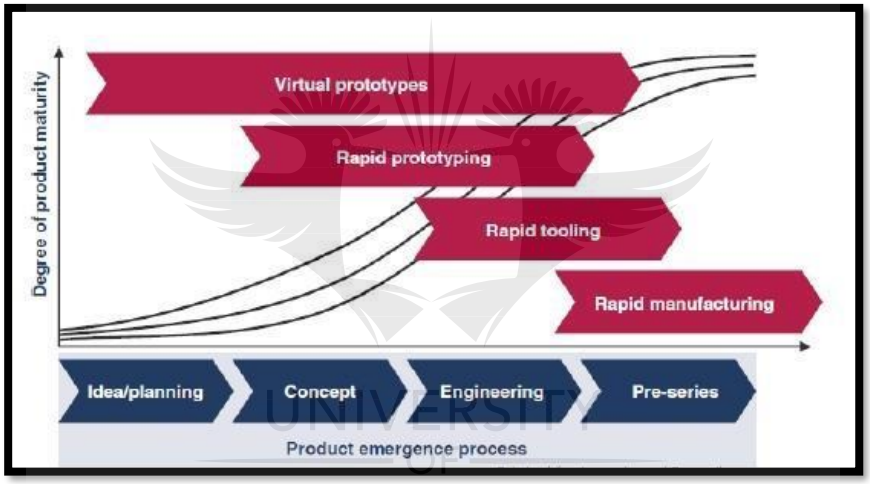

Figure 2-2: The layout of rapid technologies in the product emergence process [32]

Figure 2-3 below shows the benefits of additive manufacturing.

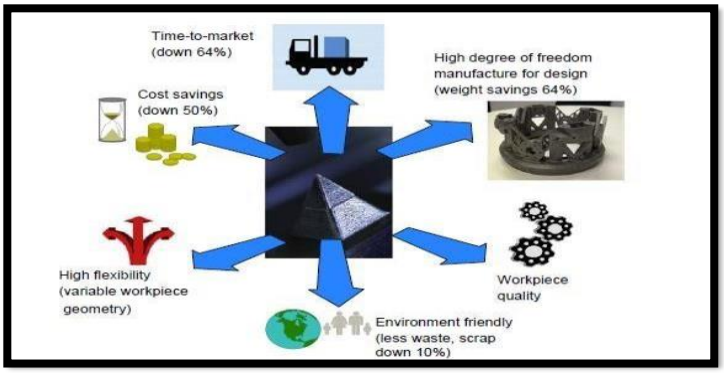

Figure 2-3: A layout showing the benefits of Additive manufacturing [33]

2.4. Classification of additive manufacturing processes

The modern day additive manufacturing processes can be grouped based on two aspects such as the shaping method and feedstock material. Figure 2-4 shows three types of feedstock materials that are utilized currently.

2.4.1. Feedstock material

The feedstock material can be classified into three categories such as solid feedstock materials, liquid synthetic resins and powered granulates. The sintering processes can only be employed when the powdered feedstock material is needed so that the desired laser beams can be utilized to consolidate and melt materials that will be applied onto each other in thin layers [32]. In most circumstances of liquid materials, the desired laser beams are utilized to polymerize synthetic resins and bond them to the latent existing layers [32]. In any case, this process also involves the utilization of solid feedstock

materials to develop the current model layer on layer by using melting followed by rapid cooling. Lastly, when solid feedstock materials with an impartial form are utilized, this usually includes layers of paper which are bonded on top of each other layer on layer [32]. Both partial polymerization and conventional bonding processes are utilized here.

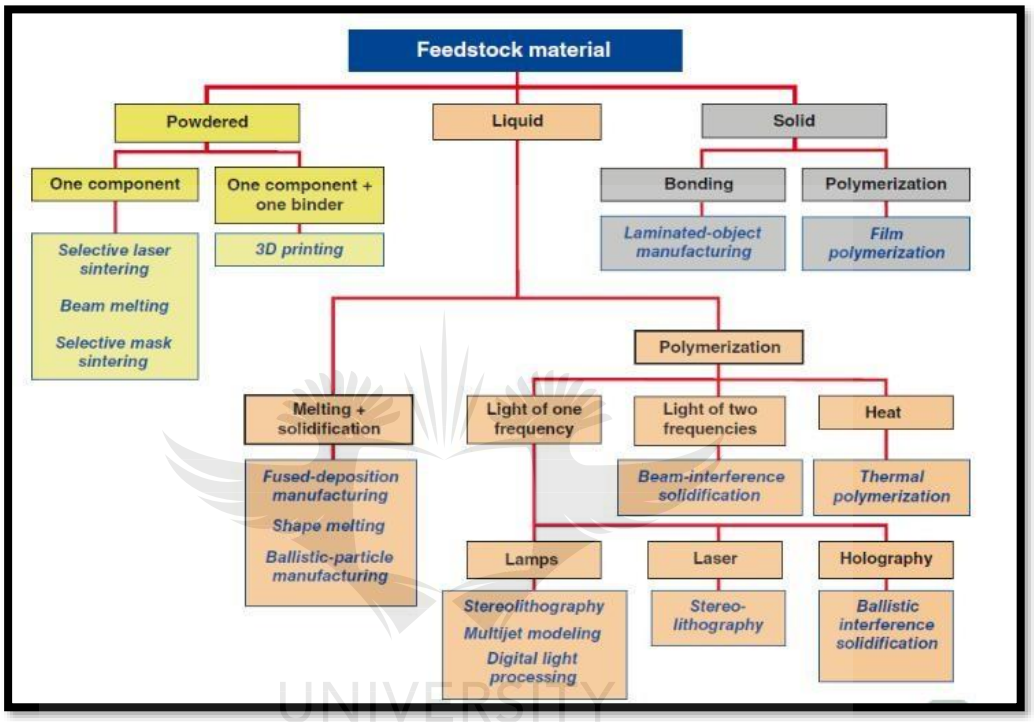

Figure 2-4: Classification of feedstock material [32]

2.4.2. Additive shaping processes

Most of the modern-day additive shaping processes work in two dimensions with single layers. Models are normally constructed with several layers, hence creating a third dimension. This is also applicable to processes that can be able to function in three dimensions directly such as fused deposition manufacturing [32]. Figure 2-5 shows the numerous additive shaping processes.

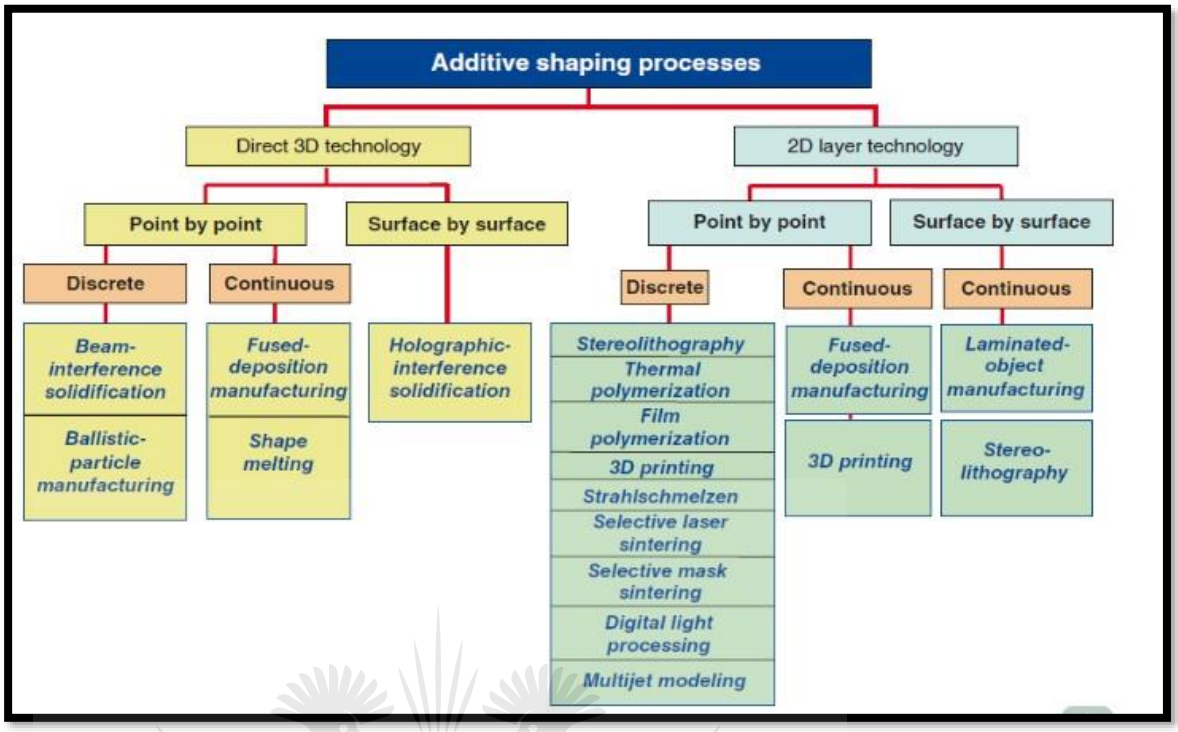

Figure 2-5: Classification of additive shaping process [32]

2.5. Technology of laser additive manufacturing (AM) methods

In the recent years additive manufacturing techniques have been acquainted as a promising technique to generate metallic parts since they can annihilate the familiar problems associated with conventional techniques. AM involves the adding of a material to the part not metal removal. Therefore, this process can be performed by creating a computer-aided design (CAD) file of the required part [34]. Afterwards, the CAD file will be transformed into layers with specific thickness that ranges between 20 to 100 µm. Finally, a 3D printer would manufacture the part layer by layer.

2.5.1. Selective laser sintering

The selective laser sintering (SLS) is process that was developed by Dr. Joe Beaman at the University of Texas at Austin in the mid-1980s [34]. The name laser sintering is utilized preferably for machines that produce plastics. The selective laser sintering process involves the physical process that utilizes two-element metal powders which are a combination of the powder particles and sacrificial binder [34]. Moreover, the binder material will be fused with powder during laser irradiation. The liquid created by the melted binder can only bind the surrounding powder after the structure has been solidified when it has cooled down. Finally, a solid layer is obtained. Figure 2-6 shows the powder-bed-based processes.

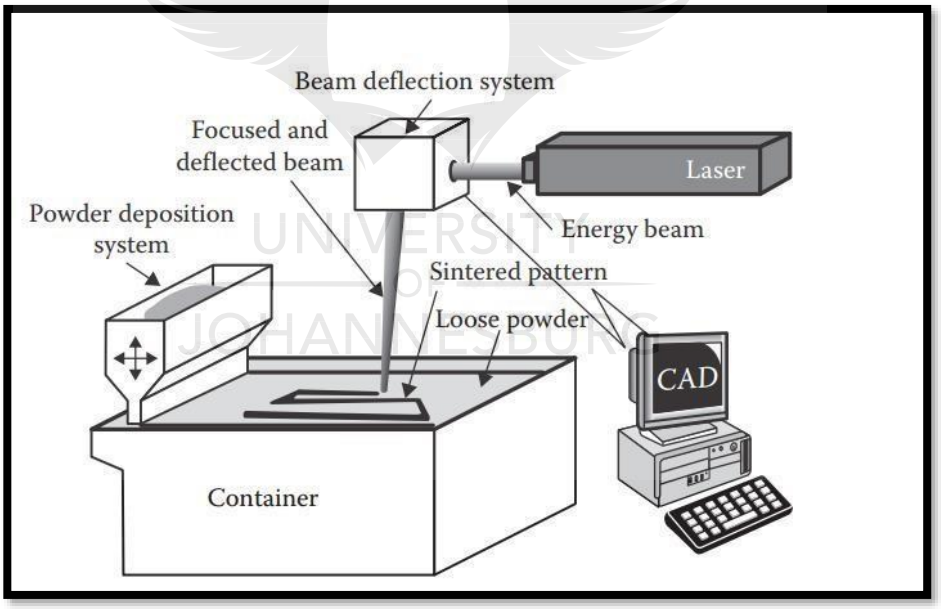

Figure 2-6: A typical layout of powder-bed-based processes during laser sintering [34]

2.5.2. Selective laser melting (SLM)

Selective laser melting can also be regarded as powder-bed-based technology that is capable of fabricating the complex parts with a density that is roughly about 100% which guarantees that the properties are the same and removes the need for post treatments. There are two big differences between selective laser sintering and selective laser melting techniques. First, Selective laser melting does not need to add elements with low melting points because it utilized integral powder. Second, higher power laser is needed for the selective laser melting process to cause the powder to be fused completely [9]. One of the issues related with selective laser melting is the residual stress which comes from high thermal gradients in the material during the melting process [9]. In addition, these residual stresses cause the part to deform. However, to be able reduce the residual stress, the material has to be preheated and the temperature inside the chamber has to be kept constant [34]. Figure 2-7 shows comparison of other laser based processes. The choice of laser has an important impact on the consolidation of powders, essentially due to [31]:

- The laser absorptivity of materials is mostly dependent on the laser wavelength
- The operative metallurgical mechanism for powder densification is evaluated by the input laser energy density.

Process	Deposition mode	Layer thickness (μm)	Deposition rate	Dimensional accuracy (mm)	Surface roughness (μm)
Direct metal laser sintering (DMLS)	Laser sintering	20–100	Depend on laser spot size, scan speed, and size, number, and complexity of parts	High, ± 0.05	14–16
Selective laser melting (SLM)	Laser melting	20–100	ibid	High, ± 0.04	9–10
Direct metal deposition (DMD)	Laser cladding	254	0.1–4.1 cm^3/min	N/A	~40
Laser engineered net shaping (LENS)	ibid	130–380	N/A	X–Y plane ± 0.05; Z axis ± 0.38	61–91
Directed light fabrication (DLF)	ibid	200	10 g/min (1 cm^3/min)	± 0.13	~20

Figure 2-7: Comparisons of other Laser-based AM processes [31]

2.5.3. Laser cladding method

Laser cladding is a new technology that is capable of melting the filler metal to a metal substrate by using fusion welding. The important part for choosing an alloy is to provide the greater part performance over the substrate. To avoid a base material to become weak, the laser cladding will add a performance layer to alleviate such environmental impacts. This process also helps in enhancing the part toughness, for instance, wear surface on hydraulics cylinders. Laser cladding provides a layer of deposited material which is attached to the surface of the part. Single layers of laser cladding are available in size of 2.54 mm thickness and on other hand are as thin 0.635 mm however they protect metallurgical integrity [35]. The laser cladding system can create a vastly

improved coating with very low of dilution, less distortion and better surface quality. There are various points of interest to utilize this technique as a quick prototyping system. Parts created utilizing this method are close to the desired shape however they will still need to go for machining. Figure 2-8 shows schematic diagram of laser cladding process.

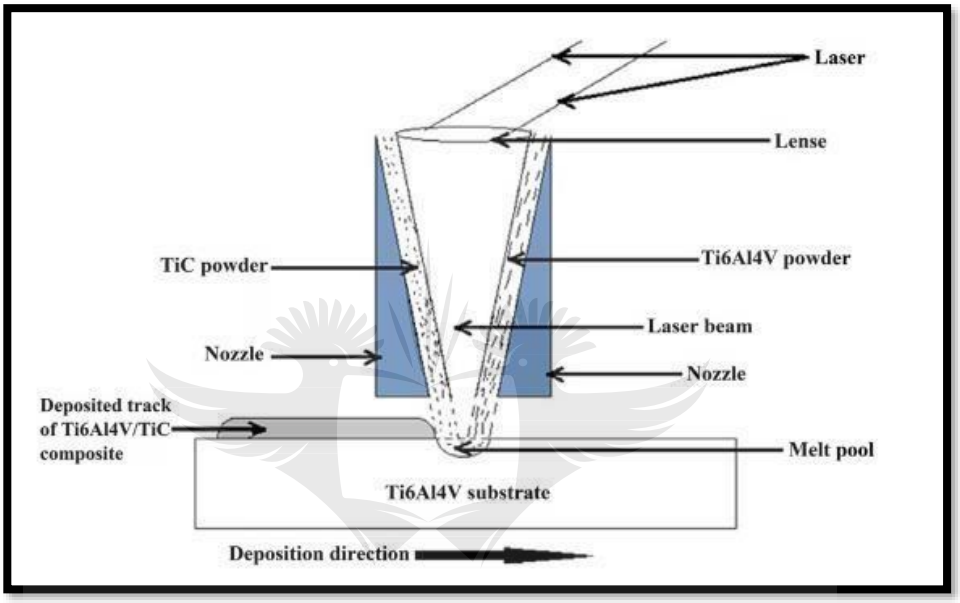

Figure 2-8: A layout of laser cladding process by filling cladding materials in synchronous feeding [36]

Figure 2-9 depicts a cross section of a bead with several parameters on dimensional characteristics. These dimensional characteristics are perceived as results that can be observed during cladding process. The different input parameters in laser cladding process affects the dimensional characteristics. In the below figure, w is the clad width, h is the clad height, θ is the angle of wetting and b is the clad depth representing the thickness of substrate melted during the cladding and added to the clad region.

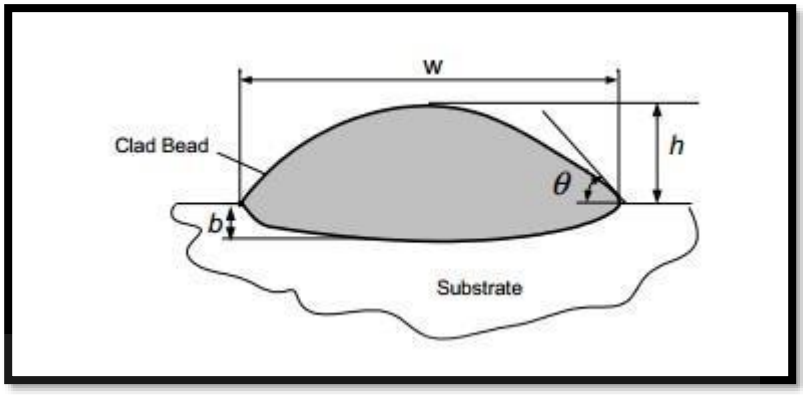

Figure 2-9: A layout of a cross section of a clad bead [37]

These input parameters influence the clad include the gas flow rate, powder feed rate, travel speed and material properties. The outputs that are needed will be analyzed after the cladding process that includes melt depth and the microstructural characteristics and also other important parameters such as dilution and hardness.

2.6. Applications of laser additive manufacturing

2.6.1. Automotive applications

The automotive industry was early to adopt commercialized AM machines and accounts for approximately 16.1% of revenue in the AM industry. The primary uses were prototyping parts to test form and fit as well as rapid product development. Large-scale producers in the automotive industry have not been able to incorporate AM into mass production parts. Unlike the aerospace industry, AM technology is cost prohibitive for most production-level automotive applications because the production volume is

significantly higher. Instead, AM has found a niche in the automotive sector for low production, high quality parts that demand performance and weight reduction. The Figure 2-10 below shows how AM can allow the frame`s design to match the stress or load capacity needed for real-world driving scenarios. The frame is 30% lighter than conventionally manufactured electric motorcycles and made of a proprietary high strength, corrosion resistant aluminium alloy [34].

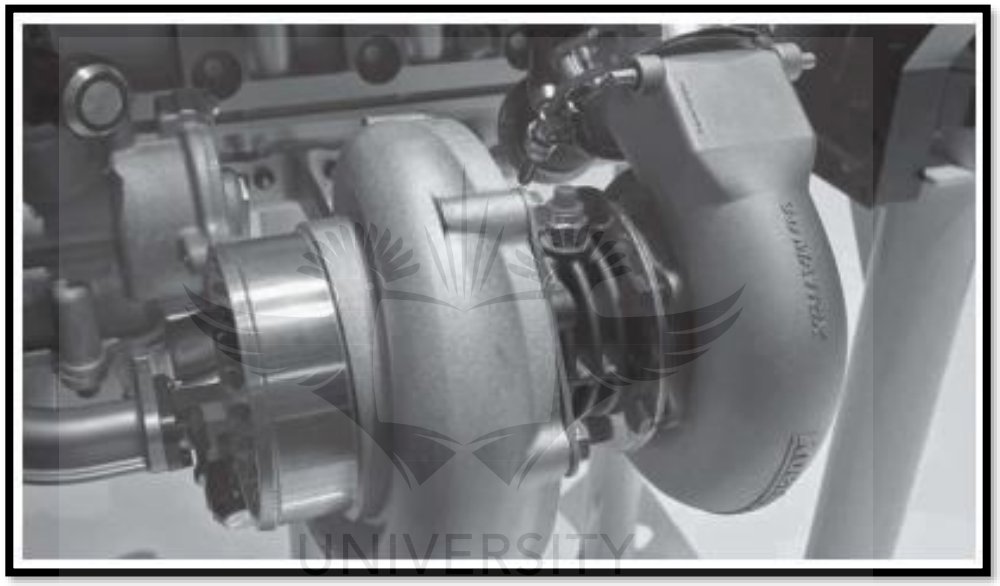

Figure 2-10: Twisted chamber turbocharger printed by SLM [34]

2.6.2. Biomedical applications

Additive manufacturing (AM) is one of the preferred fabrication methods for biomedical applications due to its high degree of fidelity and an atomically accuracy [34]. Metallic implants are widely used to restore the lost structure and functions of human bone. Current metal implants are designed to be bio-inert in nature but often demonstrate a significantly higher stiffness than natural bone that leads to an undesirable biological

response. The mechanical mismatch between bone and a metal implant often causes stress shielding. Both novel design approaches and fabrication technologies are required to achieve balanced mechanical and functional performance in an implant [34]. Figure 2-11 shows the reactivity and biocompatibility of different types of commercially available acrylates and photo-initiators for bone replacement applications.

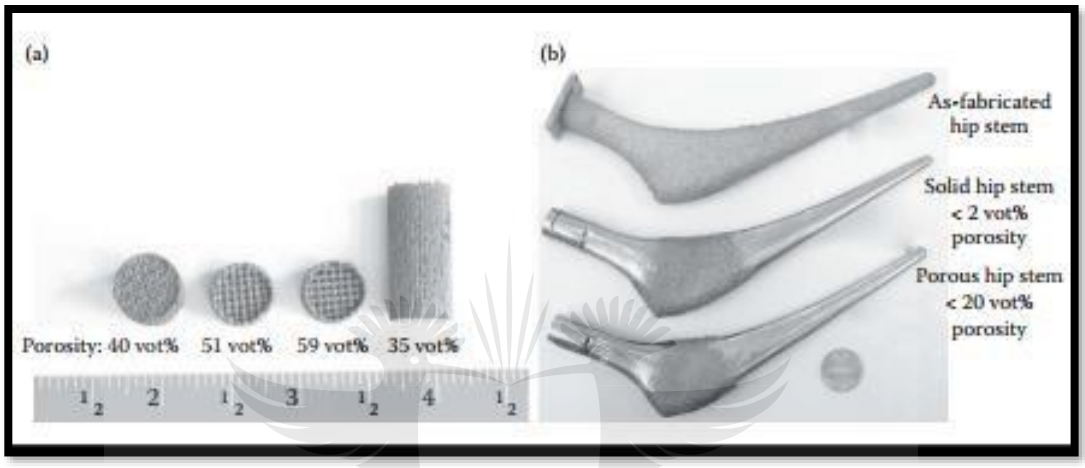

Figure 2-11: LENS processed porous titanium structures [34]

2.7. Processing parameters of laser cladding

Shah et al. [38] studied the effects of laser power, powder mass flow rate of Inconel 718 and SS316L has on the microstructure and mechanical properties such as hardness. It was concluded that titanium alloys are used for cladding because they tend to demonstrate a huge improvement on their properties when compared to the homogenous materials.

2.7.1. Laser power

Laser power is a very vital characteristic that is utilized to provide the desired heat for making the cladding process to occur. The spot area where the laser beam will be directed

and the laser power will determine the power density of the beam. It is believed that the power density is one of the essential process parameters that has an impact on the geometry of the melt pool. It was observed that specific point energy can characterize laser power [39].

2.7.2. Powder mass flow rate

Powder flow rate is an essential parameter that impacts the sample roughness of laser cladding. A higher powder flow rate, this usually causes the cladding to have a rougher surface wall. Consequently, the less powder flow rate may cause a good surface in roughness of the wall in laser cladding. During direct energy deposition of metal parts, the efficiency of the powder deposition is stated as a ratio of the nominal metal powder feed rate to the amount of particles that is directly included in the component manufacture. Powder mass flow rate is examined by the geometry of the powder flow. It was discovered that an increase in the material feed rate makes the clad width and height to increase and also enhance the efficiency of the deposition. Moreover, to get the high efficiency of powder, the powder must be fed laterally on the side where substrate moves [40].

2.7.3. Scanning speed

In some cases, some parameters are kept at a constant rate, it is discovered that as the transverse speed increases, the material that is distributed to the substrate per unit length decreases and therefore that there is an inverse relationship with clad width, melt pool depth and clad height. Hence as the scanning speed increases the width, if the height is smaller and the depth of the pool will be smaller too [41]. Scanning speed impacts the

peak temperature at the surface. For instance, utilizing a low laser scanning of 0.1 m/s, melting occurs because the peak temperature at the surface is moderately high than the melting temperature of the substrate [42].

2.7.4. Gas flow rate

In order for the powder material to be transported into the melt poo, a carrier gas flow will be utilized to help in transport. The gas is commonly utilized to locally secure the melt pool for the harmful effects of oxidation. The key gases that are utilized as the carrier are helium, Argon and Nitrogen. However, the most commonly used gas is Argon because it is extremely dense and inexpensive. The problem associated with the gas flow carriers is that they occasionally cause a pool surface perturbation that has a negative effect on clad properties. The gas flow rate also evaluates the powder particles velocity and the amount of time that will be spent by the laser beam before the cladding. It can be seen that as the particle velocity increases the laser is minimized and this therefore increases the laser power that reaches the substrate [41]. Density plays a significant role on how effective gas flow rate can be utilized. Density is one factor that affects the effectiveness of the gas when is utilized for shielding. This means the lower the density of a gas will make the flow rate to be higher as well. It is also determined by the gas nozzle, the larger the size of the gas flow rate will be allowed to flow without causing turbulent [42].

2.8. Titanium and its alloys

These titanium alloys are found to have the low weight ratio, high strength and are exceptionally resistant to corrosion that is inherent to titanium and its alloys give rise to

an extensive and varied range of successful applications which need higher levels of good performance in health facilities as well as power generation. In the greater part of these and other engineering applications, titanium has eliminated heavier and less cost-effective materials. Ti-6Al-4V is believed to be an incredible material that has many applications in a numerous of industries, the quantity of its utilization in our day by day lives is incredible and will just keep on growing with advancement in innovation and discovery of new uses for its properties. It includes great machinability and outstanding mechanical properties. The Ti-6Al4V alloy provides the good extraordinary performance on weight reduction in applications such as automotive equipment [44].

2.9. Comprehensive Review on titanium and its alloys using various additive manufacturing processes.

Lu et al. [45] conducted a comparative study of the resulting anisotropic microstructure and tensile properties of Additive Manufacturing (AM) Laser Direct Metal Deposited (LDMD) Titanium alloy (Ti-6Al-4V) components along the length and transverse direction. The fabricated components were found to be compact and with no defects. In-situ uniaxial tensile test loading was used to ascertain the various resulting modes of fracture which had occurred in the respective orientations based on the anisotropic distributions observed in the microstructure using Scanning Electron Microscopy (SEM). The anisotropic distributions in the microstructure resulted in the anisotropy found in the tensile properties. The results revealed that along the length of the components, the cross-section area had reduced and elongated greatly whereas in the transverse orientation, it was found that the components had elongated less because it had a high tensile and fracture strength. The microstructural composition of the tensile transverse

specimens constituted of prior beta grains that were columnar and short in a lamellar in structure. A tender grain boundary of alpha phases was also identified. Alpha colonies and alpha grain boundaries were observed along the grain boundary of the beta. The grains grew perpendicular to the axis of the tensile load applied, this attributed to the strengthening of the tensile and fracture properties, which were higher than in the perpendicular orientation. Alpha phases were observed in the tensile specimens which were oriented longitudinally; they had a basket-woven structure that consisted of small alpha colony sizes and short alpha platelets in contrast to the specimens oriented transversely. This attributed to the significant reduction in area and the minimum stress measured. The employed tensile testing methodology was also used to evaluate the anisotropic mechanical properties. It was observed that fracture mechanism in the transverse specimens was shear along the boundary of the prior beta grain which was caused by the boundaries of the vertical beta grains coupled with the big alpha colonies that prevented micro-crack initiations because of the resulting high strength. Equal deformation was observed on the two opposite ends of the grain boundaries and the necking that had occurred was in attribution to the composition of the small alpha grains.

Rousseau et al. [46] investigated the anisotropy in the microstructure and tensile properties of Direct Energy Deposited (DED) Ti-6Al-4V alloy in attribution to the concentration of oxygen in new and recycled reinforcement powders. The DED process is one of the few additive manufacturing processes that utilize powders that provide efficiencies of use which vary from 40-80%. It is courteous to consider environmental and economic factors in relation to the effects that reinforcement powders have on the

respective factors. Utilizing a cost-effective powder that may be reused in the process is a method of good environmental and economic consideration. Its price is determined by its level of purity. In the study, three types of powders with different grades were used which had a higher concentration of oxygen and its effects microstructurally and on the mechanical properties were characterized prior and post processing. The results revealed that the reinforcement powders which were recycled, and parts printed showed no visible pick-up of oxygen, what was identified from the recycled powder was the distribution of particle size coarsening and promotion of particles which were disintegrated. The evaluation done on the chemical composition of the heat-treated parts and feedstock powder showed that in all test conditions, there was a reduction in the aluminium element and the parts printed with the fresh reinforcement powder displayed no reduction in the Vanadium element. However, utilization of recycled powder displayed a reduction in the Vanadium content but was still compositionally valid according to its initial classification grade. It was observed that due to the deposition process the parts had a microstructure constituting of high martensitic primary alpha grains enclosed by boundaries of prior beta grains and the post processing annealing created a woven microstructure composed of alpha and beta structure. Microstructural observations showed that grains grew in the direction of build and was invariant even after annealing. Evaluation of the results revealed that the higher the oxygen content, the more Ti-α along the grain boundaries, inner grains of Ti-β and laths of Ti-α formed. Moreover, the increasing oxygen concentration had no major influence on the elongation but did improve the mechanical properties. However, the elongation in all parts was 20% after fracture.

Vilardell et al. [47] fabricated specimens of Ti-6Al-4V alloy by Laser Powder Bed Fusion (LPBF) and investigated the significance surface topography had on the fatigue performance of the specimens produced. The density of the samples was found to be greater than 99.5% with all the specimens being processed with constant processing parameters. The top and side of the surface of specimens was used to ascertain the surface topographies. The investigation was conducted by profiling the surface optically and microscopic study of focus variation were used to ascertain the microstructural evolution and surface topography. The specimens had the highest stress at the top and side after being subjected to a fatigue test by bending. The microscopy of focus variation and SEM were employed to characterize the fracture mechanisms at the surface that include the initiation and propagation of cracks. It was observed that the side surface of the specimens had a much higher roughness than the top surface, which lead to rapid initiation of cracks because of the high stress concentrations of the surface valleys. Moreover, this attributed to the low fatigue performance obtained at the side surface of the specimens. The “staircase effect” intrinsic to additively manufactured surfaces was another reason for the difference in fatigue life at the respective surfaces used on the specimens. It was found that the fatigue performance was also reduced by the scanned path of the processing laser. The cracks lateral to each other on the highly stressed surface of the specimens were nucleated which were promoted by the laser scanning path. However, the crack initiations were more influenced by the roughness of the surface than the path laser scanned.

Turichin [48] studied the effects on the technological efficiency by Direct Laser Deposition (DED) and on the generation of porosity in the microstructure of Titanium alloy produced parts. The tomography results obtained via X-ray revealed that the number of partially melted porosity and its morphology reduced in proportion to the increase of laser heat processing input. Prior to post processing, the specimens possessed high strength and had a low ductility measured from the tensile tests conducted. A desirable strength and ductility were achieved for the specimens after Hot Isostatic Pressing (HIP) at a ratio mode of laser power to process velocity of 2000/30. The percent elongation increased to 15% at the ratio mode of 2200/40. The results obtained from the X-ray spectroscopy revealed that in the composition of the microstructure was a phase mixture of alpha and primary alpha in the specimens prior to heat treatment, which formed in attribution to the initial beta to primary alpha transformation. However, subjection to HIP resulted in the dissolution of the primary alpha phase into a lamellar structure of alpha and beta phase. It was also observed that following the heat treatment was the generation of secondary alpha phase along the grain boundaries and primary alpha lamellar phase, this also promoted further growth of the primary alpha lamellar phases. The evaluation conducted on the deposited samples prior to heat treatment revealed that it had a low rate of plastic deformation and this was deduced to be the result of the metastable primary alpha phase formation.

Mahamood and Akinlabi [49] investigated the significance that the laser scanning speed processing parameter has on the evolution of the microstructure and micro-hardness property by Laser Metal Deposition (LMD) of Ti-6Al-4V reinforcement powder onto a Ti-

6Al-4V substrate. The deposition process was conducted employing a laser Rofin Sinar Nd: YAG at 4 Kw, coaxial to the reinforcement powder. The laser scanning speed was the only variant process parameter, varied between the intervals of 0.0055-0.095 m/sec and the parameters kept constant was the rate of gas flow, the power of the laser and the rate of powder flow. Optical microscopy was done to determine the metallurgical evolution in the fabricated specimens and the Vickers hardness tester was employed to determine the resulting micro-hardness property. The results revealed that the obtained micro-hardness of all the fabricated specimens were improved from the measurements done on the substrate. The observations made revealed that as the scanning speed was increased between the two intervals that the micro-hardness of all the specimens had improved in direct proportion to the laser scanning speed. The Laser Metal Deposition process is known to provide a high molten pool solidification rate, and this facilitates in the improvement of the microhardness property in parts which are produced by the process. It was concluded that obtaining desirable material properties is possible through the optimizing of the laser scanning speed of the LMD of Ti-6Al-4V, which in turn enables more control of the process.

Brusa et al. [50] investigated the mechanical performance of an additively manufactured bracket made from Ti-6Al-4V for aviation applications and modelled it numerically. The study was motivated by the limited current state of knowledge in predicting the resulting mechanical properties of new parts designed by additive manufacturing technologies. The current available literature reveals that additively manufactured parts are commonly tainted by anisotropy, reduced ductility in certain areas and defects. This occurs despite process control efforts in optimizing the manufacturing process parameters. The modelled

aerospace bracket was structurally complex and recreated through optimizing the geometry, topologically. The physical bracket was analyzed through tomography and the results was used to design a corresponding model possessing the material properties and considering the identified regions of low density and numerous defects. The material of the model designed was isotropic and homogenous based of references. This approach might have had limitations but was probed by conducting an activity for testing as well as an examination to validate the model developed numerically. Modelling in static design revealed that the numerical modelling approach enabled good strength predictability of the bracket based on isotropic and homogeneity material assumptions. Moreover, characterizing the material empirically also enabled bracket strength predictability in the design against fatigue case. A few preceding tests was conducted on the actual bracket and was a basis used to measure and evaluate the optimization methodology developed. The strength and toughness of the tensile and fracture, respectively, were compared to the wrought material of Ti-6Al-4V and deduced that the application of design criteria was a good consideration. The behavioural pattern of the static and fatigue designs was different for Electron Beam Melting (EBM) and Selective Laser Melting (SLM) additive manufacturing processes as the structure was influenced by the conditions of loads applied. However, the defects that were generated internally and the finish of the surface was where the difference was identified. Assurance of porosity through preceded identification using material tomography enabled the continuous validity of conventional test methodology that included fatigue and tensile. The concentration of porosity in the material detected through tensile testing limited the use of the properties obtained macroscopically in the modelling approach. It

was theorized that the way the internal porosities were distributed influenced the predictability of the material fatigue performance. There were a few vital concerns concerning the bolted joints of the bracket layout, but results showed that it possessed great strength supported by the preceding test results.

Krzyzanowski et al. [51] developed a numerical model of laser cladded glass reinforcement powder that was bioactive, onto a Ti-6Al-4V alloy substrate. The Finite Element methodology was devised and used to study the evolution of the stress and temperature distribution during the cladding process. Coated samples were fabricated and were investigated microscopically, the results obtained empirically served as a basis for the numerical modelling developed by FE of the process. It enabled the numerical investigation of the conditions influencing the potential of micro-cracks initiating in the clad. The time used to numerically compute the process was a factor in which the determination of the elemental sizes and quantity of the substrate and clad was based on to simulate each modelling case according to a convenient time. The processing laser was numerically set as source of heat generated volumetrically. The elements applied was a three-dimensional representation of the bio-glass reinforcement powder cladded onto the Titanium alloy substrate as a coated layer. The processing laser took on a trajectory path which was complex, and this attributed to the generated peaks of stress and temperature because of this effect, the cladded layer became susceptible to micro- cracks. The empirical results and the finite element modelling results were in good correlation with each other. The modelling results revealed that the micro-cracks had not originated internally of the substrate throughout the deposition process of the bio-glass

material since it was observed that the stress evolution within the substrate did not exceed the maximum strength during the process. Along the perimeter of the cladded coating, it was found that these areas had a high activity of thermal gradients which made the boundaries susceptible to crack initiation and propagation. The results analyzed showed that the boundaries at the beginning of each track had high thermal transients than the boundaries at the end of each track, which made the initial boundaries favourable to crack initiation and propagation.

Zhang et al. [52] developed a model to predict the temperature history field and metallurgical evolution that occurs in the solidification process of the metal during the single and successive deposition of Ti-6Al-4V alloy, employing the Direct Metal Deposition process. The simulation model developed was through the Finite Element (FE) methodology coupled with Cellular Automation (CA). The temperature simulated was presented as a coarse scale from the developed finite element model and the cellular automation model was scaled with the field of predicted temperature by an algorithm which was interpolated. The high rate of cooling was simulated, and the transient thermal field was updated which was achieved through macroscopic finite element computation. As the deposited material was cooling down and solidifying, the metallurgical grain evolution was predicted by the finite element cellular automation model. Microscopically, the cellular automation model enabled the study of nucleation, orientation of growth and crystallography, the growth of dendrite grains. The proportionality between the rate at which the grains grew and under-cooling was established by the cellular automation model and all the adjacent cells trapped were also revealed by the model. Deposition of

a single layer of material resulted in the microstructure constituting of grains which where equiaxed in structure, and for the simulation the grains were columnar for a deposition of 25 layers. The region highest on the cladded material is where larger grains grew, this corresponded to the result obtained microscopically. The empirical tests confirmed the morphology of the grains generated. The predictions of the temperature fields and grain evolution were reasonable and proved that the Finite Element coupled with Cellular Automation model developed was a valid method for direct metal deposition.

Ahmadi et al. [53] investigated the influence the treatment of transus heat and pressure (Hot Isostatic), sandblasting and etching had on the metallurgical evolution, the morphology of the modified surface and the mechanical and fatigue performances of titanium metallic meta-biomaterials which were produced by Selective Laser Melting (SLM) process. The incentive of using multiple post processes was to improve the fatigue performance of the meta-biomaterials produced. Metallurgical modification of the as-deposited Ti-6Al-4V specimens was required because the fine martensitic primary alpha structure identified in the microstructure of the titanium alloy which is not conducive for bearing conditions of various loads. The observations had revealed that the endurance of the metallic meta-biomaterials had improved twice as much when the as-deposited materials were subjected to surface modification by sandblasting and metallurgical redesign by Hot Isostatic Pressing. The results revealed that the method of laser pulsed vector showed no growth of grains, preferentially, it behaved more isotropic than with the conventional STL laser continuous method. Sudden failures in the specimens had occurred as a result of the generated internal porosity and stresses applied residually,

these factors had promoted the initiation of cracks which prevailed through the specimens. The microstructural evolution was the main contributor to the phenomenon. Microstructural analysis revealed that there was a transformation into a matrix of alpha and beta phases which were highly ductile and a reduction of manufacturing defects in attribution to the Hot Isostatic Pressed treatment. It was observed that there the fatigue performance was not improved as well as its endurance ability when the specimens were subjected to the two conditions of transus heat treatment. An improvement was observed only when the specimens were subjected to the combination of heat treatment and Hot Isostatic Pressing. The metabiomaterial fatigue life had improved significantly due to the removal of the incomplete fused material particles and stress induced compressively on the surface of the structs when the specimens were sand blasted. The conventional method of manufacturing components in three-dimension was not efficacious and so the post processing techniques used had to be tailored to transform the martensitic primary alpha structure of the as-deposited specimens. The ability of the specimens to tolerate fracture was improved by the sequential combination of HIP, sandblast and etching, which also promoted an organic reaction.

Oyelola et al. [54] studied and reported the behaviour in which Titanium alloy Ti-6Al-4V specimens were machined and the integrity of its surface. The specimens were fabricated by the Direct Laser Metal Deposition (DLMD) process, utilizing wire of raw material. The study was carried out to further investigate the effects that machine tools with two different inserts had on the as-deposits, at invariable machining conditions. The current state of technologies of the AM laser processes have a few elemental limitations that are being

addressed such as the requirement for most additively manufactured as-deposits to be machined for desirable results. The specimens had adverse effects on the integrity of the surface as well as its ability to be machined due to the solidification process which had occurred at rates which were not uniform and the defects which were generated. The surface of the specimens was analyzed, and it was found that the dominant stresses were compressive and induced lateral to the circumference of the surface. The machining tool which was coated induced compressive stresses which were significantly higher than the tool inserts with no coating, at a ratio which was higher as well. The proposition was that to optimize the machining operation on the as-deposits, the requirement of the cutting force and the inner conditions of the specimens can be related to the input process by employing a control system. This was proposed as the solution to machining specimens which had components that are spread randomly and laser cladded components that are functionally graded.

Xu et al. [55] conducted a study to investigate the significant effects that gum metal (Ti-36Nb-2Ta-3Zr-0.3O) reinforcement powder had on Titanium alloy Ti-6Al-4V substrate when deposited onto the material with direct laser. Only two coatings were applied which were analyzed based on the metallurgical evolution, corrosion performance and the tensile performance. The results obtained from the Energy Dispersive Spectroscopy revealed that on the second coated layer the toxic elements (Aluminium and Vanadium) were eradicated from the substrate material which proved to show that surface modification of Ti-6Al-4V with the gum metal does provide improvement of the performance. Based on the results obtained, observations revealed that the second gum

metal coating had an elastic modulus which was low in attribution to the single columnar beta phase which was oriented independently. The first cladded coating had martensitic secondary alpha which were prevalent in the layer. Moreover, the elastic modulus at the second coated layer was measured to be 75 GPa, which had reduced by 40% from that of the substrate and revealed from the test results conducted through Nanoindentation. The corrosion performance of the laser deposited gum metal coated substrate in Sodium Chloride (NaCl) at 3.5 wt% had improved and revealed by electro-chemical tests. This phenomenon was achieved because of the promotion of beta phase in the cladded layer. The study proved that titanium alloys may be biocompatible through the improvement provided by coating the material through direct laser processing. Moreover, depositing gum metal powder through direct laser processing onto Ti-6Al-4V alloy is a confident methodology in biomedical applications because of the ability of integrating the materials beneficial characteristics.

Mishra et al. [56] investigated the machinability performance of Titanium Ti-6Al-4V alloy by using machining tools which were textured and textured coated. The work focused on comprehending the efficacy of these machining tools by conducting empirical and numerical modelling (Finite Element) methodology. Nd:YAG Laser fibre (nanosecond) equipment was used to produce the textured (chevron) cutting tools and the subsequent coating applied was TiAlN using the Physical Vapor Deposition process. The two-dimensional numerical simulations utilized textured and textured coated cutting tools in comparison to the effects of using standard and standard coated tools by turning process. The simulations were pertained to the influence of the machining speed, the radius of the

tool edge, the tool feed and applied coating. The numerical modelling results were confirmed by the empirical tests which were conducted with the coated and non-coated textured cutting tools based on their efficacy regarding the average coefficient of friction, the contact length of the tool chip, required machining forces, performance of how the chips disentangled and the induced adhesive stresses that sheared between the coatings and substrate. The numerical modelling results pertaining to the length of contact, required thrusting force and machining force correlated well with the empirical test results. The other numerical simulation aspect which was validated by empirical tests was that of applying different cutting speeds for "Interface Multipoint Micro-cutting." The length of contact, the low curl radius of the chip, machining force and coefficient of friction were reduced when the textured cutting tool coated with TiAlN was used compared to the alternative tools which were developed. The coated textured cutting tools operated at changeable feeds reduced the primary machining force by 9.6-10.7% and 17-19.5% in comparison to the standard cutting tools which were not coated. The effectiveness of the textured and textured coated cutting tools had Improved as the feed was increased, hence increasing the length of contact. It was observed that the textured and coated textured cutting tools had a reduction in the contact length of the tool chip in contrast to that of the standard cutting tools. The combination of texturing and coating the cutting tools led to the significant decrease in the length of contact of the cutting tools by greater than 30%. The variation in the length of contact of textured cutting tools were incapable of being predicted in machining by the models which are theoretically available. However, the varying machining forces may be predicted for textured cutting tools by simulating the length of contact of the tool chip. The observations done showed that the

chips formed from machining the surface were disentangled when the textured and coated textured cutting tools were used and provided a better finish to the surface than compared to the use of standard non-coated cutting tools. In addition, the decrease in the lower curl radius of the chip of the coated textured cutting tools allowed the created chips to flow smoothly. The rake face and flank experienced a reduction in the peak shear stress for the coated textured cutting tools, shown by the numerically modelled results. The cutting tools which were coated had a less probability of experiencing coating failure during the operation because of mechanical interlocking. Hence, the reduction of the shear stresses in textured coated cutting tools attributed to the reduction of the substrate to fracture and failure of the cutting tool coating. The high machining feed and speed used in operation with the textured coated cutting tool had still improved the performance in machinability of the Ti-6Al-4V.

Seo and Shim [57] investigated the effects that track spacing had on the fabricated metallic materials which were induced with cell pores that were open and closed. The Laser Melting Deposition process was employed to create the metallic materials consisting of porosity. The metallic powder used was Ti-6Al-4V alloy coupled with a foam agent known as TiH_2, which created the two types of pores in the material. The phenomenon in which the metallic foams were created was in attribution to the high-power laser which was used in the process to fuse and deposit the powder mixture as it was being sprayed. The analysis carried out focused on the significant effects that the varyingly spaced tracks had on the characteristics of the foams formed, on the dimensions, and distribution of the pores created. The track spacing was the main

deposition process parameter but other parameters were considered and investigated as well, which include the rate at which the powder is fed, the content of the foam agent and the intensity of the laser used. The foaming agent used created the pores when the deposited track beads had a much larger width than the spacing of the tracks. The molten pool of metal varied according to the varying spacing of the tracks created, which was consequent to the open cell porosity that was promoted within the tracks. Therefore, the observations confirmed that in controlling the generation of pores, the spacing of the tracks need to be controlled. In addition, numerous open cell defects were generated with moderately increased the spacing between the tracks because of the molten pool surface tension that was created. Although, it was observed that increasing the track spacing more led to a reduction in open cell defect generation due to the empty pockets being filled entirely by the flow of the metallic molten pool. The results revealed that the porosity generation was contingent to the rate of the solidification process of the metallic molten pool because more porosity was generated as the rate at which the powder mixture was increased and reducing the laser intensity. The closed cell defects were identified by the processing parameters which were considered (the laser intensity and rate of the powder feed), the content of the foaming agent and the way the oriented tracks overlapped each other. The molten pool cooled at a very slow rate because the adjacent distance between the deposited tracks was small and due to this, the TiH_2 foaming agent in the reinforcement powder emitted gas and decomposed continuously before the solidification process was complete. More thermal energy was generated and retained as the adjacent deposited tracks were made smaller, it was also observed that this attributed to the increase of porosity in the porous metal material. It can be deduced based on the results

that the respective deposition processing parameters influenced the amount of porosity, the distribution, shape, size and the tensile performance of the porous metallic material that was fabricated. The radical intuition is that the desired metal foam defects may be achieved by optimizing the processing parameter values in accordance to what porosity type is being generated. Moreover, in applying a foaming agent in combination with the metallic reinforcement powder and controlling the spacing in which the tracks are deposited is consequential to the generation of open and closed cell porosity in the fabricated metallic material. The main future recommendation of the study is to investigate the tensile performance of the fabricated porous metallic material as the processing parameters are individually controlled.

Tan et al. [58] investigated the effects that Ti-6Al-4V alloy coating thickness had on the metallurgical evolution, tensile performance and fracture performance when cold sprayed onto Ti-6A-4V substrates. This is a new state of technology for coating substrates by spraying the reinforcement powder without the need to heat it in order to create a bond. This new technological method of using cold spraying to create coatings on materials has supposedly the capability to repair worn out parts that are made from Ti-6Al-4V and other metal alloys that are light weight. The components which are subject to damage due to corrosion or wear require coatings of variation in thickness at high quality in order to be repaired by Ti-6Al-4V alloy. So, this study addressed the matter by coating the Ti-6Al-4V substrates with varying thickness. The analysis revealed that as the subsequent coating layers were deposited, the metallurgy and tensile performance of the Ti-6Al-4V coating such as the level of defects, strong adhesion and high microhardness were retained. This

makes it a promising repair process in applicable industries. The tensile test used was the glueless method which ascertained the strength of the bond at the interface. Observations showed that the thin coated layers were able to sustain higher points of concentrated stress than the thick coated layers, when the flexure characteristics were investigated. A 2.7-3% level of defects was found in the Ti-6Al-4V coatings at each cross-section done. Due to the plastic deformation and shear adiabatic instability bonds created in the particles which were sprayed, there was no severe change in the thickness across the coating as was analyzed on the cross-section morphology of the surface and the microstructure. However, as the subsequent coatings layers were deposited, the roughness of the surface had a 0.1% increase as the coating thickness had increased. The Ti-6Al-4V particles were work hardened when cold sprayed and this attributed to the coatings having a much higher microhardness average value of 370 $HV_{0.3}$ than both the Ti-6Al-4V reinforcement powder and the substrate itself. The bond strength was found to be higher than 65 MPa at the coalesce surface of the coatings and substrates that fractured along the adhesive glue. However, the bond strength at the interface was found to even reach 90 MPa when the tensile test was employed using the glueless method. It was observed that the coatings delaminated off the substrate surface and there was failure at the interparticle as the thickness of the coating had increased, resulting in the reduction of the flexure strength of the coating. The fracture investigation conducted revealed that the fractured coalescence surface had brittle and local ductile fractures hitherto the pull-out method of facture testing. Within the splats - the areas of material jetting - is where the bonding occurred and this was the region where the ductile fracture

points were observed, whereas the bonding at the south pole to the splat is where the brittle mode of fractures were observed.

Rotella et al. [59] investigated the effects that the turning machine process had on the surface engineering of conventional wrought and additively manufactured Ti-6Al-4V alloy parts. The Titanium alloy materials which were additively manufactured included Direct Metal Laser Sintering (DMLS) and Electron Beam Melting (EBM) processes. The modifications of the microstructure, nano-hardness and the layers which were deformed plastically were investigated to ascertain the degree of which the integrity of the material surface and machinability were affected by the production processes used. The analysis was conducted on the chemical, mechanical and morphological aspects of the fabricated materials prior and post-machining. The analysis revealed that the fabrication processes used had affected the integrity of the surface for all the completed parts. The materials which were fabricated by the different production processes and machining operations might have all had the same Ti-6Al-4V material alloy but were all different in terms of their metallurgical characteristics and tensile properties. The observations made on the roughness of the surfaces revealed that the wrought parts had a much better quality than the components which were produced by the additive manufacturing processes. The performance of the additively manufactured parts was different in terms of size of the layer was affected and the anisotropy in the hardness at the surface and underlying layers. The results revealed that the processing parameters used for the turning operations were optimized for the wrought parts and special attention was still needed to optimize the machining parameters for the parts that were additively

manufactured. The surface of the additively manufactured parts was the least susceptible to fret initiation of fatigue than of the wrought parts due to the varying hardness which were achieved on the surface of the additively manufactured parts, post-machining. The technique used to fabricate the parts is what needed to be considered to bring the processing parameters of the turning operation into optimization. The general trend observed for all the parts fabricated was that as the turning speed was increased it increased the material hardness and reduced the roughness on the surface, however, despite this, it was of great importance to still ascertain the number of changes that resulted from the parameters of the turning process. Although the metallurgical composition of the fabricated parts was retained, the manufacturing techniques used such as wrought, Electron Beam Melting and Direct Metal Laser Sintering influenced the degree to which the metallurgical, mechanical and topographical properties were affected by the turning operation process.

Mahamood and Akinlabi [60] carried out a study that investigated the effects that Laser Metal Deposition (LMD) processing parameters had on the hardness behaviour of Titanium alloy Ti-6Al-4V parts additively manufactured by the LMD process. The design of empirical statistical method using complete factorial was devised and used to characterize the significant effects that the LMD processing parameters had on the resulting hardness performance. The reinforcement powder used was a Titanium Ti-6Al-4V grade 5 alloy which was deposited onto the substrate of the same chemical composition. The process parameters that were considered included the speed at which the laser scanned, the laser intensity, the rate at which the gas flowed and the rate at

which the powder was deposited onto the substrate. The set parameters of the LMD process had its primary effects during the process as well as potential effects when they interacted and so these were vital to quantify, and design of experiment methodology employed had the capability to measure these effects. The hardness analysis was carried for each specimen produced, and the procedure which was followed pertained to varying the parameter values between minimum and maximum intervals, resulting in the totality of 16 empirical tests. The results revealed that when the laser processing speed and the rate at which the powder was deposited increased, the hardness of the material improved. However, as the laser intensity was increased, the hardness property started to reduce. In the case of the rate of gas supplied, the variation of this parameter had no significant effect on the hardness performance of the specimens, as it only decreased minimally.

Oliveira et al. [61] conducted a study in which the corrosion performance of Titanium alloy (Ti-6Al-4V) was investigated in attempt to improve the property by application of nitride coating deposits, namely TiN and TiAlN/TiAlCrN by plasma assisted physical vapour deposition (PVD) technique in a hydrochloride (HCl) solution of 2 M at varying temperatures of 25, 60 and 80˚C. An open circuit potential (OCP) against time intervals, a spectroscopy of electrochemical impedance and potentio-dynamic polarization methods were used to measure the behaviour of the corrosion. The results revealed that the uncoated titanium alloy substrate demonstrated a higher corrosion density and lower spectroscopic electrochemical impedance in comparison to the corrosion behaviour measured for the coated alloy. Indicating that the coated alloy provided good corrosion

resistance for the titanium alloy. Observations showed that the uncoated titanium alloy was reactive and transitioned from active to passive when submerged into the HCl solution. Whereas the Tin and TiAlN/TiAlCrN coated alloy was nonreactive. The low current density of the corrosion and high values of impedance attributed to the superiority of the corrosion resistance of the applied coatings. Observations at 25˚C showed that a single layer (2.2 μm) of TiN coating enhanced the corrosion resistance of the titanium alloy than the multiple deposited layers of TiAlN/TiAlCrN. The TiAlN/TiAlCrN deposited coating had a thickness of 6 μm and a low number of interfaces (N=6). The aluminium content present in the composition of the TiAlN/TiAlCrN coating made it susceptible to react when in contact with the HCl solution. The corrosion resistance was invariable at 60 and 80˚C for both nitride coatings deposited on the titanium alloy. Potentio-dynamic polarization results revealed that at 25,60 and 80˚C, the TiAlN/TiAlCrN coating was spalled on the surface of the alloy but the TiN coating remained intact.

Dzugan et al. [62] investigated the fracture performance - at a small scale - of small Ti-6Al-4V specimens fabricated by Selective Laser Melting (SLM) and Selective Electron Beam Melting (SEBM) by ascertaining the microstructure and mechanical properties resulting from the effects of the specimen thickness, position and build direction. The study developed a systematic method in which the small sized specimens – excised from larger parts – were employed to ascertain and document the resulting microstructure by local property characterization in which also determined the developed porosity, through tomography, and tensile properties. This approach enabled processing variations (additively manufactured conditions) to also be determined from the fabricated additively manufactured specimens. The results obtained and reviewed, revealed that the

orientation of deposited layers as well as the thickness and location of the specimens attributed to the anisotropy found in the microstructure and tensile properties. There were tensile properties which were affected by the excising of the superficial as-deposits. The system developed in the study was a cost-effective approach especially in relation to quality control of additively manufactured components. The method enables the small specimens to be placed at different locations in the additive manufacturing chamber, the ability to mate to component parts and remove from component parts. The anisotropy inherent in the thermal gradient of fabricated specimens have great potential to attribute to the large anisotropic tensile properties resulted when the three methods are employed. Study still commences in ascertaining these differences. In order to ascertain properties with great validity, the study showed that it is of importance to investigate the positioning, thickness and orientation of the additively manufactured specimens. It is also of importance to consider the surface roughness and other surface contributors of the fabricated specimens as they effect the resulting tensile properties.

Farayibi [63] conducted a study in which the surface of laser cladded Titanium alloy Ti-6Al-4V was improved by employing Plain Water Jet (PWJ) and Pulsed Electron Beam Irradiation (EBM). The current state of knowledge states that the laser cladding method can be used to improve the lifespan and repair worn out parts that have high replacement costs. One of the main concerns is the resulting surface finish of laser cladded components; ridges forming and a poor overall surface finish. This study addressed this issue by developing an approach where surface finishes of components may be achieved to specific desires. The PWJ and EBM was applied sequentially in the process to create

a uniform surface of low roughness than initial laser cladded components that have poor surface finish of high roughness. Prior to the post-processing, the surface observed had ridges measured to be 200±18 μm (peak to trough) and 49 μm waviness. The PWJ applied to the surface of the cladded components had a pressure head of 345 MPa impinged at 90˚, 3mm stand-off distance, a traverse speed of 250 mm/min and 0.25 mm overlap during milling. The sequential process resulted in the removal of the ridges, with a 480±10 μm surface depth after milling. The waviness, surface roughness and surface straightness achieved was 14.9 μm, 12.6 μm Ra and 44 μm, respectively. These were achieved after the PWJ process, which owed to the surface having defects characterized by a poor layer of cracks, deep pores, staggered surfaces and underlayer gaps. However, this poor surface layer owing to the PWJ process was rectified when the surface was subjected to the Pulsed Electron Beam Irradiation (EBM) of 50 pulses at 17 J/cm^2. The defected surface was melted, removing most of the rough edges, burrs and gaps, resulting in a uniform and straight surface with a 6.2 μm Ra final roughness.

Molaaei et al. [64] employed the Powder Bed Fusion (PBF) process to fabricate titanium alloy Ti-6Al-4V tubed components of thin-walled structure which were used to investigate the impact post processing Hot Isostatic Pressing (HIP) has on the fatigue performance and on the multi-axial load conditions applied, as well as the effects that the roughness of the surface and orientation has in the process. The specimens were subjected to deformation conditions that included torsional, axial, in-phase (combined) and axial+torsional loadings that were 90˚ out-of-phase. Build orientations at 45˚ (diagonal) and vertically were studied to ascertain their significance on the fatigue behaviour. The effect that the roughness of the surface had on the fatigue behaviour was assessed by

subjecting specimens that were surface machined and as-built to a series of fatigue tests. The impact of the HIP process was also investigated by subjecting heat-treated specimens to the process and evaluating the significant effect. The effects of the varying input processing parameters and fatigue data were evaluated and compared from dual PBF machines. Comparisons were made between the HIP specimens that were subject to torsion to the behaviour of the heat-treated specimens subject to torsion and to the wrought specimens that were cyclically deformed; for the purpose of ascertaining the significance of the HIP process. The results revealed that the PBF specimens that were subjected to the HIP process underwent a transformation in microstructure and was consequent to internal defect constriction and fusion. This owed to the correlation found in the behaviour of the wrought and HIP processed specimens that were subjected to axial and torsional loads. The additively manufactured specimens that were subjected to the HIP process attributed to the reduction in ductility, which resulted in the specimens being minimally softened cyclically in the regards to plastic deformation, in contrast to the degree of cyclic softening experienced by the wrought specimens. The HIP treated materials experienced no excessive hardening cyclically when the 90˚ axial+torsional out-of-phase load was applied, the same was deduced for the wrought specimens. The HIP process on the PBF annealed surface machined materials attributed to the evolution of the alpha martensitic particles – that were low in ductility – to alpha/beta phase which was ductile, and to the reduction in structure and fusion of the internal defects. This microstructural evolution led to result of the detected shear failure in the Low Cycle Fatigue (LCF) and the High Cycle Fatigue (HCF) regions after the post processing treatment. The PBF materials that were surface machined annealed had shear failure in

the LCF area and throughout its longer life, it was tensile, signifying that in the HCF area, the internal defects were predominant. The failure results obtained for the materials that were machined surface annealed were also achieved for the as-built materials that were subjected to HIP processing. Analysis of the fatigue performance in consequence of the varying loads applied revealed that the additively manufactured HIP treated specimens and the wrought specimens had corresponding behaviour. The ductility of the materials that were HIP treated had improved and this was consequence of the evolution of the microstructure, the reduction of the internal defects and the remedying of the residual stresses. Observations showed that the results measured from the von-Mises equivalent of the multiaxial deformation data based on the varying load applications did not correlate well with the data obtained from the fatigue tests of the torsion, axial, in-phase (combined) and the out-of-phase (90˚) axial+torsion loadings. However, a better correlation was achieved with the cyclic deformation data from the predicted fatigue life curve of the planar Fatemi-Socie critical parameter. In completion of the HIP process applied to the materials, the volume of the manufacturing defects decreased; reducing their structure, and this resulted in the additively manufactured annealed materials to have a considerably shorter fatigue life in the HCF than the materials that were HIP treated. This was an improvement however, the post treatment only removed some of the partially fused particles, the gas entrapped pores and other superficial residual defects, which all are potential sites for initiation of cracks. The HIP post treatment not only reduced the internal defects, but also remedied the direction anomalies caused by the additive manufacturing build process. This accounted for the materials not having considerable anisotropic effects after HIP treatment. When the materials were subjected to the torsional load condition, the

threshold of fatigue failure was on the external surface due to the inclining stress, whereas the threshold of the initiated crack was unclear for the axial and axial+torsion (combined) load conditions as the fatigue failure could have occurred at the manufacturing defects or at the internal or external surface of the material. The fatigue failure behaviour of the materials HIP treated were significantly different for the various conditioned surfaces. The results revealed that the HIP materials that were surface machined had longer fatigue lives than the HIP materials that were superficially as-built. This occurred because although the post treatment reduced the manufacturing defects, the length of the fatigue life is affected by the surface roughness and generated micro-cracks, which are factors that are not affected by the HIP process. It was observed that the variations in the processing parameters and PBF fabrication from machine-to-machine attribute to great significance in anisotropy of the thermal rates, microstructural evolution and the nature of the defects developed. These are all important factors that govern the effects on the fatigue behaviour of the materials. The morphology, dispersion and positioning of the generated defects in the additively manufactured materials are the characteristics that are influenced by the additive manufacturing processing parameters, the powder metallurgy and the thermal rates.

Yang et al. [65] employed the Finite Element Method (FEM) to validate and predict the thermal and mechanical performance of titanium alloy Ti-6Al-4V additively manufactured by direct energy deposition Laser Engineering Net Shaping (LENS) process. The numerical model developed was “thermo-elastic-plastic” representing three-dimensional mapping. The main incentive of their study addressed one of the significant impediments

in additive manufacturing that limits the technology from being completely accepted widely in broader industrial fields, is the generation of thermal residual stresses and distortions in the fabricated high functioning components. The study contributes to the current state of knowledge that include validation of the developed model by comparing – via magnitude and mapping - the modelling distortion observed on the base surface of a thin parent material with the measurements made empirically by employing a laser scanner that provided three-dimensional mapping. Whereas the more conventional method was to compare the numerical results with the empirical results by the point-wise approach to validate the proposed model, this limited the potential knowledge perceived. Also, the study proved the significance of employing quasi-static simulation as a means of conducting computations in a cost-effective way, by conducting quasi-static and dynamic modelling and comparing the obtained results with those achieved mechanically. The incentive was to contribute to the lack of publications done in measuring how effective the quasi-static mechanical methodology is in the transient LENS process. The additively manufacturing building process was modelled. The modelling results and the empirical results were used in comparison with each other to validate the thermal behaviour that was analyzed. The comparison was based on the point-wise thermal history, which was also valid for the thermal transfer through the parent material across its thickness. The magnitude of distortion as well as the distorted pattern at the base surface of the parent material where similar for the empirical and the simulation results, and this was used to validate the mechanical modelling, which is more esoteric than the previous point-wise method of comparison done in the past. The analysis performed on the contraction induced bending, coupled with the numerical analysis in terms of the stress field

computed longitudinally within the larger and smaller dimension of the walls were used to profoundly explain the map representing the distortion. The effects of modifying the surface through the building process and the detailed empirical heat transfer convection measurement can be of consideration for future recommendations of this work to achieve greater validity and accuracy. However, on-line optimization of the additively manufacturing process by employing Finite Element Method technology in the industry will require a methodology that provides more accuracy and efficiency.

Biswal et al. [66] investigated the effects that porosity defects have on the fatigue performance of additively manufactured Ti-6Al-4V alloy. The focus was based on how the shape, location, size and other morphological characteristics of empirical gas entrapped pores influence the fatigue life performance of the material. A finite element simulation was initially conducted based on an elastic-plastic model to compute the change of the local mean stress, the stress and strains at the localized areas and the plastic deformation that occurred cyclically within the perimeter of the isolated pore defects. The elastic-plastic model developed of the morphology of the gas pore was spheroid and elliptically spherical, which were used in the modelling analysis. The fatigue life was predicted using the method of determining the life of the strain. The Hot Isostatic Press (HIP) post process was applied to the additively manufactured Ti-6Al-4V and the S-N data obtained was used as a standard to predict the fatigue life performance of the materials, conditioned in being pore-free. The finite element results revealed that the location and shape of the isolated gas entrapped defects governs the factor of the stress concentration (K_t). In addition, although the geometric size of the gas pore is inconsequential of the prediction of the

fatigue life, the cross-section area bearing the load decreases due to enlarged pores. Spherical gas pores were characterized as an internal defect from the when their location was measured to be four factors more than the pores diameter proxy to the free surface, and the stress concentration factor of this type of pore was found to be 2.08. Surface Pores that were hemi-spherical had a stress concentration factor of 2.1. Elliptically-spherical internal pores had a stress concentration factor of 2.5. The type gas pore that was found to be critically important was the spherical pores that were found at the subsurface which were a pore diameter away from the free surface. Their stress concentration factor had increased from 2.2 to 4.3 contingent to the distance from the free surface. The internal gas pores that had geometrically evolved from being originally spherical to elliptical at a factor of two was found to have a stress concentration of 2.08 that had increased to 2.5. The literature synthesis provided in previous year publications on the Selective Lase Melting (SLM) of Ti-6Al-4V was used to calibrate the application of the non-linear mixed hardening rule that was used by Biswal [66] to model the relationship the materials had subjected to the cyclic deformation load condition. The mean stress that was locally measured was found to have relaxed attributed to the effect of the cyclic plastic deformation which had occurred at the root of the gas pores. This phenomenon was governed by the morphology of the gas pores, the ratio of the stress and the application of the stress amplitude. The strain-life relation equation that was formulated by Smith-Watson-Topper was used with the locally computed maximum stress and strain amplitude obtained from the finite element model, to predict the fatigue life performance including the local strains which were high and the relaxed mean stress that was measured locally. The procedure of predicting the fatigue life performance was validated

with the literature that was published on the additively manufactured Ti-6Al-4V powder-based alloys experimental results that included knowledge of gas pores location, size and shape being the sites of crack initiation. The work was further investigated through parametric study which confirmed and provided more comprehension that the fatigue life performance of the material was influenced by the shape and location of internal pores and less on their size. The strength of the fatigue had decreased consequent to the isolated porosity defects and this was accounted for by the employing of an S-N curve in the parametric study.

Khatri and Jahan [67] conducted a study investigating the various possible wear mechanisms that dominate when using machine tooling to machine titanium alloy Ti-6Al-4V. Three machining conditions were used that include dry machining, excessive coolant and Minimum Quantity Lubrication (MQL). The machine tools used was one uncoated carbide and the other was Titanium Aluminium Nitride (TiAlNi) carbide coated. Both cutting tools were used set at the same machining process parameters to machine the titanium alloy material. The machining parameters considered were the cutting speed, which was set at a high speed but thereafter kept constant, the tool feeding rate and depth of cut were the invariant parameters used in the multiple tests conducted in the end mill machining of the material. In completion of the multiple experiments conducted in the dry, excessive coolant and MQL machining conditions, it was observed that the tool wear mechanism that was the most prominent was abrasion during the machining of the material. However, during the dry machining condition, abrasion tool wear was most dominant followed by MQL condition with the least occurrence and excessive coolant

displayed the very least occurrence of abrasion wear. The tool cutting faces namely the rake and flank faces are the two tool geometries which are responsible for the life of the tool and the surface roughness finish, they both showed occurrences of tool wear abrasion being dominant. During end milling of the titanium alloy material, high excessive heat was generated and the tip of the carbide tools experienced cooling in periods which attributed to the generation of thermal fatigue, this resulted in the wear of the tip of the tool as well as the chipping of the edge that was observed as also a dominating tool wear mechanism. During the machining in dry condition, it was found that the tool wear mechanism second in dominance was adhesion. Machining in the MQL condition showed a reduction of the chipping of the edge and adhesion of the generated chips. The MQL machine condition had reduced the dominating occurrence of plastic tool deformation of the tool edges and flutes which were prominent during the dry and excessive coolant machine conditions. When the coated (TiAlNi) carbide cutting tool was used in the excessive coolant and MQL machining conditions, the coatings started to delaminate, and this was more dominant in the two wet conditions than in dry machining. This signified how effective it was to machine materials in the dry condition than with an application of a coolant with coated cutting tools. From the results obtained, it was deduced that the most productive and efficient way to machine titanium alloy Ti-6Al-4V materials is in the MQL machining condition than in dry machining and excessive coolant because of the least dominance of tool wear mechanisms that occurred during the MQL condition.

Sun et al. [68] probed the effects that Selective Laser Melted (SLM) Titanium alloy Ti-6Al-4V processing parameters had on the macrostructure, metallurgical evolution and tensile performance. The process parameters have a significant influence on these factors considered, including the morphology of the surface, density, evolution of the microstructure, accuracy of the fabricated dimensions and the mechanical performance of the Titanium alloy components processed by SLM. The fabricated components were also examined for fracture and the mode of failure was characterized. The results of the investigation showed that the density had increased in proportion to the increase of the processing laser power coupled with the reduction of the speed of the laser scan. Moreover, for a laser power equivalent to and exceeding 175 W, the density became less susceptible to the laser power. The speed in which the laser scanned on the surface of the substrate had influenced the morphology of the surface of the scanned tracks in such a way that the initial microstructure was ordered and visible but evolved into being nonuniform and unclear as the parameter was increased. Morphological observations along the side of the surface showed the prominence of the adhesive powder, flow path of the melt pool and the areas which overlapped, attributed to the increase of the laser scanning speed. In addition, round structures shaped like a ball had formed on the microstructure. In terms of the accuracy of the fabricated components: the building process occurred in the z-direction and the effects found on this axis was of size shrinkage and in the x- and y-direction was affected by “periphery spreading”. The analysis conducted by X-ray Diffraction (XRD) revealed that the predominant phase present in the fabricated components was the primary alpha which was martensitic.

Zhang et al. [69] conducted a study to investigate how the absorption of light during the Selective Laser Melting (SLM) process was affected by the various defects and sizes of the reinforcement powder particles. The reinforcement power was layered onto the Ti-6Al-4V substrate and the laser was irradiated along the layer. The process was developed numerically in which models were design – closed-packing, and the methodology used to vary the way the packing was filled was established according to what Horsfieled had devised. The mechanism used to simulate the absorption of light by the powdered layer was based on “ray tracing”; the interaction between the laser beam and the material. The “integrating sphere” was used to make the reinforcement powders - of varying particle sizes and defects – susceptible to measuring the absorbed light. The closed packing methodology developed and used, the computations of the intensity of the light irradiated onto the layer and the absorption of light through the accumulator of light intensity were validated by the empirical results obtained for the prepared powders which absorbed light. It was numerically ascertained that the absorption of light by the layer of reinforcement powders and integrating sphere measurements was found to be 70%. A relationship was observed-as the defects in the layer reduced, more light was absorbed through the layer, but the degree of light absorbed had decreased once the number of defects had reached a certain number while decreasing. This phenomenon had occurred because more light was being reflected than absorbed. More light was being absorbed when the sizes of the reinforcement powder particles were reduced. Observations led to the conclusion that the behaviour of the absorption of light varies according to which position the light was irradiated on the closed packing model. In instances when the light was irradiated between the interspaces of the spheres, there was more light absorption due to the

random dispersion of scattered light and when shone onto the spheres directly, there was more reflection light which then reduced the degree of light absorbed.

Tan et al. [70] investigated the thermal, metallurgical evolution and mechanical performances of the Titanium alloy Ti-6Al-4V which was processed by Selective Laser Melting (SLM) and subjected to multiple tracks and multiple layering. The model developed encapsulated all three factors which made it possible to predict the variation in thermal energy, the transformation phase in solid-state and the induced residual stresses. The phase state transitions such as shrinking, vaporization, cooling, melting and solidification where all included in the development of the model which also considered the phase transformation in solid-state. The heat source was volumetric which established the powder beds absorption and scattering of the laser. This heat transfer conduction process which had occurred was evaluated by thermal analysis. The solid-state phase transformation caused a change in the volumetric strain, which was ascertained by the thermal histories that measured the evolution of the volumetric fraction in the microstructural phases. It was seen that the thermal histories and the solid-state phase transformations had induced strains which was in consideration by a constitutive law of a proposed elasto-plastic that was used in evaluating the generated stress fields. The numerical modelling revealed that the residual tensile stresses were reduced, however, the residual compression stresses were edified; this was all in attribution to the solid-state phase transformation which was taken into consideration in the investigation. Moreover, the results revealed that along the direction of which the scanning was conducted, the component stress induced in the singular printed coat was greater than

the other bi-component stresses. It was discovered that at the bottom area of the part which was coated with four coats, the peak von Mises stress was achieved in that region.

Mishra and Kumar [71] developed a numerical model based on the thermal-fluidic transport that takes place during the process of fabricated Ti-6Al-4V by Selective Laser Melting (SLM). The process was simulated using a volumetric source of heat and the investigation focused upon studying how the Ti-6Al-4V reinforcement powder layer was influenced by the volumetric energy which was absorbed. The only processing parameters which were varied were the laser intensity and the scanning speed, which were employed to numerically design the SLM single- and multi-tracks. An empirical method was also developed and was used to validate the results achieved by numerically modelling the process. Thermal, molten pool size and shape measurements were published empirically and used for numerical validation. Moreover, energy densities between low (30 $J \bullet mm^{-3}$) to moderate (70 $J \bullet mm^{-3}$) are where the best numerical and empirical results were correlated. The defects which had formed during the deposition of the multiple tracks were numerically modelled and the predictions were well correlated with the empirical results at a specific range of energy densities. The study had showed that in processing Ti-6Al-4V parts by Selective Laser Melting, the optimized range of processing is at the energy densities of 50-70 $J \bullet mm^{-3}$. The findings showed that the thermal gradients and cooling rate were high at instantaneous locations on the front of the solidification interface; ordered at 10^7 $K \bullet m^{-1}$ and 10^6 $K \bullet s^{-1}$, respectively. These were found when the solidification parameters including the temperature gradient magnitude, solidification front velocity, cooling rate and interface stability factor were computed. The

solidification planar had a critical limit which was above the interface stability factor and remained this way.

Wang et al. [72] studied the significant effects that defects, and metallurgical anisotropy induced by the Electron Beam Melting (EBM) process of Titanium grade 5 alloy had on the mechanical performance. The samples were oriented in three different ways in the building process. The investigation focused on the morphology of the defects and microstructure, the distribution of the grain boundaries, the tensile properties, fracture behaviour and the way they were interlinked. The results obtained revealed that in all three sample orientations with reference to the substrate, characteristic defect anisotropy regarding the morphology and prevalence had occurred in the EMB Ti-6Al-4V samples. The porosity generated were spherical and columnar in structure and their sizes were acquainted with the defect anisotropy. The findings showed that during the EMB process in the vertical, horizontal and diagonal sample orientations, the columnar defects always had its major axis at right angles to the direction of the build. The mechanical properties were influenced significantly by the way the columnar defects were oriented respective to the direction of the tensile load applied. Characteristic anisotropy of the microstructure had the second dominance over the tensile performance. Very fine ductile dimples were formed in attribution to the alpha + primary alpha grain boundaries which initiated and propagated intergranular cracks. However, fractography analysis revealed that chevron fracture of microcracks had initiated at the columnar defects. When the samples were subjected to tensile loading lateral to the columnar beta grain boundaries, the tensile properties had improved which indicated that the grain boundary structures were vital in

the improvement of the mechanical performance of the samples. In addition, there was no delineate that the prior beta boundaries contributed in any way to the initiation of the cracks.

Rubino et al. [73] investigated the potential microstructural and surface advancements of the Friction Stir Process (FSP) on Electron Beam Melted (EBM) plates made from Ti-6Al-4V alloy. The tool used for the friction stir process was pin-less in efforts to redeem the unsatisfactory finish of the surface, induced manufacturing porosities and reduced tensile performance of the superficial as-layer which was affected. Three friction stir processing conditions were employed which included an invariant tool rotational speed of 700rpm and varying tool advancing speed of 100, 112 and 125 mm/min. The friction stir process resulted in the final surface finish to be reduced by 80% for all three processing conditions. The process reduced the manufacturing defects. However, the compositional material that made up the distinct microstructural zones was not affected by the varying tool speeds i.e. when the advancing tool speed was increased from 100 to 112 and 125mm/min, the stirred area had reduced from 0.20 to 0.18 then 0.14mm/min. The area in which transition took place had reduced from 0.3 to 0.15 then 0.05mm at each increasing advancing tool speed.

Vrancken et al. [74] investigated the potential and effects of employing Concentrated Solar Energy (CSE) for the first time as a new technique to heat treat Titanium Ti-6Al-4V alloy which was produced by the Selective Laser Melting (SLM) process. This method of heat treatment asserts itself amongst the other conventional heat treatment processes

and proposes as an alternative. The specimens were subjected to heat treatment in solar furnaces which were horizontal and vertical, SF40 and SF5, respectively. The investigation established the significant effects on the hardness, the weight gained or lost and the microstructural evolution of the SLM specimens. Argon atmosphere was used during the process of heat treating the as-specimens in both solar furnaces – SF40 and SF5, a 60˚C/min rate of heat was applied in the process on both sides of the beta-transus. This was achieved when the heat treatment on the specimens were complete in the horizontal solar furnace at a temperature of 705˚C-Air Cooling (AC) mode below the beta-transus. The microstructure of the heat treated specimens in the horizontal solar furnace at 850˚C and in the Furnace Cooling (FC) mode had equiaxial grains in the alpha phase observed and microstructure similar to basket waves. The specimens heat treated in both solar furnaces at horizontal: 1015˚C – Air Cooling, 850˚C – Furnace Cooling and 1050˚C – Furnace Cooling; vertical: 850˚C and 1050˚C – Furnace Cooling, were observed to have promoted alpha case. This formation of the alpha case was supposedly in attribution of the environment of the heat treatment within the solar furnace it being contaminated by elements, namely CO_2, water vapour, Oxygen, CO and Nitrogen. An alpha lamellae structure was formed from the original primary alpha and the structure was a matrix of beta, consequential to the heat treatment temperature of 1015˚C being applied above the beta-transus, thereafter, heated at 850˚C – Furnace Cooling. Alpha colonies were also observed, however, the clouds led to an incomplete residence time of 50min from the full 150min. Heat treatment at a temperature of 1050˚C above the beta-transus resulted in the microstructure being lamellae with a matrix of alpha+beta, which had transformed from the initial primary alpha microstructure. Alpha colonies and a Widmanstatten

microstructure were formed. There was a formation of primary alpha phase elongated in structure, as well as an alpha+beta structure which was transformed from the initial martensitic primary alpha after the specimens were heat treated below the beta-transus in the vertical solar furnace at a temperature of 850˚C. The SLM as-specimens were contaminated during the heat treatment process in the horizontal and vertical solar furnace, coupled with the formation of the alpha case all contributed to the weight gained by the specimens. The weight varied the most in the specimens which were heat treated at the temperatures higher than the beta-transus (1015˚C and 1050˚C) and close to it (850˚C). The investigation showed that this process of heat treatment ought to be optimized when employed, but, nonetheless, Concentrated Solar Energy serves as a reliable heat treatment alternative process of SLM Ti-6Al-4V materials than the conventional processes. The solar furnaces might create a contaminated atmosphere inside during the heat treatment process but it is identifiable and can be eliminated, moreover, there is more accurate temperature control of the solar energy in the heat treatment process which is feasible at high rates of heating temperatures. The cycle of the heat treatment process was short due to the ability of meeting the specific treatment temperature in a short time at the rate of heat of 60˚C/min used in the process.

Stoffregen et al. [75] produced Titanium Ti-6Al-4V alloy specimens by employing the Selective Laser Melting (SLM) process and the fatigue performance of the specimens were analyzed by investigating the strengths of the fatigue by characterizing the range of low and high life cycles. The specimens were subjected to strain control at constant amplitude. The reinforcement powder was deposited onto the material by laser at right

angles to the axis of the specimens in an additive fashion. The specimens were manufactured into circular Tensile-shaped specimens and the fatigue tests were conducted on them at standard temperature. A treatment was applied to all the specimens to “stress release” them. Notch sensibility was conducted on the specimens of a second bath to investigate the phenomenon in the material. Displacement control was used to conduct the tests. The metallurgical analysis revealed that the morphology of the microstructure constituted of needle-like structures in double phases possessing favourable transitioning and minimal defects. Characterization of the material was based on the tensile performance, fatigue life cycle range and the incorporated equations of Basquin and Coffin. The results showed that the cyclic curve was relatively low in contrast to the monotonic curve, which was in attribution to the higher strains induced that caused the cyclic-softening behaviour analyzed. The alloy is known to have low ductility and great strength which influenced the transitioning cyclic life to be low – with reversals of approximately 250. The equations employed and the conducted fatigue test results subjected under strain control were viable in the investigation of fatigue performance, and 164 reversals were achieved for the transitioning fatigue life. A factor of the notch sensibility of material in terms of the cross-section of the circular notch was measured to have a stress concentration (K_t) of 1.7 and quantified to this was the dynamic stress concentration (K_f) which had the relationship to increase with increased fatigue life, increasing from the low to high fatigue cycle alluding to 1.42. Multi-nucleation was observed from the Scanning Electron Microscope (SEM) results, moreover, the cracks were observed to have originated superficially and propagated into the cross-section.

Wu et al. [76] fabricated Titanium Ti-6Al-4V alloy components using the Wire Arc AM process with Gas Tungsten as the only local shielding gas: GT-WAAM. The geometry of the build as well as the tensile properties of the fabricated components were investigated in terms of the influence of the thermal performance during the Additive Manufacturing process. Computations were done to study the accumulation of heat and thermal performance during the GT-WAAM process by employing in-situ measurements of the temperature at subsequent deposited layers. The viability of fabricating Ti-6Al-4V components by using GT-WAAM technology was assessed by means of evaluating the Influence of the heat generated and accumulated by the process – under local shielding gas - on the metallurgical evolution and tensile properties of the components. The phenomenon was investigated by using SEM, OM, EDS, XRD and conventional tensile load tests. The results obtained from the empirical measurements showed that there was anisotropy in the tensile properties and in the characteristic features of fracture due to heat generated and accumulated during the process along the direction of the build. In addition, this attributed to the anisotropy due to the influences in the evolution of the microstructure, the oxidation layer of the surface, the resulting sizes of the grains and the crystalline phase, which had all varied according to the accumulation of heat. Based on the results, it was deduced that to produce quality Ti-6Al-4V components with desirable tensile properties, the inter-pass temperature had to be limited to 200˚C and below when fabricating the components by means of GT-WAAM technology under local shielding gas. Along the height of the build there was a phase transition in the evolution of the microstructure as the structure of pseudo-lathes in a matrix, lamellae structure, a structure of basketwaves and alpha colony structures were developed; they had influenced the

characteristic features of fracture and the tensile properties of the fabricated components. It was noted that to improve the ductility of the material, the alpha colony structures formed needed to be controlled. The inter-pass temperature along the layer determined the coupling effect of the predominant surface oxidation layer and the minimal influence of the metallurgical evolution on the anisotropy of tensile properties at various locations of the walls of the coating. This study serves as a reliable reference for processing control and optimization of Ti-6Al-4V components fabricated by Wire Arc AM process in terms of the findings provided regarding the thermal accumulation and effects on the specified properties investigated.

Zhang et al. [77] developed a Cellular Automation (CA) model for two-dimensional simulation and prediction of the microstructure in terms of the transformation phase in solid-state and the rate of solidification processes based on thermal cycles of multiple spatial variable. The model developed considered the transient heat histories and thermal distribution in the fabrication process of producing Ti-6Al-4V alloy specimens by employing the Selective Laser Melting (SLM) technique. The incentive was to address the challenge of manipulating the microstructure and properties to what is desirable by predicting the metallurgical evolution of the SLM specimens. The various heat cycles attribute to the complexity of thermal histories which was the primary challenge for the incentive. The simulated results of the Cellular Automation model in terms of the beta grain and martensitic morphology were verified by empirical results based on single-and multi-track, cuboid and thin-walled specimens. The Cellular Automation model developed proved to be a feasible model in predicting the microstructural evolution during the

fabrication process of Ti-6Al-4V alloy specimens through Selective Laser Melting, under the multiple induced heat cycles. During the simulation of the Selective Laser Melting process of Ti-6Al-4V alloy four stages were observed namely; the stage when the powder melted, a stage where there was mush created, a stage where there was a multi-phase and a final stage of phase transformation in solid-state. Moreover, three zones were also observed namely; the region where the powder melted, a region that was re-melted and a region which was reheated. The heat flux direction and the spacing of the hatch between the overlapped adjacent tracks deposited induced by the heat cycles in the melt pool influenced the morphology and direction in which the prior beta grains grew. In addition, a size measurement of 100µm was recorded for the prior beta grain in the melt pool of the single-track.

Tian et al. [78] employed the Laser Polishing (LP) technique to modify the surface - particularly the surface roughness - of a Titanium Ti-6Al-4V alloy part which was fabricated by the Electron Beam Melting (EBM) Additive Manufacturing process. The incentive was to investigate the feasibility of using Laser Polishing to improve the quality of the surface of parts EBM additively manufactured. The study also addressed the possible effects of Laser Polishing on the fabricated parts in terms of the residual stresses induced and the metallurgy of the surface. The surface of parts additively manufactured which are rough and fatigue susceptible have the potential to be improved in-situ by the Laser Polishing technique that provides smooth and precise processing. The empirical results revealed that the surface roughness of the additively manufactured parts were reduced by more than 75% based on the millimeter scale and the microscale showed the

surface roughness achieved was Sa = 0.51µm, equivalent to the surface finishing produced by various surface machining processes such as CNC. Moreover, the defects promoted in the EMB parts of high concentrations of stress were eliminated by the Laser Polishing process, with no material being wasted. The additively manufactured substrate was subjected to 200µm deep Laser Polishing and the resulting surface layer had a variant grain structure and a texture that was different from the as-materials. The modified surface layer had a minimal increase in hardness in attribution to the epitaxial columnar grain regrowth of which was promoted in the polished surface layer. In addition, the regrowth of the grains was in a different direction in contrast with the EMB material and originated from the substrate towards the re-melted zone. This phenomenon was contingent to the new re-direction of the solidified layer and the direction of laser scanning during the process. Microstructural analysis showed that the Heat Affected Zone (HAZ) created in the material had a depth of approximately 450µm, which comprised of a fully annealed beta region that was measured to be 300µm in surface depth and also a transition region which was minimally transformed. The modified surface layer of the additively manufactured part had improved and had a fine microstructure which - as previously stated – had a slight hardness increase at a surface depth of approximately 450µm, which was equivalent to the depth of the HAZ. The Laser Polishing processing parameters induced surface residual stresses of as high as 580MPa that had gradually decreased with increasing depth into the material. However, standard heat treatment may be applied to the Laser Polished parts to relieve the high induced surface residual stresses.

Wu et al. [79] fabricated Ti-6Al-4V specimens by using the Wire Arc AM (WAAM) process coupled with Gas Tungsten gas (GT) and an investigation was conducted that ascertained the relationships developed between the corrosion performance of the specimens immersed in 3.5% NaCl solution. The resulting effects of the directional microstructural evolution and compositional phase in the Ti-6Al-4V specimens were also studied. The empirical tests conducted to ascertain the relationships include a corrosion test conducted electrochemically, diffraction patterns through XRD, micro-hardness testing and microstructural analysis through optical microscopy. The Ti-6Al-4V wrought specimens produced were used as reference in terms of their corrosion performance to judge the significant improvement or underperformance of the GT-WAAM specimens to their counterparts. The process was evaluated based on two orientations with reference to the substrate and it was found that during the additive manufacturing process, the resistance to thermal conductivity varied through the material considering the orientation. In the case of the direction of build which was vertical with reference to the substrate; it was found that the rate of solidification was slow in this directional plane which promoted the formation of lamellae alpha grains that were large in size and hard. The alpha grains were woven together by a Widmanstätten structure. Whereas in the scanning horizontal direction, the rate of solidification measured in that plane was found to be relatively fast and promoted the formation of primary alpha grains which were soft and much smaller. The empirical results revealed that due to the anisotropy found in the additively manufactured specimens - in terms of the microstructural evolution, the sizes of the different grains, the structure of the phases formed and the orientation - they were more prone to corrosion in the scanning direction than in the build direction. It was observed

that in both the scanning and build directions, the thickness of the passive film was low in comparison to its standard wrought counterparts. This was in attribution of the lamellae alpha and needle-like primary alpha phases which formed as non-symmetrical structures. Moreover, this was consequent of the low corrosion resistance and high rates of corrosion exhibited in the as-fabricated specimens. This study proved that there are still improvements which need to be implemented in the Wire Arc AM process for the application of Ti-6Al-4V parts in the fields of high corrosion. The life service of the material will be short in application and the focus needs to be in addressing the anisotropy of the resulting microstructure.

Dhanda et al. [80] employed the laser cladding process and created in-situ coatings of desirable strength and low coefficient of friction and subjected the Ti-6Al-4V components to sliding wear. The investigation was conducted by firstly placing the reinforcement powders - Ti, B_4C and Hbn-mixture on the Ti-6Al-4V substrates, followed by irradiating laser onto the surface to create the coatings and surface engineer the substrate. Various laser beam scanning speeds were used in the process. Scattering of the reinforcement powders were observed in-situ deposition of the coats and this was due to reactions of in-situ Self-propagating High-temperature Synthesis (SHS) in the process of irradiating the surface with the laser. It was suggested that thin laser coats were more environmentally friendly than the deposition of bulk coatings. Observations showed that placing 100µm layer thick reinforcement powder had the potential to only produce a laser coating thickness of 60µm. These SHS reactions had occurred when the powder layer was increased to 400µm. Within the matrix of the coatings, compounds such as TiB, TiB_2,

TiO_2, TiN and TiC formed due to the interaction of the laser with the reinforcement powders and the substrate. Micro-hardness analysis showed that the average hardness of the Ti-6Al-4V substrate was approximately 345HV and the improved hardness was 2200HV which was found within the coating at a laser scan speed of 2500m/min. The sliding wear performance of the coatings was tested against a Tungsten Carbide (WC) ball applied at 10N and the results showed that the coating of 2200HV hardness had less wear and satisfactory coefficient of friction measured to be 0.1-0.16**.**

Riedlbauer et al. [81] investigated the Selective Electron Beam Melting (SEBM) of processed Ti-6Al-4V by applying experimental measurement and macroscopic simulation of the melt pool characteristics. FEM simulations and experimental measurements were done to measure the various scanning speeds laser beam powers and line energies to analyze the depth, width and lifetime of the molten pools of the powdered material. FEM was used to simulate the melt pool width and lifetime of the process and the results were compared to the experimental measurements. The Temperature distribution in SEBM process was simulated with a thermal finite element simulation tool that was developed by the researches. The experimental measurements were conducted by building thin walled structures using an ARCAM AB A2 SEBM machine. All the processing parameter combinations investigated coincided well with the numerical and experimental results achieved for the lifetime of the pools of molten. The relationship observed was that as the line energies were high, the lifetimes increased linearly, and remained constant for constant line energy at higher scanning speeds. The wall built by the SEBM process had a defining thickness used to approximate the molten pool width. There was a good

correlation observed between the simulated molten pool width and the wall thickness, as the results revealed that they were near constant over the wall height. The increase in line energies reduces its influence on the molten pool width, as confirmed by the simulations results. Only for various process parameter combinations was the molten pool depth determined by simulations; with constant line energy resulting in near constant melt pool depth. Higher line energies increased the molten pool depth. The temperature history within the material is prevailed by the process, which influences the mechanical properties of the part fabricated. The researchers intend on using the simulation tool developed to conduct further investigations on this matter by simulating the different scan paths of the SEBM process. It was stated that less defective parts are to be produced when there are more homogeneous temperature distributions, so different scanning paths are to be compared for spatial homogeneity. The various processing parameters used interact critically to determine the dimensional accuracy and quality of the parts fabricated by the process.

Vajpai et al. [82] investigated the possible improvement of the performance of Ti-6Al-4V alloy components that are in service. To strengthen the alloy, a unique microstructural design was proposed, called “harmonic structure”, where the microstructure design is heterogenous containing grain areas that were fine and coarse and topologically distributed. Improving the properties of Ti-6Al-4V was of interest because the alloy possesses a desirable combination chemical and mechanical properties, that are utilized in the aerospace and biomedical industries. Its material is structurally advanced owing to its wide range of applications. Mechanical milling was used controllably to create the

harmonic structure of the Ti-6Al-4V alloy by using the process of powder metallurgy in which the (Ti-6Al-4V) pre-alloyed powder was severely plastically deformed and consolidated by plasma sintering. Consequential to the mechanical milling process, the distribution of the grain size was bimodal with the area close to the surface of the particle containing a “shell” region of nanocrystalline structures that was roughly deformed and the region of the core being encompassed with coarse-grained structures. When the milled powder was plasma sintered, it formed the harmonic structure. The Ti-6Al-4V harmonically structured design possessed strength and ductility properties that were significantly enhanced, exhibiting greater toughness and improvement than the traditional Ti-6Al-4V microstructure grains. The resulting harmonic structure design of the Ti-6Al-4V alloy improved the mechanical properties, allowing for stable local plastic deformation by the uniform distribution of strain during the initial deformation stages.

Chastand et al. [83] investigated the fatigue performance of Titanium Ti-6Al-4V samples fabricated by Selective Laser Melting (SLM). Several fatigue tests were performed - inclusive of both High Cycle Fatigue (HCF) and Low Cycle Fatigue (LCF) tests – to conduct the fatigue performance evaluate of the Ti-6Al-4V alloy. Three process parameters were considered in comparison with each other; the orientation of the built, post-machining and Hot Isostatic Press (Heat Treatment). An analysis was conducted on the three processing parameters that effected the fatigue properties and fractured parts. An analysis of the fractured surfaces was conducted to identify the parameters of defects that are critical. The tests of the two-loading domain (HCF and LCF) displayed the effects of the heat treatment (HIP) and the surface roughness. The fatigue life was improved,

and the size and number of defects were reduced by HIP. The heat treatment (HIP) process attributed to the formation of a varied microstructure, and the improvement of the ductility. There was a high number of surface defects on the as-built parts with a high surface roughness. This critically effects the fatigue performance. The two different manufacturing directions dispersed lower than the one batch that was dispersed, therefore resulting in no great variation between the two manufactured directions. The fatigue properties of the regional parts that were un-melted were considered to not have great anisotropy. The results of the LCF tests confirmed ductility anisotropy in which the microstructural texture of anisotropy was used to explain the phenomenon. The fatigue lifetimes were evaluated and an identification and classification of the least to most critical types of defects were done. The fatigue graphs were used to compare and classify all the different defects that were observed on the fractured surfaces. Other parameters of importance of the defects were identified, such as the size, positioning and concentration. The areas of the surface that had a cluster of defects or the largest defects had a zone near the surface with most initiation fracture defects located. There were various types of defects that initiate fracture on parts fabricated by SLM, which made it complicated in predicting the fatigue lifetimes. The properties of the fabricated specimens improved when heat treated (HIP) and polished. Developments are still in process to accurately locate the positions and size of defects through controlled methods and remedying their presence. Moreover, the methods developed enables ease in predicting the fatigue life. The Titanium Ti-6Al-4V specimens fabricated by SLM and are stress relived possess fatigue properties that are in correlation with the fatigue properties of casting, and in correlation with wrought processing when heat treated (HIP). The fatigue life of the SLM

fabricated parts was accurately predicted when the location and size of the defects are determined. The direction of manufacturing also has an effect and is equally important to study.

Leicht and Wemberg [84] studied and compared the mechanical behaviour of two additively manufacturing process techniques; Selective Laser Melting (SLM) and Electron Beam Melting (EBM) of Ti-6Al-4V fabricated powder, using Digital Image Correlation (DIC). Two different layering orientations were done on the fabricated Ti-6Al-4V powder samples; the tensile direction was parallel (X) to the single set of built samples and perpendicular (Z) to the other set of samples. Exactly half of the SLM samples fabricated were heat-treated. The strains that were localized were ascertained by subjecting the samples to tensile quasi-static loading tests complemented with Digital Image Correlation. The mechanical properties such as the yield of strength, Young's moduli, fracture elongation and ultimate tensile strength was determined for all tensile tests conducted. The microhardness values were obtained by performing Vickers hardness tests on the metallurgical prepared surfaces. All the samples were observed under an Optical Microscope (OM) to perform microstructural analysis. It was observed that all the samples produced by the two additive manufactured techniques, showed several layering of prior β grains that grew in the direction parallel to the build direction. This was caused by the layers being repetitively melted. Because the prior β grains are aligned parallel to the build direction, all the manufactured samples had unequal mechanical properties along the different axes. There was a potential connection to the regions containing the prior β grains by the local strains that were perpendicularly elongated to the direction of tensile

for all the SLM and EBM samples built parallel to the tensile direction. This observation was achieved by conducting an analysis using DIC. Whereas, the EBM and SLM samples built perpendicular to the direction of the tensile showed localized strains that elongated in the direction of tensile. Moreover, DIC analysis showed that the strain concentrations are found at the regions where there are grains, and anisotropic result in the mechanical behaviour was not caused by the layers built. The SLM samples built perpendicular to the tensile direction showed homogeneous strain fields. It was reasonably assumed that critical failure may be initiated at the areas where there are high strains. It was stated that further studies of the results be conducted to determine whether there should be necessary precautions taken regarding the manufactured components build direction. This study deduced that manufacturing with different processes results in the achievement of anisotropic mechanical properties. A higher hardness, ultimate tensile strength and yield strength was achieved for SLM manufactured samples. It is the α'-phase and microstructure of the material that was responsible for resulting mechanical properties. The ultimate tensile strength and the yield strength of the SLM samples heat treated reduced, but the microhardness remained constant. As much as there are differences in the mechanical properties of the two processing techniques, the difference was minimal. The comparison was made between the resulting mechanical data and the data achieved using DIC. It was concluded that high quality components may be produced using both processing techniques because very few defects were observed, indicating that the processes were in good control. Neither one or the other of the EBM and SLM was chosen to the best manufacturing technique because the profits and mechanical properties desired of the components were well balanced.

There are still current challenges being faced with additive manufacturing technologies. One of the limitations is to improve the efficiency of the entire process, but this consequentially increases the rate of mass deposited and reduces the time for post-processing. According to Turichin et al. [85], optimizing the distribution of the laser power beam attributes to the molten pool shape and size to the modified, which improves the rate of deposition. The requirements of the surface roughness promoted macroscopic waviness, which influence the post-processing cost and time. A possible solution to this problem was to use beam oscillation. The study conducted was on the fabrication of Ti-6Al-4V by Laser Method Deposition (LMD) with continuous beam oscillation. A simulation was carried out in which the molten pool shape and size were analyzed based on the effects of the processing parameters. A function method developed by Green was used to analytically solve the problem of heat conduction. The moving heat source that were normally distributed generated temperature fields, which were also investigated. The results showed that there was a rapid 53% reduction of the heat flux of the heat source that was distributed normally, when the amplitude of the oscillation was increased to the radius of the laser beam. The oscillation amplitude allowed was low and had minimal influence on the peak molten pool width value, when the beam radius was large. The wall surface was smooth, with no present macroscopic waviness, which was promoted by using beam oscillation and observed when a microscopic analysis was conducted.

Mulay et al. [86] studied the microstructure and mechanical properties of additively manufactured titanium alloy Ti-6Al-4V by Direct Metal Laser Melting (DMLM) technique,

compared to the properties of Mill-annealed Ti-6Al-4V alloys processed conventionally. The resulting metallurgical and mechanical properties of Ti-6Al-4V produced by DMLM are usually significantly anisotropic. The resulting anisotropy of the microstructure was analyzed based on the direction of the build. The results obtained revealed that the samples additively manufactured had a microstructure that consisted of mainly homogenous needle-like distributed structures, which produced less anisotropy in the mechanical properties, with respect to the direction of build. Other engineering materials such as aluminium alloys and stainless steels that are direct metal laser melted have rather contrasting resulting properties than compared to that of titanium alloy Ti-6Al-4V. The alloys mill-annealed showed high anisotropic microstructure and mechanical properties; it was observed that the grain morphologies were anisotropic and had a dense texture and the yield strength and hardness showed high anisotropy, with respect to the test direction. It was found that the testing direction had no significant influence on the resulting yield and hardening response of the DMLM produced materials, with respect to the direction of build, whereas the properties of the mill-annealed materials produced depended on the test direction. The materials produced by DMLM had a much higher stress saturated concentration than the mill-annealed samples because of the higher rate of initial hardening, but the yield strength initially obtained were in close correlation with one another (DMLM and mill-annealed) and may be compared. The modelling results of polycrystal plasticity of the mill-annealed materials revealed that the dense texture and grain morphologies confirmed the anisotropy behaviour of the microstructure and mechanical properties. The anisotropic results of the yield strength and rate of hardening

obtained in both the IP and TT mill-annealed samples was highly influenced by the strong texture than the grain morphologies, which was confirmed by the modelling results.

Waghmare et al. [87] conducted a study in which the cladding method of Tungsten Inert Gas (TIG) process was used to deposit a thick coating of composite Ni_xTi_Y, i.e. NiTi and $NiTi_2$, including a $TiAl_3$ composition that was sort of intermetallic and Titanium that was unreacted, on titanium alloy Ti-6Al-4V substrate. The composite powder was mixed with Nickel (Ni) and Titanium (Ti), in which the ball-milling route was used to prepare the mixture. The TIG current that was employed in the process was used to control the heat input, which governed the resulting microstructure of the NiTi composite coating that was produced. This was based on the analysis that was conducted on the microstructure. The results of the hardness obtained from the Vickers micro-indenter revealed that there was an improvement as the hardness measured for the cladded NiTi layer was approximately 680 ± 60 $HV_{0.05}$ and the hardness of the Ti-6Al-4V substrate was measured to be 320 $HV_{0.05}$. This improvement was attributed to the NiTi, hard $NiTi_2$ and intermetallic phases that formed, this was confirmed by the analysis done on the cladded layer by employing EDS and XRD. The grain form and structure as well as the mechanical properties of the cladded layer were significantly affected by the current processed by TIG. The low current of 40A and 50A employed and the coating and substrate being limitedly mixed, resulted in the cladded layer having a significantly higher hardness than the substrate, but the hardness suddenly reduced to the value of the substrate after the cladded layer. The hardness of the coating was significantly low and had slowly diminished in the direction of the interface; the coalesced coating and substrate, due to the high current that was

used to compensate for the substrate layer which was diluted. The behaviour of the coating wear resistance (abrasive) was improved by 9.5 when worked against the abrasive disc, when compared to the wear resistance of the uncoated titanium substrate that was measured by the loss of height. The enhanced process current that was used resulted in the value of the wear being increased. The characteristics of the wear and the hardness of the deposited coating was heavily affected by processing current, which the grain morphologies and concentration of phase composition formed were predominant in the result of the wear and hardness properties. Industries of biomedical and mechanical components may implement the application of composite NiTi coating since there was an improvement on the hardness and wear characteristics, which is usually of major concern in industry applications.

Ali et al. [88] employed the laser power surface cladding process, by using coating composite of Tungsten Carbide (WC) with an alloy powder that was Nickel based (NiCrBSi), cladded onto a Titanium alloy (α/β) substrate. The ratio of the composite metal layer coating used to metallurgically bond with the substrate consisted of 60% Tungsten Carbide and 40% NiCrBSi. This was performed by using an Nd:YAG laser that produced a perpetual wave of 2.2 kW, which consisted of a concentric system of a jet-nozzle and powder feed. The different layers resulting from the process, consisted of three microstructural zones: the coating, coalesced surface and the substrate. From the observations conducted, it was revealed that the NiCrBSi alloy matrix consisted of a uniform distribution of hard Tungsten Carbide particles embedded in the cladded area. Whereas, at the zone of the interface, had little Tungsten Carbide material resulting in structures that were more epitaxial and arborescent. The intent was to improve the

abrasion wear resistance of the titanium alloy substrate by achieving a uniform distribution of crack and defect free hard WC particles. The cladding process parameters were optimized to obtain desirable mechanical properties and the desired porous and crack free, WC distribution. The final samples fabricated were microstructurally examined, and hardness and wear tested. The X-ray Diffraction (XRD) system was used to identify all the phases formed. The interface had the composite coating powder partially melted around it, due to the high temperature input that was produced, but most of the particles were retained. At the lowest heat input of 18 J•mm^{-2}, the clad layer shallowest had a thickness of 195 µm, and the highest heat input of 60 J•mm^{-2}, produced the deepest clad layer thickness of 1083 µm. The substrate consisted of beta and alpha Titanium phases, but the metallic matric clad consisted of beta-WC, W_2C, Ti, TiC, and Ni matrix phases. There was no formation of TiC phase on the microstructure when observed, between the 18-30 J•mm^{-2} heat input, and the highest heat input attributed to the Tungsten Carbide particles being dissociated but only partially, of consequence to the high specific heat input that initiated a chemical reaction at the interface. A relationship between the laser coating and the incident heat input was found to be in direct proportion. The relationship between the hardness of the coated composite layers on the substrate and the increased dilution ratio was also found to be in direct proportion. The wear resistance of the coated layers was found to be improved by 400 times, when compared to the wear resistance of the uncoated Ti-6Al-4V substrate. This was confirmed by the wear 'pin-on-disk' test that was conducted. One of the main objectives was to produce a composite coating layer in which the WC particles are uniformly distributed with no pores nor cracks, this was achieved at the optimum process

heat input of 59.5 J•mm^{-2}. Its abrasive wear resistance was adequately improved, and the hardness was found to be 1200 HV. Studies reveal that due to the poor tribological properties of Ti-6Al-4V Titanium alloys, it is limited in its application and this study conducted by (Ali, et al. 2017) achieved good improvement on the wear characteristics.

Neikter et al. [89] investigated, characterized and compared the different microstructures and hardness of produced by five additive manufactured techniques on the substrate of Ti-6Al-4V Titanium alloy. The five various techniques used was: Shape Metal Deposition (SMD), Laser Metal Powder Deposition (LMpD), Laser Metal Wire Deposition (LMwD) and the Selective Laser Melting (SLM) technique. The characterization of a few metallurgical features were namely: the grain size of the prior beta (β), thickness of the alpha (α) lath, the size of the alpha colony and alpha grain boundary (GB—α). It was discovered that the SMD technique resulted in minimal variation in the size of that α lath on the Ti-6Al-4V substrate microstructure, and greater variation in the size of the α lath was produced by the LmwD-0 technique. The powder Bed Fusion (PBF) resulted in small grain size of prior beta in the manufactured samples. The SMD process produced the biggest prior beta grain size. The direct energy deposited Ti-6Al-4V materials promoted parallel bands to form, and PBF didn't not promote any parallel bands. The highest material hardness was produced by the SMD and LMpD processes. It was discovered that depositing the layers with LMwD at two-minute intervals, produced a fine microstructure to form than to deposit the layers continuously. It was found that as the cooling rate of the additively manufactured materials was decreased, the α phase formed in the grain boundaries of

the prior beta, increased. This was prominent in the materials that were built continuously using LMwD. There was no pronounced formation of any GB-α produced by using the LMpD process. It was observed that a finer and intertwined fabricated material microstructure was achieved by employing the SLM process and a few prior beta grains that were promoted, in contrast with the EBM method. Many alpha grains were formed with the LMwD-0 process than any of the other DED methods that employed a wire, then the LMwD-2 and SMD methods. The EMB process had more alpha grains that formed than SLM, and the two PBF methods used promoted more alpha grains than the LMpD process. The conclusion made was that as much as the build may be the same, there will still be great variations in the metallurgy and hardness of the materials additively manufactured at constant process parameters.

Muhammad et al. [90] carried out an investigation where the creep behaviour of Ti-6Al-4V alloy was additively manufactured by Laser Powder Bed Fusion (LPBF), at atmospheric conditions. The process parameters such as the size and direction of the scan were varied. The testing technique used was depth-sensing indentation, which focused primarily on the mechanisms that were dislocated. The testing technique used was instrumented and is commercially known for being a well suited and trustworthy method to perform characterizations, non-destructively. Hence, it was used to ascertain the plastic deformation – at a rate dependent – and mechanical properties at a smaller scale. This technique achieves this well at ambient conditions and at higher temperatures for metallic and alloy materials. A two-stage method (load and unload) was used to perform the indenting creep tests at 250mN, 350mN and 450mN varying loads at 400

seconds load-holding time. The method devised by Oliver/Pharr was used in the study to analyze the parameters used in the creep tests such as the exponent of the creep stress, the effect of the size of the indent and the rate at which the creep was conducted. The analysis was done at varying A.M scan size and direction. A metallurgical analysis was conducted where O.M and S.E.M were employed quantitatively to ascertain the correlation achieved of the property of the creep tests, the considered parameters and the microstructural evolution in the Ti-6Al-4V material. The results quantified revealed that the Ti-6Al-4V substrate at ambient conditions are still subject to creep influence. The varying peak loads and holding time was dependent on creep process parameters. The creep was primarily dominated by the motion of dislocation of the laser powder bed fused titanium alloy material at ambient conditions. This was affirmed from the values obtained from the exponent of the creep stress. Direct comparison to conventional wrought Ti-6Al-4V was made. The stress and depth relationship were graphically represented and from it “geometric necessary dislocations” was discovered, which were result of the effect the size of the indentation had on the alloy. The creep rate was found to be higher for samples that were scanned vertically and lower for samples scanned horizontally.

Buciumeanu et al. [91] conducted a study whereby an investigation and characterization of the performance of tribo-corrosion of Titanium alloy Ti-6Al-4V, which was fabricated by various manufacturing and processing procedures. An Open Circuit Potential (OCP) was used to analyze the different alloy samples produced by employing the methods of Cast, Hot Press (HP) and Laser Engineer Net Shaping (LENS). The OCP analysis constituted

of contact testing of reciprocated sliding alumina. It was quantified that the resulting tribo-corrosion performance of the titanium alloy specimens produced was dominated by the manufacturing/processing methods employed. The results obtained revealed that the wear characteristics and corrosion properties of the alloy specimens fabricated by Casting or Hot Pressing, were poorer compared to the LENS Ti-6Al-4V samples produced. The LENS process caused local cooling rates that were ultimately high and resulted in the hardness being higher with minimal variation in the chemistry in the titanium alloy specimens produced. This did not only affect the hardness, but also the strengthening of the powder, which all together influenced the final corrosion properties of the part. The microstructural study conducted revealed that employing different manufacturing methods resulted in varied microstructures. The Hot-Pressing samples produced, had a lamellar structure that consisted of phases of α+β material, whereas a columnar structure was observed for samples produced by LENS that consisted of interlayers of Widmanstätten material. The one factor that was not dependent on the manufacturing/processing methods was the Coefficient of Friction (COF), which never varied for all Titanium alloy samples that were investigated. The corrosion property of the Ti-6Al-4V specimens produced by all methods varied when there was no application of mechanical load. The unreactive layer on the Casting and Hot-Pressed produced specimens were eradicated when application of a mechanical load was introduced, but that of Tanium alloy samples produced by LENS were only partially removed.

Promoppatum et al. [92] studied the mechanical and thermal properties as well as the material development of Titanium alloy Ti-6Al-4V components produced by the process

of Direct Metal Laser Sintering (DMLS). Moreover, these properties were ascertained by the development of numerical modelling and experimental tests. The progressive development of the thermal property during the DMLS process was predicted by employing finite element modelling of the Ti-6Al-4V specimens. The DMLS process parameters that were measured were the thickness of the coating of 30 μm, the laser power at a maximum of 400 W, a scanning velocity at a maximum of 7 m/s and 100μm diameter laser beam. The modelling and experimental results were in good correlation with each other. Certain defects were generated from the manufacturing process such as un-melted regions in the products, insufficient fusion and the balling effect. These defects were quantified by the results obtained from numerical modelling. The relationship and influence of the process parameters were ascertained by the process window established analytically, numerically and physically. The formation of the melt pool and the resulting mechanical properties are characteristics of the specimens that were primarily dominated and defined by the density parameter of the energy deposited in the process, and the lowest laser scan speed was quantified when the time for the heat to transfer through the material was measured. It was deduced that to achieve complete melting, the density of energy deposited should at minimum be equivalent to the thickness of the powder coating. Moreover, a high amount of energy density needs to be supplied. Reducing the melt pools ratio of length-to-width to less than π, prevents the balling effect. Spheroidization may be promoted in the melt pool when there was excess laser power and scan speed. It's more feasible to establish a processing window by primarily using Numerical analysis, with comprehension of the analytical and theoretical criteria. It was time efficient in constructing the guideline when this procedure was used, because only

a few test samples was required. In addition, introducing new parameters will allow for easy construction of the guideline. Specimens produced with densities of energy deposition in regions of complete fusion and melting may result in the roughness of the surface and hardness being uniform. This was expected from the exact complete fused scanned path. Varying the scan speed and laser power may always promote the generation of columnar grains with the other traditional process parameters being at a conventional range. The columnar structures are compact and are small in width attributing to the dominance of the diameter of the laser and space of the hatching on the grain size of the columnar structures. Given that the layers deposited are all scanned in one direction.

Pratap and Patra [93] conducted a study in which the performance of the wettability as well as the bio-tribological properties were focused on for improvement in Titanium alloy Ti-6Al-4V, by employing a surface modification technique (mechanical micro-texturing). The surfaces were micro-textured by three different tools including milling with a micro flat-end and ball-end, and micro drilling. These three micro surface modification methods were used to produce dimpled structures on the surface. Moreover, the circular indentations all had a diameter of 200 μm. The Coefficient of Friction (COF), roughness of the surface, hardness, and wettability of the surface were ascertained attributed to the effects of the different geometrical micro-surface machining. The prosthetic hip-joint was used to quantify the COF with regards to in-vitro condition and the contact angle was regarded to quantify the surface wettability. The micro-tool selected and resulting penetrating depth determined the dimensions of the dimple, which varied for each end

geometry. The surface of the Titanium alloy that was not textured (NTS) had a high affinity for water and the application of mechanical micro-surface texturing enhanced the phenomenon. The Surface conditions pre-textured, the surface and geometrical texture all combined are the roughness factor, which improved the wettability performance. The two textured surfaces that showed similar improvement in the performance of the wettability in comparison to the surfaces not textured (NTS) and Micro Flat-end Textured (MFETS) was the surfaces textured with the ball-end (MBETS) and micro-drilled (MDTS). There are only two surface micro-machining methods that were considered to meet desired biomedical implant requirements, which were the ball-end and drilling micro-textured surfaces. A wide region of contact was formed the width of the lubricated layer was squeezed, which increased the speed and loads of sliding. As a result, this increased the COF of all micro-textured surfaces. The ball-end geometry improved the hardness of the surface and wettability, in addition, the dimpled textures were able to enclose the remains generated from wear. These properties achieved by MBETS resulted in the COF being the lowest compared to the MFETS, MDTS and NTS. The surface hardness and good lubrication achieved by MBETS allowed for a much smoother surface patterning where there was wear, compared to MFETS, NTS and MDTS. These micro mechanical surface machining techniques are proved to be among the most suitable and reliable methods for fabricating titanium alloys and biomaterials in similarity.

Book and Sangid [94] employed Digital Image Correlation (DIC) at high resolution to investigate the strain localization in Ti-6Al-4V produced by Direct Metal Laser Sintering (DMLS) and thermally refined and the resulting impact of the variations in the

microstructure. The specimens were mill-annealed and stress relieved and experienced monotonic and cyclic loading. Before a material fails, it experiences strain locally. The DMLS process produced Widmanstätten microstructures in which the prior beta (β) was a critical phase in strain localization of the Titanium alloy microstructures produced by DMLS. The characterizing method carried out experimentally also revealed that for each prior beta phase boundary, enclosed its own micro-textured area, and constituting of major grain orientation axis and texture that was separate from the other phase boundaries. It was observed that several local strains occurred compactly attributing to slip being activated followed by slip being transmitted over the prior beta phases, because of the oriented regions micro-textured. In addition, the time for cracks to initiate may be reduced when the slip transmission is prevented at every prior beta boundary by retarding the strain. There are no boundaries (grain and phase) within the alpha (α) lathes, and since it has no barriers the strain developed inline of the alpha laths major axis. It was observed that there was major axis angle alignment of approximately 45˚ with respect to the directional load of the slip systems that were oriented in the huge alpha lathe phases. This resulted in strain being accumulated in the alpha lathes and defined it to be a shear strain highest in terms of macro scale. Based on the contention of slip system geometry over neighbouring grains, it was observed that the prior beta structures had an alignment of alpha lathes on either side, which facilitated the transmittance of slip over the regions that were micro-textured. Results showed that there was promotion of slip transmission across the micro-textured areas as the shear strain at macroscopic scale was increased. The results obtained from high resolution digital image correlation of the strain highly developed was confirmed by alpha lathe mapping of Schmid's' factor applied to prism

slips. There was widespread strain that was accumulated in alpha lathes on basal slipping structures for specimens that were loaded cyclically. Due to the interacting and compatible grains in the polycrystal structure, stress states occur in complex conditions in every grain and mapping used by Schmid's factor does not record this phenomenon, which in contrast was observed that the high factor map values had regions in which the strain accumulated was followed. It was shown that when size of the prior beta grains was reduced in the initial solidification process by elevating the rate of cooling and implementing a method of building in which the material that was already solidified will not be re-melted by reheating. In addition, in reducing the size of prior beta grains means that micro-textured areas may also be reduced to oppose slip possible amongst micro-textured areas. The results obtained and confirmed shows that the method used was reliable in improving the performance of Titanium alloy Ti-6Al-4V produced by the DMLS build process.

Vora et al. [95] studied the corrosion and wear performance of bio-implant alloy Ti6Al4V after it was laser surface nitrided. A continuous wave Ytterbium fiber laser system was used to process the samples in a nitrogen gas atmosphere. A potentiostat was used for electrochemical tests conducted in a stationary simulated body fluid. Corrosive wear was measured by means of a pin-on-disk tribometer. The results showed that the corrosion behavior of the laser surface nitrided samples were superior and the corrosive wear analysis showed a reduction in the wear rate. Thus, the authors deduced that laser surface nitriding of Ti6Al4V will improve its properties.

Guo et al. [96] analyzed the corrosion behavior, antibacterial action and cytotoxicity of Ti-6Al4V-xCu alloys fabricated by selected-laser-melting. The specimens were prepared by selective laser melting Ti-6Al-4V powder with 3 increasing amounts of copper powder and 1 without copper. To observe the microstructure and phases, an optical microscope, SEM and XRD were used. A standard potentiostat was used to conduct electrochemical tests. The results showed that the laser treatment of Ti-6Al-4V increased its corrosion resistance and it was also found that the increase in copper content reduced the corrosion rate. The alloys with a higher copper content exhibited excellent antibacterial properties and good cytocompatibility.

Zhao et al. [97] investigated the corrosion performance of a Ti6Al4V alloy scaffold that has been manufactured by selective laser melting and electron beam melting for implantation in vivo. The Ti6Al4V alloy samples were manufactured with electron beam melting (EBM) and selective laser melting (SLM) using similar procedures and conditions. SEM-EDS and XRD were used to analyze the surface investigation, metallic constituent distribution and phases present. Electrochemical tests were conducted in a 3.5% NaCl solution to observe the corrosion behavior of the samples. The SLM sample had the best corrosion resistance, however the EBM sample exhibited better resistance to crevice corrosion. The authors therefore conclude that both surface modification techniques improved the corrosion resistance and can be used in vivo.

Chikarakara et al [98] examined the surface alteration of Ti-6Al-4V by employing high speed laser surface treatment. A CO_2 laser was used to irradiate specimen at three

different irradiance levels and three different times. The effect of the change in process parameters on the surface was evaluated by optical microscopy, SEM, XRD and a Vickers hardness tester. The results showed that the smoothness of the laser melted layer increased with a rise in irradiance and residence time. The hardness was found to have increased by 67%. The authors there agree that laser surface modification of Ti-6Al- 4V improved its properties.

2.10. Summary

From the literature reviews, it can be concluded that surface modification of Ti-6Al4V alloy is a possible technique that can be used for improving its corrosion resistance, hardness, microstructure and wear resistance properties. Some authors agreed that the laser surface modification with additional elements can improve the surface properties while others agreed that laser surface melting with no additions can enhance the surface of Ti-6Al-4V alloy. The focal point of this work will be how Al-Si-Sn-Cu coatings will affect the surface properties of Ti-6Al-4V alloy.

This section of the report covered the description of additive manufacturing, the benefits of its application in industry and comprehensive review on titanium and its alloy using various additive manufacturing processes and techniques. Laser cladding of titanium and its alloy were studied to gain more understanding about their applications. Literature reviews related to this study were evaluated to help with the expectation of the research results. The next chapter of this report is the experimental design for this research study.

CHAPTER THREE: EXPERIMENTAL DESIGN

3.1. Introduction

This chapter presents the experimental design needed to conduct this investigation. The equipment, materials, procedures of the laser cladding and for characterization of the coatings are described.

3.2. Research Approaches

The surface characteristics of a material can be altered by employing surface modification in order to achieve the desired and required properties for specific applications. The surface of the alloy is the intended area for modification and not the bulk of it, therefore laser cladding of Ti-6Al-4V/Al-Si-Sn-Cu of different proportions were employed. The phases present and microstructure were observed with X-ray diffraction (XRD), optical microscopy (OPM) and scanning electron microscope (SEM). Wear techniques, and microhardness tester were used to evaluate the hardness and wear performance.

3.3. Materials and Preparation

3.3.1. Substrate cutting and cleaning

Ti6Al4V plates were sectioned by means of the Struers Mecatome T300 machine shown in Figure 3-1. Water was used as a coolant during the cutting of the alloy to avoid excessive heating and deformation of the substrate. The substrate used in the deposition operation was a solid titanium grade 5 Ti-6Al-4V which had a volumetric dimension of 100

x 100 x 5 mm^3. A cleaning preparation was conducted on the substrates whereby they were sandblasted to remove the surface impurities and to roughen the surface layer of the material to aid the metallurgical bond of the clad to the surface of the substrate. All the residue after sandblasting was washed off with acetone and then dried with air.

3.3.2. Powder preparation

Aluminium (99.9% purity), Silicon (99.9% purity), Tin (99.9% purity) and Copper (99.9% purity) powders were used for this study. The powders were mixed in different proportions with the Turbula Shaker Mixer as shown in Figure 3-2. The powders were mixed in dry conditions at room temperatures at a rotational speed of 72 rpm. Mixing was carried out for 16 hours for each powder composite.

The composition of the mixed powders was:

Al-10Si-10Sn-2Cu

Al-12Si-10Sn-5Cu

Al-15Si-10Sn-10Cu

3.3.3. Laser powder deposition

The Direct Laser Metal Deposition (DLMD) was conducted by employing the Ytterbium Laser-System with wavelength 1.06 μm operates at 3kW maximum power and incorporates a Kuka-robot for the operation of controlling the process of deposition. Figure 3-3 shows the laser system. Laser deposition was completed varying the scan speed while power was kept constant. The process parameters are shown in Table 3-1.

Table 3-1: Process parameters for laser deposition of Al-Si-Sn-Cu/Ti-6Al-4V Composite coatings

Laser power	900-1100 W
Laser scan speed	0.8 - 1.2 m/min
Laser beam diameter	2 mm
Powder flow rate	2.0-3.0 g/min
Shielding gas flow rate	Argon (2.0) L/min

3.3.4. Metallographic preparation

After laser deposition, the samples were prepared for metallographic analysis. The samples were cut to dimensions of 10 mm x 10 mm x 5 mm. They were the mounted using the mounting machine shown in Figure 3-4. They were mounted in way as to expose the cross-section of the samples. Grinding was the next step, SiC emery papers with roughness of 600 µm, 800 µm, 1000 µm and 1200 µm, using water as a lubricant. Polishing was done with Aka-Chemal cloth and 2 µm fumed silica solution was used as the lubricant. Grinding and polishing was completed with the machine shown in Figure 3-5.

3.3.5. Microhardness testing

The Vickers Micro-Hardness Tester was used to ascertain the hardness property of the samples by applying six indentations on the cross-section from the deposit, through the

HAZ until the substrate. A test force of 100gf was used with a dwell time of 15s as shown in Figure 3.6.

3.4. Experimental procedure

The Direct Laser Metal Deposition (DLMD) was conducted by employing the Ytterbium Laser-System which operates at 3kW maximum power and incorporates a Kuka-robot for the operation of controlling the process of deposition. The deposits were designed and manufactured at The “Council for Scientific and Industrial Research, National Laser Centre (CSIR NLC), Pretoria, RSA.” The laser head of the Kuka-robot irradiated the laser through the centre nozzle which created a molten pool on the substrate and the reinforcement powders were deposited into the melt through the concentric nozzle by using argon gas to accelerate the powders. The argon gas was also used to protect the deposition process from oxidation

3.5. Microstructural and Phase Characterization

3.5.1. Metallographic preparation

The deposits were subjected to metallurgical preparation, whereby they were cut transversely and prepared for material characterization process, according to the Struers standard guide (ASTM E3-11) for the metallographic preparation for specimens. Kroll’s reagent was used to etch the samples for 15s then the necessary material characterization tests were carried out that included observing the microstructural evolution using SEM and optical microscope.

3.5.2. Microstructural analysis

The microstructural features were analyzed by employing the optical microscope: BX51M Olympus. The deposited zone of the cross-section was the area of focus in accordance of ASTM F728-81 standard [100].

3.5.3. Phase analysis

ASTM E1426-14 standard [101] was used for analyzing the quaternary coatings phases via X-ray Diffraction (XRD)

3.5.4. Wear characterization

A wear test machine was used to assess the wear resistance of the modified surface in accordance of ASTM G99-17 standard under ambient conditions [102].

3.5.5. Numerical Modelling

The influence of these processes and reinforcement proportions will be determined on the mechanical and wear properties of the coatings. Numerical modelling using COMSOL multiphysics 5.3 was developed to reveal the thermal and mechanical behaviour in the coated samples.

3.6. Detailed experimental matrix

3.6.1. Substrate

Base metal considered in this research is titanium alloy grade 5. Exceptional properties of titanium alloy have extended its application in automobile, chemical processing industries, manufacturing, medical and aerospace. Table 3.2 shows the base metal chemical composition

Table 3-2: Base Metal Chemical Composition (Ti-6Al-4V Alloy)

Elements	Ti	Al	V	Fe	O	C	N
Wt.%	Bal.	6.2	3.9	0.2	0.01	0.12	0.005

3.6.2. Etchants

The solutions required for this study are sodium chloride solution, Kroll's reagent and acetone.

3.7. Experimental matrix

A set of nine laser cladded samples were produced in accordance with the design parameters in Table 3-3 and lists of variables in Table 3-4. The laser power was varied between 900 W and 1100 W while the gas flow rate was kept constant. The scanning velocity was varied between 0.8 and 1.2 m/min. The shielding used was argon and the laser beam was 2 mm.

Table 3-3: Experimental L9 Orthogonal matrix design

Sample no	**Laser Power (W)**	**Scan velocity (m/min)**	**Powder fed rate (g/min)**	**Gas flow rate (L/min)**
1	900	0.8	2.0	2.0
2	900	1.0	2.5	2.0
3	900	1.2	3.0	2.0
4	1000	0.8	2.5	2.0

5	1000	1.0	3.0	2.0
6	1000	1.2	2.0	2.0
7	1100	0.8	3.0	2.0
8	1100	1.0	2.0	2.0
9	1100	1.2	2.5	2.0

Table 3-4: List of variables and parameters

Variables	Parameters
Independent variables	• Powder flow rate
Dependent variables	• Dilution • Time • Track height • Track width • Powder efficiency • Metallurgy properties • Wear rate • Hardness
Constant variables	• Laser scanning speed • Track length • Shielding gas flow rate • Laser power • Laser spot size • Ambient temperature & pressure • Number of layers

3.8. Equipment

3.8.1. Struers cutting machine

Mecatome T300 machine was used in this research for the cutting of samples as shown in Figure 3-1. The machine was used to cut the samples to a required size. The machine is operated manually and can cut even long samples. Depending on the hardness of the metal to be cut, the cutoff wheel can be changed to different materials.

Figure 3-1: Struers Mecatome T300 cut-off machine

3.8.2. Tubular mixer

Turbulent mixer is used to mix powders as they differ in particle size and weight to utilize homogeneous as it rotates at a definite speed for hours as shown in Figure 3-2. It operates by tumbling solids inside a spinning vessel. The impressive efficiency of the tubular shaker-mixer originates from the use of rotation, translation and inversion as per the geometric theory according to Schatz.

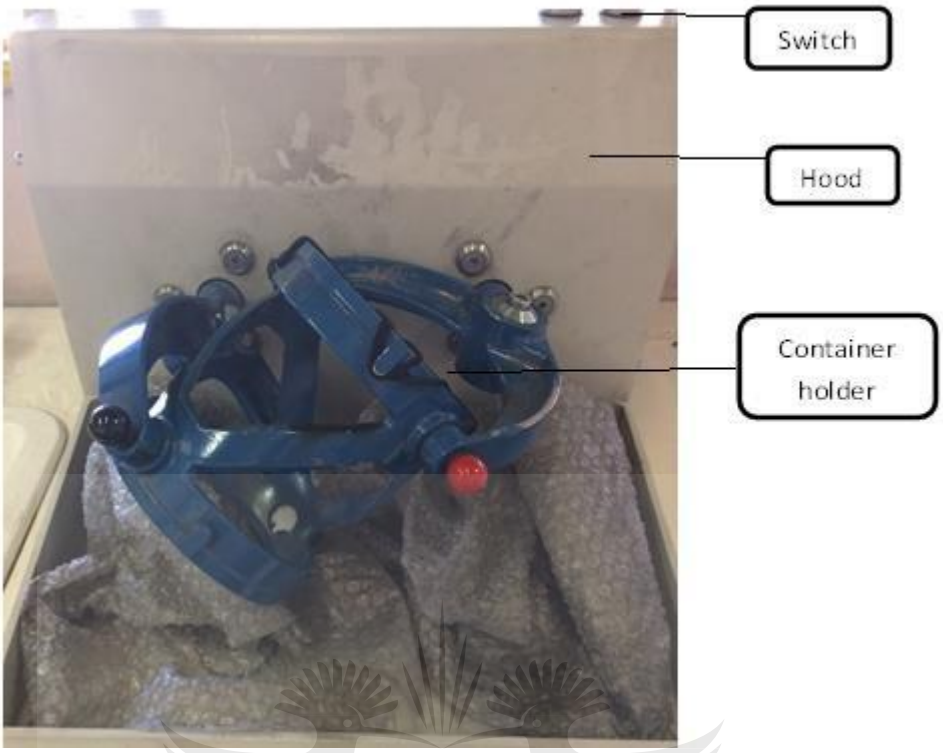

Figure 3-2: Turbulent Shaker-Mixer machine

3.8.3. Laser

A continuous wave 3.0 kW ytterbium laser system (YLS) was used for this experiment. The laser is pumped using laser diodes through the neodymium doped Yttrium Aluminium Garmet medium. The optical fibre directs the laser beam to the focusing lenses. Argon gas is used as a shield to prevent oxidation. Figure 3-3 shows the laser machine used with the powder feeding compartments.

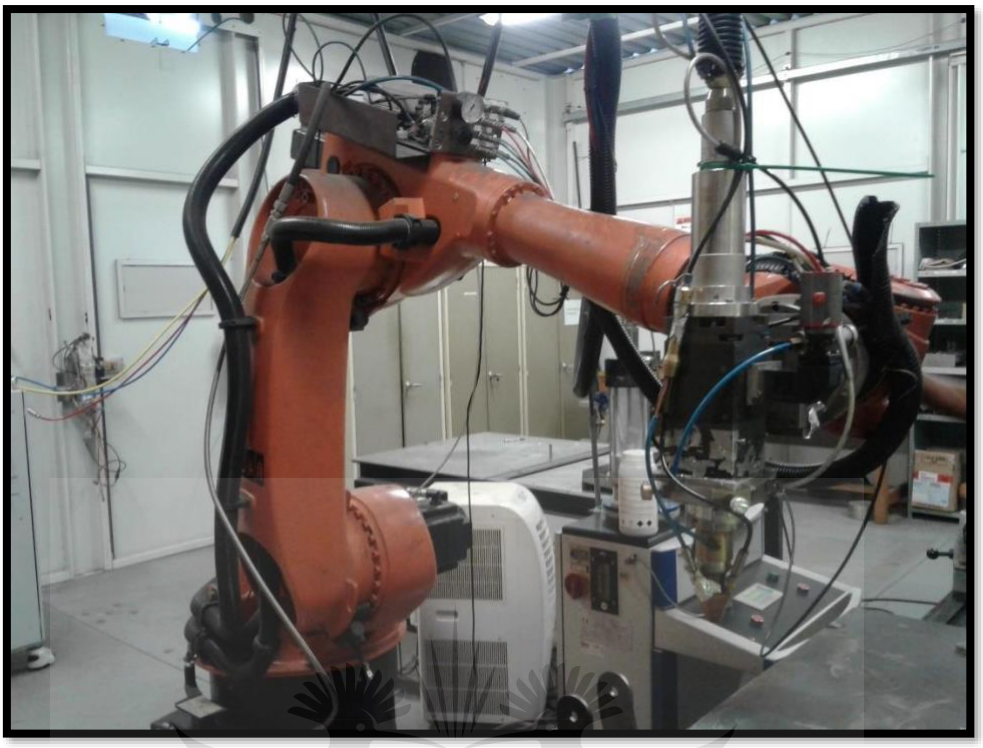

Figure 3-3: Ytterbium Laser System

3.8.4. Mounting Machine

Figure 3-4 depicts a Struers mounting press machine. It is used to embed samples in a resin for better handling by means of hot mounting. A thermosetting resin powder is used, and it is melted at high temperatures and pressures. This is ideal for materials that are not easily affected by heat and pressure changes, for such materials, cold mounting should be used.

Figure 3-4: Struers Mounting press machine

3.8.5. Grinding and Polishing Machine

Figure 3-5 shows a Struers grinder/polisher. The machine is equipped with a rotating wheel on which the emery paper or cloth is placed and a tap. For grinding, SiC emery papers are used with water as the lubricant. Grinding is done to achieve a smooth, plane surface. In order for the samples to have a mirror-like finish, they are polished with different clothes and suspensions depending on the metal. The grinding method was performed by using the Struers grinder/polisher in accordance of the ASTM E3-11 standard.

Figure 3-5: Struers Grinding and polishing machine

3.8.6. Hardness tester

Figure 3-6 shows a Vickers micro-hardness tester. It is used to obtain the hardness of a material by measuring the diameters of the diamond created by the indenter on the surface. A Vickers hardness tester was used to test the hardness of the materials. This equipment, shown in Figure 3-6, makes indentation on the sample surface and reads the hardness value based on the degree of penetration of that indent. The machine is also equipped with an optical lens which allows the user to choose the correct/desired focus area.

Figure 3-6: Vickers micro hardness tester

3.8.7. Optical microscope

Figure 3-7 shows an optical microscope. This type of microscope uses visible light and magnifying lens, light is directed vertically through the microscope objective and reflected back through the objective to an eyepiece or view screen. The light focuses directly on the sample and observed by eyes using eyepiece. The microstructure is captured by the displaying screen which is generated by the normal light-sensitive camera inside the optical microscope.

Figure 3-7: Optical microscope

3.8.8. Scanning electron microscope/Energy dispersive spectroscopy (SEM/EDS)

A field emission scanning electron microscopy used in this research is shown in Figure 3.8. Samples compositional characteristics and morphology are revealed through SEM. The specimen surface received the electron beam and therefore generate signals. The image is formed through the detector which acquired the signals generated and then handled into an image. Specimen elemental composition are revealed via energy dispersive spectrometer which is connected to the microscope. The electron gun contains field emission cathode where high and low electron energy narrow in terms of probing

beams are generated. Damaging and charging of samples are minimized and spatial resolution are enhanced through this channel.

Figure 3-8: Scanning Electron Microscope and Energy Dispersive spectroscopy

3.8.9. X-Ray diffraction (XRD)

Figure 3-9 shows the Ultima IV X-ray diffractometer. An X-ray technique is a resourceful, non-destructive technique that reveals detailed information about the chemical composition and crystallographic structure of natural and manufactured materials. These techniques are based on observing the scattered intensity of an X-ray beam on a sample as a function of incident and scattered angle, polarization, and wavelength or energy. The diffractometer is equipped with pre-aligned, fast and interchangeable modules which

make changing the optical path easy. Its characterization capabilities are appropriate in large part of the fundamental principle that each element has a distinctive atomic structure allowing unique set of peaks on its X-ray emission spectrum.

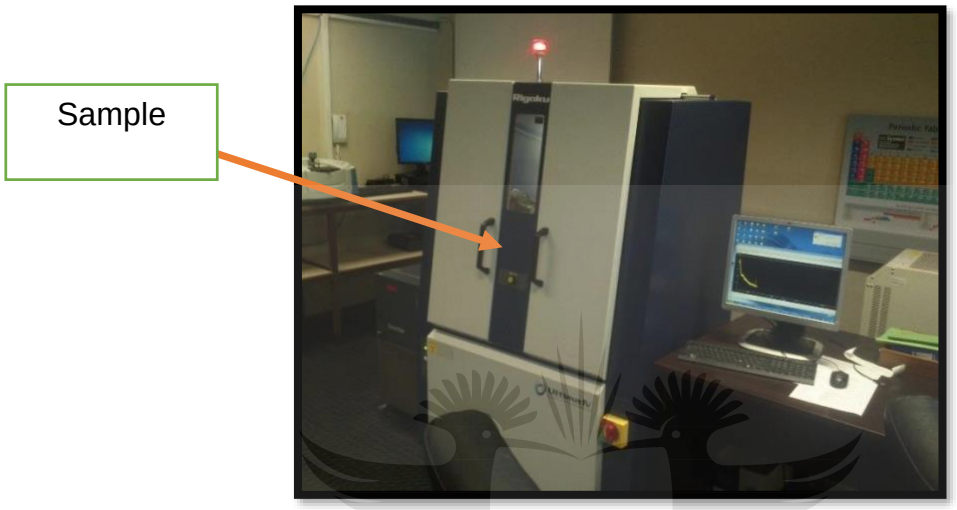

Figure 3.9: Ultima IV X-Ray Diffractometer

3.8.10. Wear tests

The wear test was carried out at 15N force. The quaternary samples were sectioned into 2 x 1 cm area and were fitted into samples holder inside the machine. The speed of sliding was set at 2 m/s in order for the samples to experience reciprocating motion from the pin disk. The coefficient of friction of each sample was recorded at 15N force. The time taken for each sample was 17 minutes to record the coefficient of friction. The base metal coefficient of friction was also determined in order to compare the wear performance of the quaternary coatings.

3.9. Summary

The tests were carried out according to the procedures defined in this section. The result can be found in the next section. The sample preparation conducted by the laser cladding process and the experimental testing procedures conducted were analyzed in this chapter. The microhardness, XRD, SEM-EDS, optical microscopy and wear resistance tests were conducted successfully according to the relative ASTM standards. Chapter 4 presents the results acquired.

CHAPTER FOUR: RESULTS AND DISCUSSION

4.1. Introduction

The aerospace industry is usually considered as the first industrial technologies and innovative materials systems industry, due to its advancement and piloting ways. The efficiency of aircraft performance is enhanced by material development. Weight savings, cost-effectiveness, improved thermal capabilities are what matters whilst developing new materials. Materials such as titanium alloy and aluminum alloys are considered for aerospace application because they are lightweight materials and can improve the efficiency of the aircraft energy use. Due to the fewer strengths in these alloys, they can provide the needed strength-to-weight by merging the two alloys, compared to low alloy steels. In this chapter, we shall be looking at the analyzed results that were obtained from the conducted experimental are work. The results include microstructure characterization, XRD, SEM-EDS, microhardness profiling, wear resistance and mechanical properties

4.2. Parent Material

Figure 4-1 shows the microstructure of the parent material (Ti-6AI-4V alloy) magnified at 100x. The underlying layer used in this research study was a Ti6Al4V plate. The alloy's attractive properties include excellent biocompatibility, high corrosion resistance, and high-temperature strength, which can be applied in the medical, aerospace, automobile and chemical processing industries. Figure 4.2 indicates the SEM/EDS of titanium alloy substrate. Several titanium alloys are engaged in engineering uses owing to their performance and higher strength [29, 31] which is contrary to their pure form. Ti-6AI-4V

alloy is sustainable in the aerospace industry and this is because of the alpha and beta stabilizers, used to supply the needed specific strength within the different high-temperature varieties. The beta grains are the black dots whereas the alpha grains are white dots as shown in Figure 4.1. A study done by Mahamood et al. [60] shown the microstructure of titanium characterized as beta and alpha grain structures. Enhanced mechanical properties are provided in the α-phase of the alloy and these properties are high hardness and wear resistance. Whereas improved relative strength against harsh environments is offered in the β-phase of the alloy.

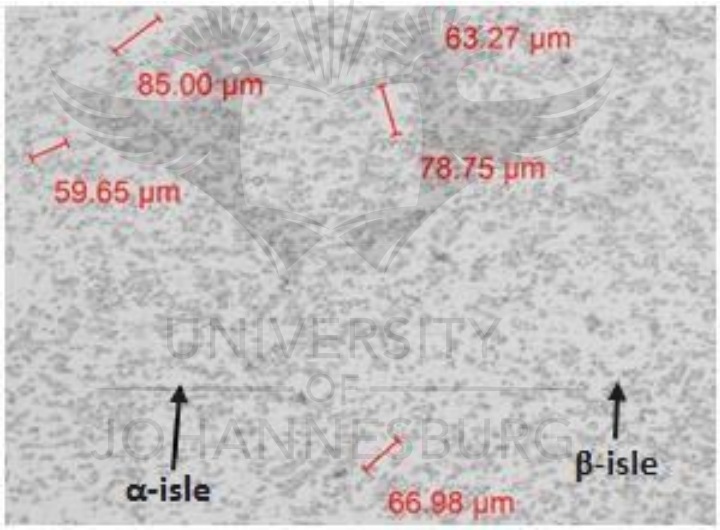

Figure 4.1: Substrate (Ti-6Al-4V) microstructure

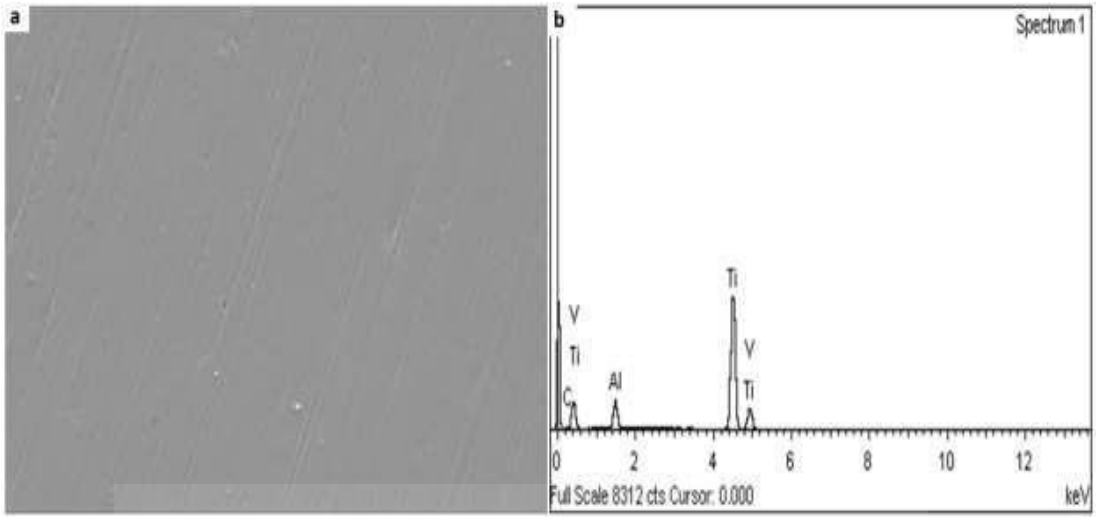

Figure 4.2: SEM/EDS of Substrate (Ti-6Al-4V)

4.3. Reinforcements Characterization

The powders mixed in dry conditions at a rotational speed of 72 rpm. For every composite powder, the mixing process takes 16 hours. The composition of the mixed powders consisted of 73-12-10-5 wt. percentage of Al-Si-Sn-Cu and 65-15-10-10 wt. percentage of Al-Si-Sn-Cu. In this experiment, a continuous wave of 3 KW ytterbium laser system (YLS) was used. The optical fiber is what directs the laser beam to the focusing lenses. To prevent oxidation, Argon gas of 2.0 L/min was used. The powders (Ai-Si-Sn-Cu) were fed into the feeder, and coaxially deposited on the substrate through a laser beam. The work-piece and the nozzle head's distance was 2 mm. Tracks overlapping was set at 70%. 900 W and 1000 W levels of laser power were employed. The optimized laser parameters used: a beam diameter of 2 mm, powder flow rate of 2.0 g/min, scan speeds of 16.7 mm/s and 20.0 mm/s.

4.4. Microstructures

A high power laser of 3000 W was used to clad the layer on the substrate which has a small spot diameter. Through a focusing lens at a certain speed, the beam is released onto the specimen. Molten metal oxidation was avoided by using an inert gas with the powder injection. The injected powders into the molten pool are of different quantities. For all the variable parameters of the experiment, AI powder weight percentage varied between 65 and 73 percent at different speeds. The variation of the Si powder composition when at different speeds was between 12 and 15 percent. At the same time, the Sn content remained consistent, with the Cu powder varying between 5 and 10 percent. To obtain an identical mixture with equally distributed particles and to avoid inadequate melting of quality coatings with high pores, because of the reinforcement the Sn content remained consistent, with the Cu powder varying between 5 and 10 powder particles that are poorly molten. The particles cannot conform to the surface due percent. To obtain an identical mixture with equally distributed particles and to avoid to their inability to form splats when the coatings are formed. Therefore, the solidification contagion, the Tubular Type T2C was used. When the laser power is low it causes an of the splats lead to the formation of pores and cracks. Additionally, several un-melted and incompletely melted particles can be found in the deposited coatings with low laser power. The increased speed of the reinforcement particles that displays a proper flow of molten liquid is brought about by the increase in distribution, and spheroidization [6, 15, 103]. The level of pores that would be found in the coatings is triggered by the rate of deposition. As featured on Figures 4.3, 4.4 and 4.5 laser power; also noting that an increased laser power causes improvement, standardized

coatings fabricated at 900 W showed a microscopic level of apertures when compared to coatings fabricated at 1000 W. The reason for the high level of pores at a higher powder feed rate, is because of the partially melted reinforcement powder deposited at the nozzle tip of the beam. The insufficiency of initial laser power to melt reinforcement powder at a higher powder feed rate within a limited slot of time is what produces partially melted powder in the molten pool, which in turn creates a high level of pores formed in the coating as shown in Figure 4.7. Owing to the increased powder feed rate, the constructed coatings with uniform microstructure, caused by the synergy between the laser beam and the reinforcement powders, showed no porosity and the same sample showed the highest Energy input of 29.94 J/mm^2. A minute pore in the microstructure with the energy inputs of 22.5 and 25.0 J/mm^2 is seen in Figure 4.6. The properties of the coated materials may experience a decline as a result of this. Furthermore, the shapes of the pores induce failures in the materials. Consequently, the thorough use of the optimized laser process is a way to avoid pores that may destroy the properties of the coatings. As an option for minimizing the pores formed in the microstructure, merging the laser process parameters with a low powder feed rate is effective [21, 104-106]. The distance from the Ti-6AI-4V alloy substrate determines the peak temperature distribution in the molten pool. There is a notable affiliation between the powder feed rate and laser scanning speed.

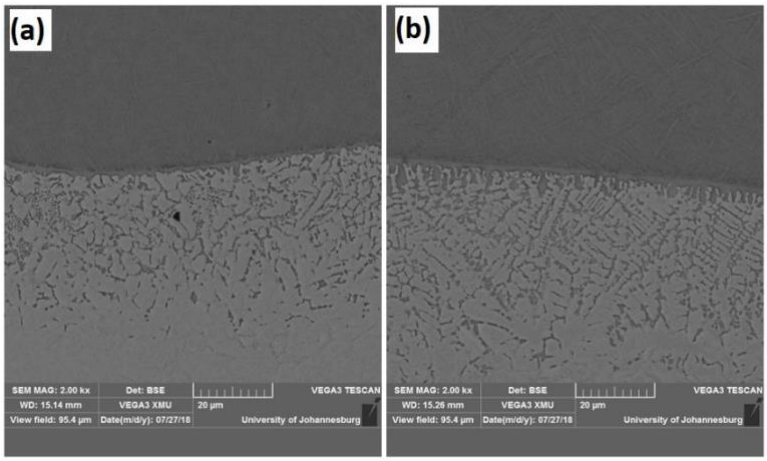

Figure 4.3: SEM Images Cross-section of Al-15Si-10Sn-10Cu Coatings at scanning speed of 16.7 and 20.0 mm/s and laser power of 1000 W.

The optical micrographs of Al-15Si-10Sn-10Cu is shown in Figure 4.3. Dendrites grains are shown in the fabricated coating. The interfacial zone as a junction with high bond strength has various chemical reactions that ensue between the coatings and the substrate. Thus, as the result of an efficient metallurgical bonding, the mechanical property of the coating-substrate system was enhanced. The change in microstructural positioning is seen from the mid-region of the coating coming up to the interfacial zone. The cause of this is as a result of the dependence of the temperature gradient ratio and the solidification rate, which is solidification during laser cladding on the solid/liquid stability variable. The noted rapid cooling through the substrate was caused by the rapid heat dissipation, which was produced by the high-temperature gradient and the high cooling rate. The directional grain growth in the coating as promoted by this is seen in Figures 4.4a and 4.4b. Therefore, when observed the fine dendritic microstructure which resulted from the fast cooling rate is visible [2, 106, 107].

Figures 4.4a and 4.4b display the dendrite structures and formation, where the coarse dendrite structures were caused by low laser speed longer interaction of powders with a laser beam at low scan speed (16.7 mm/s). An activated reduced rate of cooling emerges from the low scan speed that enables the longer interaction time, in turn forming granular dendrites [108]. Refined grains, which happened at higher scan speed (20.0 mm/s) are shown in Figures 4.3b and 4.4b The synergy between the laser beam and the powders reduce produce a high cooling rate. The reduced grain sizes are actualized after solidification and result from the rapid nucleation created by this high cooling rate [109-111].

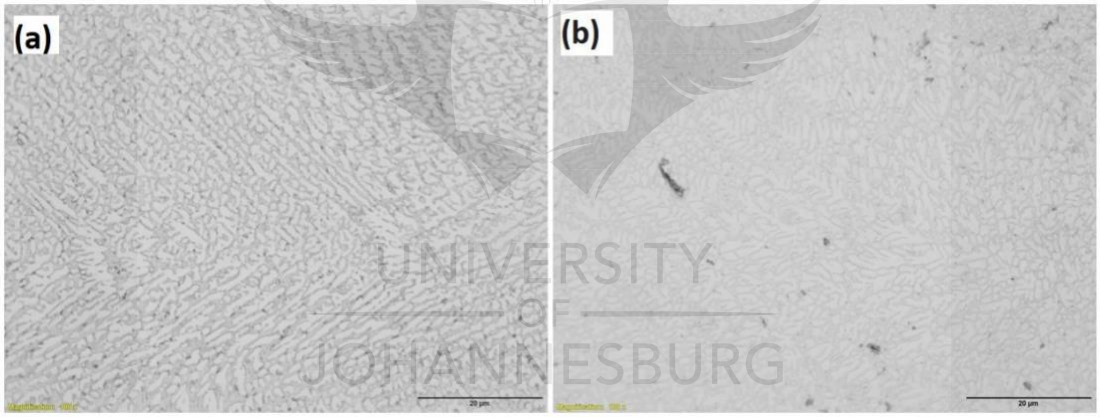

Figure 4.4: Optical Micrographs of Al-15Si-10Sn-10Cu at 16.7 mm/s and 20.0 mm/s scanning speed and laser power of 1000 W

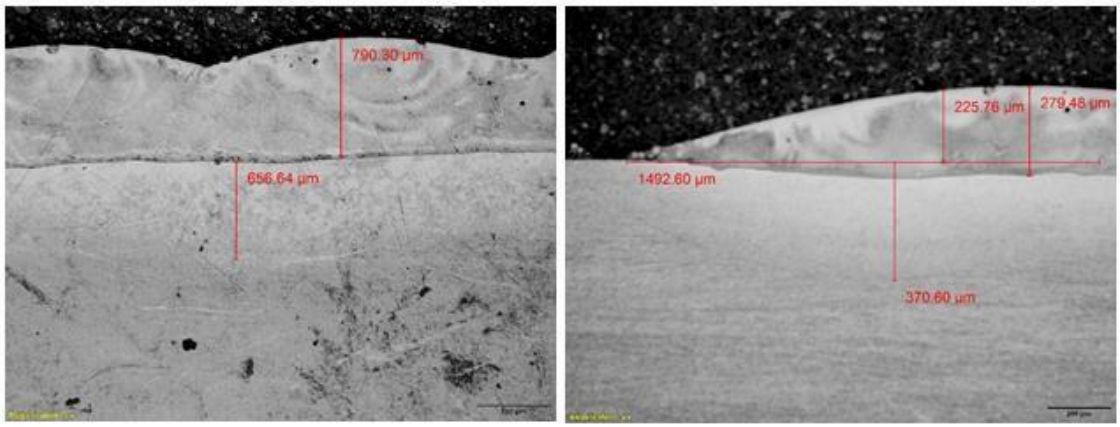

Figure 4.5: Optical Micrographs Cross-section of Al-15Si-10Sn-10Cu at 16.7 mm/s and 20.0 mm/s scanning speed and laser power of 900 W

A blend of substrate and reinforcement powders melt due to the irradiation of laser energy onto the base metal. Subsequently, the matrix of the coating forms as a solid solution of Al-Si-Sn-Cu and Ti solidifies. Molten powders interact with the base metal and form complex phases, resulting from the irradiation of the laser energy [112]. Optical micrograph of Al-12Si-10Sn-5Cu is shown in Figure 4.8 with different heights and widths of coating.

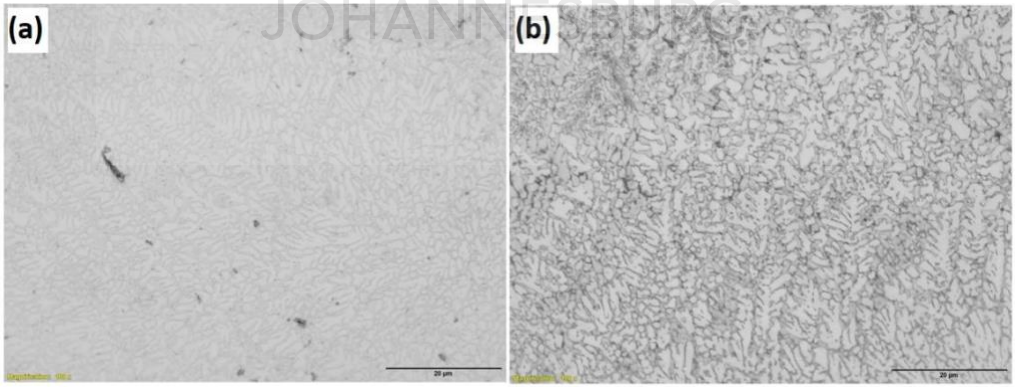

Figure 4.6: Optical Micrographs of Al-12Si-10Sn-5Cu at 16.7 mm/s and 20.0 mm/s scanning speed and laser power of 900 W

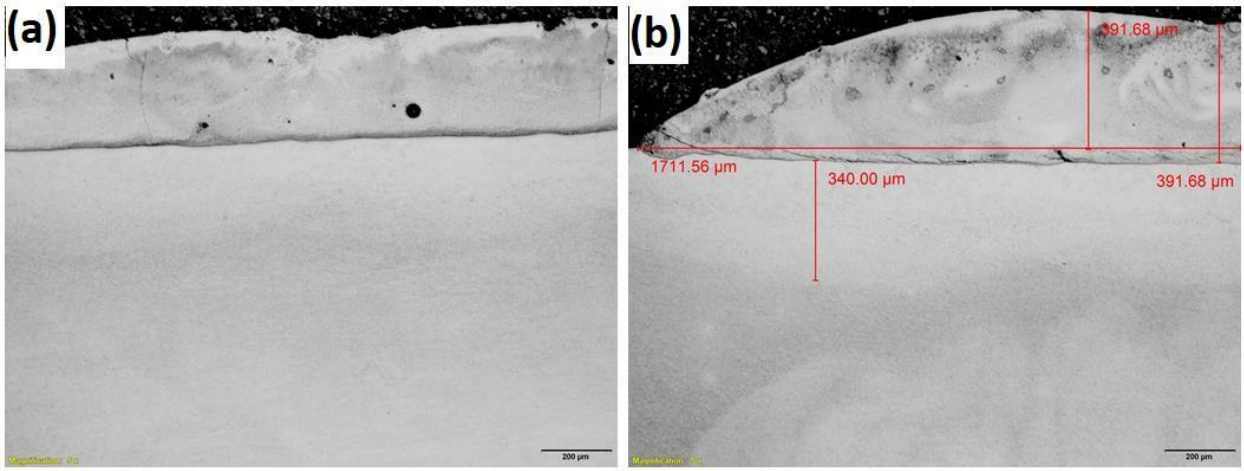

Figure 4.7: Optical Micrographs Cross-section of Al-12Si-10Sn-5Cu at 16.7 mm/s and 20.0 mm/s scanning speed and laser power of 1000 W

Figure 4.8: Optical Micrographs Cross-section of Al-12Si-10Sn-5Cu at 16.7 mm/s and 20.0 mm/s scanning speed and laser power of 900 W

High cooling rates form dendritic structures within the coatings. The major factors that determine the formation of the dendritic structure are the thermal gradients within the substrate during cooling and the cooling rates as shown in Figures 4.9 and 4.10. The faster and slower cooling rate causes the spacing of the dendritic arm [113-118]. The reinforcement particles inside the melt pool draw gas into the molten surface. Therefore,

if the solidifying anterior speed of the melt pool is progressive compared to the leaving speed of the pulled gas, gas foams become stranded inside the coatings creating clefts [119]. This substantiates with other researchers the connection between increased convection time and reduced pores in the coatings [120]. The conclusion that can come from this is that molten pool size influence the coating mechanical properties acutely.

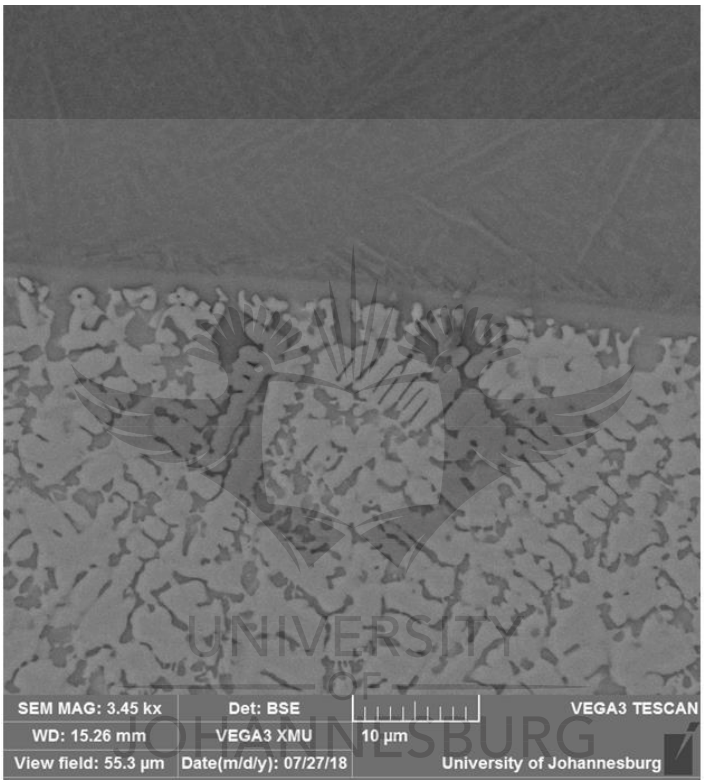

Figure 4.9: SEM Image Cross-section of Al-15Si-10Sn-10Cu at 16.7 mm/s and 20.0 mm/s scanning speed and laser power of 900 W

Several authors had claimed the relationship between increased wear resistance with silicon in the presence of aluminum, however, under lubricated conditions especially for starting engines, it would have poor seizure resistance properties. Exceptional materials can be generated with a lengthy use through the combination of the properties of different materials. Ways in which these properties can further be improved include cautiously

controlling the ratio and distribution of the ingredients of a composite in addition to the processing conditions. The refined grains become nuclei to form elongated and thin columnar grains, at the point where more layers are added (Figure 4.10). The influence on the microstructure is by cause of any processing parameter that would affect the energy density and thermal history, considering that thermal history may have determined the microstructural development [121]. The development of grain growth is brought about when a layer of the material is added to the pre-existing layer, and then having the unchanged solid region at the top of the pre-existing layer re-heated.

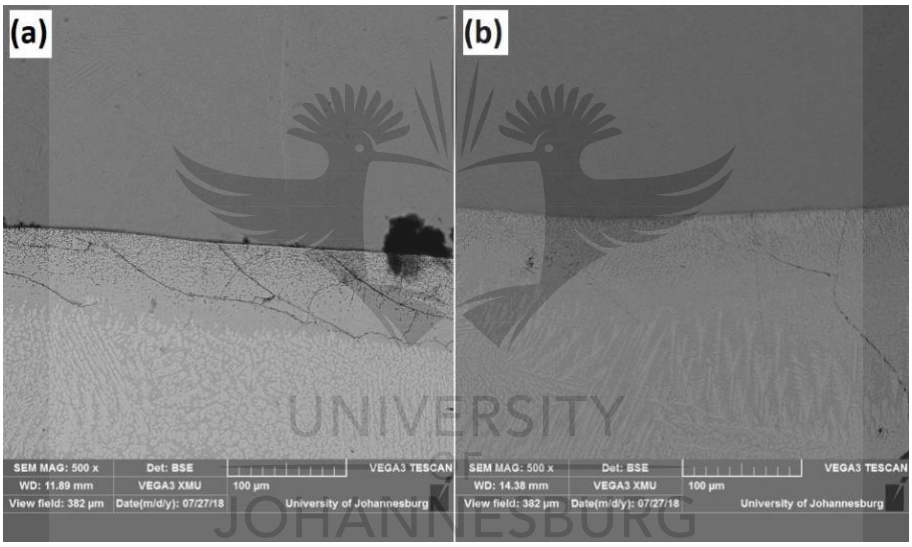

Figure 4.10: SEM Images Cross-section of Al-12Si-10Sn-5Cu at 16.7 mm/s and 20.0 mm/s scanning speed and laser power of 1000 W

The thermal gradient between the melt remaining and the columnar grain acted as a restriction for the directional growth of the columnar grains. Seed crystals are represented by the melted off arms of the columnar grains which have been fused into the liquid caused by the turbulent convection current in the liquid. Equiaxed grains are formed by these [122, 123]. The turbulent Marangoni convection current is the momentum and

turbulence that occurs in the melt pool, which in fact is brought about by the blowing of the powders into the melt pool through the argon gas which carries the powders during laser metal deposition. A decrease in the aspect ratio of columnar grains comes into effect by the increase in equiaxed grains as the build height increases. Processing conditions on grain structure with its influence was also noted. The microstructural development can also be affected by other processing parameters such as the powder flow rate as suggested by the results. Therefore, the microstructural development may have been conclusively determined by the input energy density, which could be defined by laser power, scanning speed, powder flow rate, and thermal history. Hence, we see the influence on microstructure when any processing parameter affects the energy density and thermal history [122].

Al-Si-Sn-Cu Coatings resulted in a martensitic microstructure seen in Figure 4.11, with more acicular alpha grains appearing when the scanning speed was increased but a few beta grains at the top of the deposit. Acicular alpha martensite is also referred to as alpha-prime microstructure [15]. Figure 4.12 provides the SEM image cross-section of laser surface alloyed Al-10Si-10Sn-5Cu/Ti-6Al-4V. The scan speed was raised from 16.7 mm/s in (a) to 20.0 mm/s in (b). Acicular alpha grain structures appear in both (a) and (b) but have a much shorter length in (b) than in (a). Evidently, more grain structures were promoted in (b) and appear finer since increasing the scan speed consequently increases the cooling rate because of less material interaction time [49]. The increase in line energies reduces its influence on the molten pool width, as confirmed by the simulations results. Only for various process parameter combinations was the molten pool depth

determined by simulations; with constant line energy resulting in near constant melt pool depth. Higher line energies increased the molten pool depth. The temperature history within the material is prevailed by the process, which influences the mechanical properties of the part fabricated.

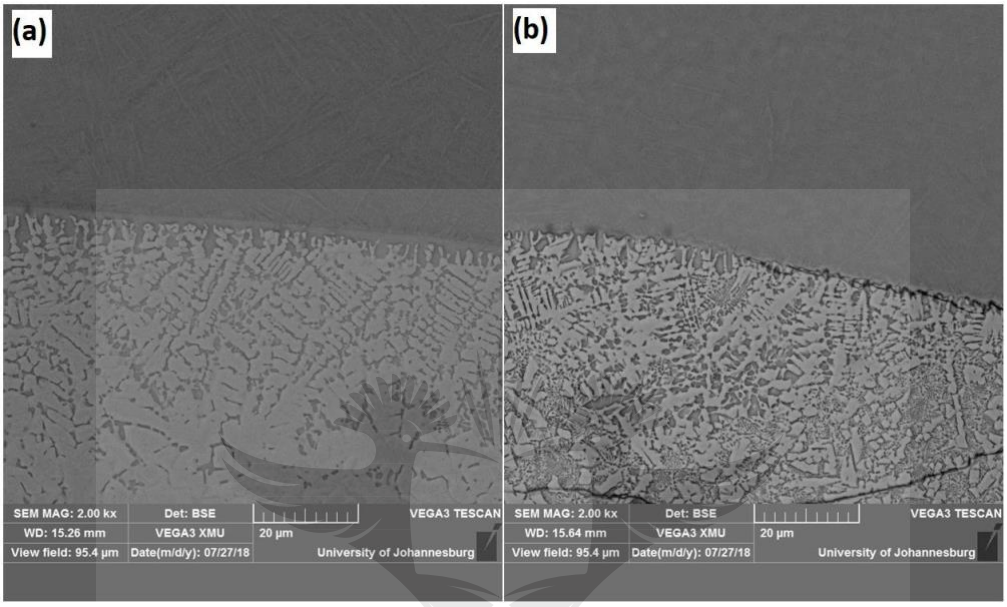

Figure 4.11: SEM Images Cross-section of Al-15Si-10Sn-5Cu at 16.7 mm/s and 20.0 mm/s scanning speed and laser power of 900 W

From Figures 4.7 and 4.8, the Heat Affecting Zone (HAZ), pores and the Fusion Zone (FZ) are detectable in the microstructure. The heat-affected zone is impacted by the heat input during the laser cladding process, which is worth observing. The radius of the heat-affected zone changes, when specifically looking at the dilution of the coating. At the bottom of the coating, we see the planar crystal and then the cellular crystal along the direction of solidification. We see dendrites at the interior and top regions in coatings from the microstructures. In addendum, the cooling theory is capable of explaining how the

grain size decreased along the distance from the fusion line. The high-temperature gradient and low growth rate refer to the planar grain seen at the interface between coating and substrate. High rapid cooling, which correlates with the direction of heat flow (Figure 4.12) shows how grains grown in the form of columnar dendrites are induced in the interior and top regions of the coating. Despite this, due to the instability of heat flow in the molten pool, the direction of dendrites at the upper part of the coating is more even compared with that in the middle [7, 18, 103, 124].

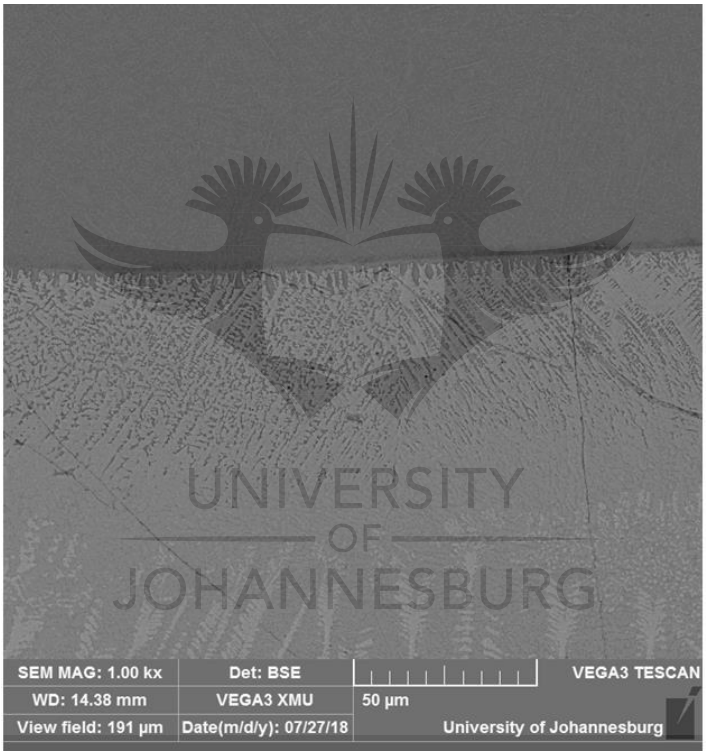

Figure 4.12: SEM Image Cross-section of Al-15Si-10Sn-10Cu at 20.0 mm/s scanning speed and laser power of 1000 W

Also, in Figure 4.10b, there was less pronouncement of the black flecks and numerous needle-like growth, which was as a result of active intermetallic compounds that have

been formed. These intermetallic compounds are hard materials formed from the matrix and second phase particle. They gradually build up at the grain boundaries, thereby preventing dislocation movement and causing stain hardness.

Columnar dendrites are caused by the low solidification velocity and high thermal gradient at the bottom of the melt pool and above the solid/liquid crossing. The high solidification velocity and low thermal gradient at the upper part of the melt pool create an equiaxed microstructure from the middle to the top section of the composite. The degree of melting increases as a result of an increase in laser power. Another visible increase due to the increased laser power was in the columnar grains and dendritic microstructure. An increase in dilution with an increase in the laser scanning speed is brought about by the clad area above the substrate decreasing more significantly than the clad area below the substrate. A decrease in the clad height also has a slight effect on the clad width, this is all due to the increasing laser-scanning speed (Figures 4.7 and 4.8).

The advancing scan speeds were varied for the two processing conditions and it was observed that the microstructural zones identified were susceptible to change as the scan speed was varied. A change in grain size as a result of scan speed changes had been reported in the literature [105, 114, 125]. Quick rate of cooling as the materials solidify with enhanced microstructure was also reported by other researchers [109, 110, 115] as a result of the scan speed changes. The kinds of stresses (tensile/compressive) that would be introduced into the coatings are determined by the change in thermal expansion coefficient of the base metal and the coatings.

4.5. XRD Analyses

The two phases (alpha and beta) standardly present in the Al-Si-Sn-Cu/ Ti-6Al-4V composite coating can be altered by employing the various available processing procedures and prior heat conditioning, which influence the morphology and distribution of the grains. It is of importance to take note to the rate of cooling of the alloy once it has been heated to and above the beta transus temperature as the metallurgical modifications occurs during this process [126]. The microstructural evolution that is commonly evident is that of the formation of large lamellar beta grains which are fully homogenous, fine alpha colonies with bi-modal constituents, or the alpha-beta structures that from equiaxed [127].

The confirmed presence of intermetallics are responsible for the enhanced hardness profiles of the cladded samples with increase in the wt. % composition Si and Cu. At laser power of 1000 W, these intermetallics were synergetically formed from the matrix elements (Ti, Si, Al, Sn) and Cu. It is noteworthy that these intermetallic compounds have excellent match of properties viable for tailored applications in applications that require high temperature strength, good wear resistance, and microstructural integrity. Aside from the control sample, Ti, Al_3Ti, Ti_3Al, $CuTi_2$ intermetallic were present in Figures 4.13 and 4.14 of the cladded quarternary coatings [peter odetola]. The XRD spectrum for Ti6Al4V/Al-12Si-10Sn-5Cu quaternary coatings at laser power of 900 W and scanning speed of 16.7 mm/s is shown in Figures 4.15 and 4.16.

Dilution effect from the base metal mixed with the reinforcement materials in melt pool during melting and solidification to form intermetallic Ti, Al_3Ti, Ti_3Al, CuTi, TiV, Ti_2FeCu

and $CuTi_2$ seen in Figures 4.15 and 4.16. In-situ metallurgical reactions is responsible for the formation during the cladding process. Diffraction peaks of titanium and titanium-aluminium from the XRD spectra resulted from high laser power and scanning speed of 1000 W and 16.7 mm/s. The weight percent of titanium and aluminium are the highest in the composition therefore leading to titanium-aluminium (Ti_3Al) formation and existence of α & γ phases. Hardness values, yield strength and tensile strength enhancement respond to increased weight percentage of copper in the quaternary composition. This corresponds to the researches in the literature. FCC and BCC combined structures from initial FCC were formed as a results of weight percent decrease in copper and weight percent increase of aluminium in the composition. As reported [7, 18, 103], formation of BCC phase was stimulated by aluminium while formation of FCC was stimulated by copper. Copper is widely renowned as one of the β-stabilizing elements.

Formation of β-Ti phase was as a result of atomic migration of copper during solidification in the Ti lattice. β-matrix crystallographic structure area more open by the migration of copper into the lattice of titanium. Naturally, copper and aluminium are not easy to work with as a result of difference in reflectivity and diffusivity and metallurgical bonding is one of the requirements. The quality of the metal deposition depends on the ability of the two materials for absorption of photons by reinforcing them with excellent materials [124]. When α-phases is strengthened by solid-solution, the possibility of Ti-Cu mechanical properties enhancement is very high with intermetallic compounds precipitation.

The XRD spectra shown in Figures 4.13 and 4.14. Figure 4.13 includes an irregular shaped AlTi phase as distributed in a Ti-matrix. This was done at laser power of 1000 W

and scanning speed of 20.0 mm/s. At optimal parameters, Al_3Ti peaks could be seen along with Ti and CuTi peaks. There is a relationship between melt pool, time, solidification rate and temperature of the reinforcements during the formation of aluminium titanium phase. In the matrix, chemical composition is linked with the formation of primary crystal. This is because primary crystal crystallization comes after the gradient of chemical composition. The difference in densities is responsible for the migration of the primary crystal. The main factors responsible for the hardness influence of Al-Si-Sn-Cu/Ti6Al4V are the size and shape of reinforcements, formation of hard intermetallic and reinforcement distribution gradient type at high laser power.

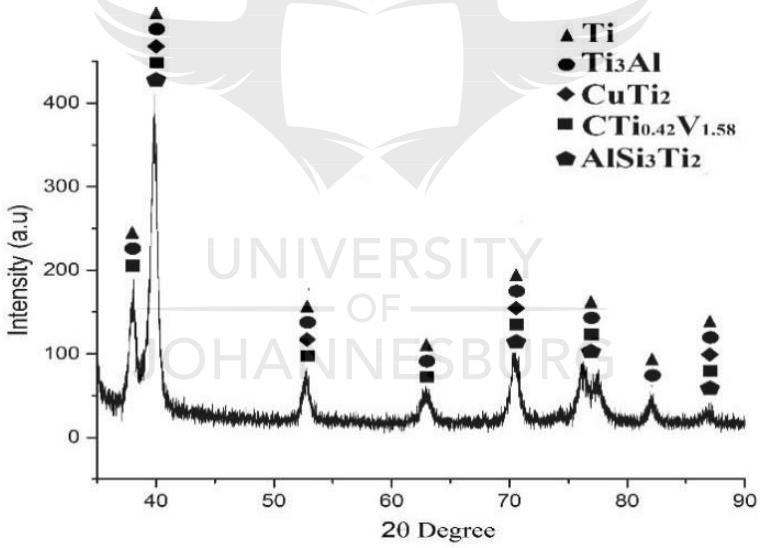

Figure 4.13: XRD Spectrum of Al-15Si-10Sn-10Cu Coatings at 20.0 mm/s scanning speed and laser power of 1000 W.

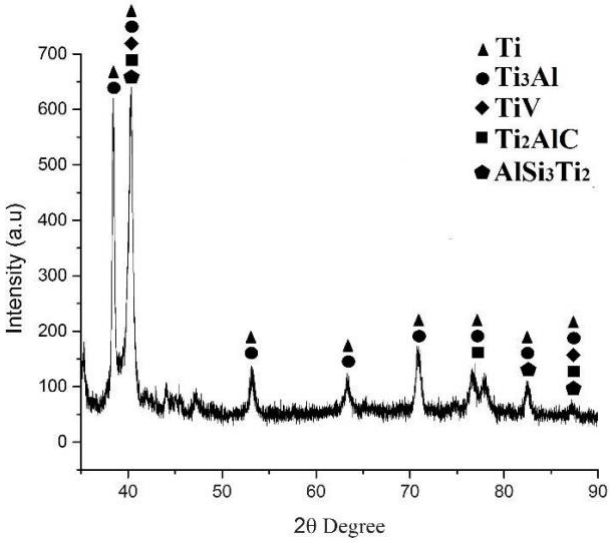

Figure 4.14: XRD Spectrum of Al-15Si-10Sn-10Cu Coatings at 16.7 mm/s scanning speed and laser power of 900 W.

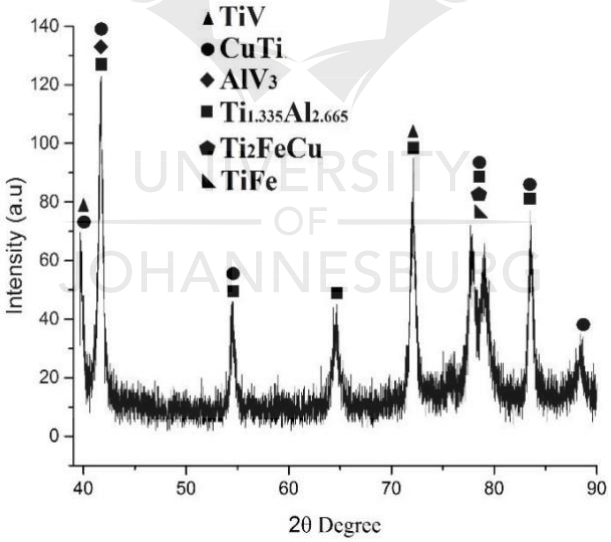

Figure 4.15: XRD Spectrum of Al-12Si-10Sn-5Cu Coatings at 20.0 mm/s scanning speed and laser power of 900 W.

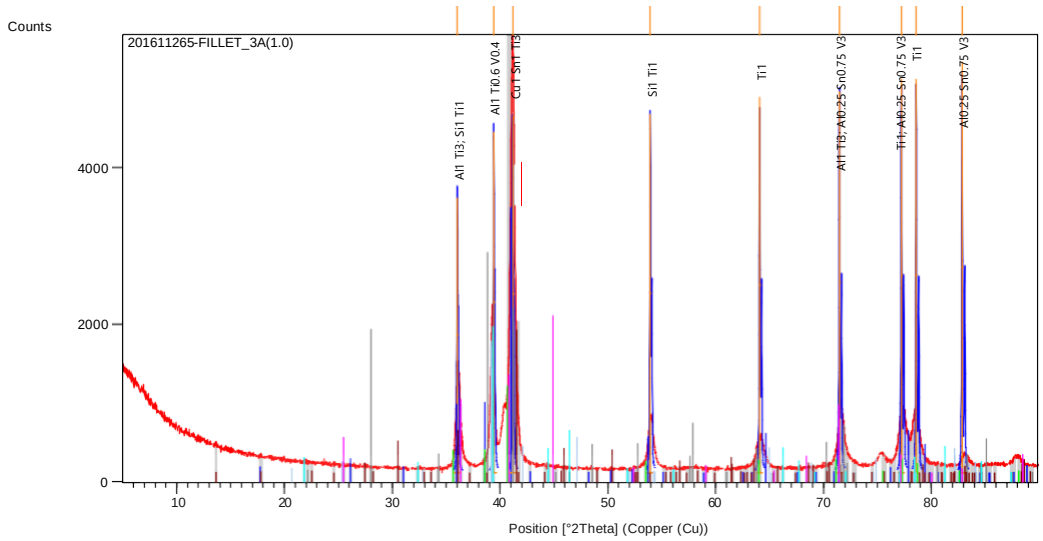

Figure 4.16: XRD Spectrum of Al-12Si-10Sn-5Cu Coatings at 16.7 mm/s scanning speed and laser power of 900 W.

4.6. Hardness and Wear Resistance

Figure 4.17 shows the microhardness of Al-Si-Sn-Cu quaternary coatings. The improved hardness as revealed by all quaternary coatings was as a result of solidification mechanisms and hard intermetallic formation. Observation of a trend in the hardness values as shown in Table 4.1 shows increased scanning speed 20.0 mm/s with increased copper weight percent. Several hard intermetallic contributed to the enhanced hardness property and microstructures of the Al-Si-Sn-Cu quaternary coatings such as SiTi, $CuTi_2$, Ti_3Al, $AlSi_3Ti_2$, $Al_{0.25}Sn_{0.75}V_3$ and $AlTi_{0.6}V_{0.4}$. Increase of 10 weight percent of copper is responsible improved hardness due to the presence of $CuTi_2$ hard phase as shown in Figures 4.13.-4.16. The microhardness results indicated that sample D, Al-15Si-10Sn-10Cu (deposited at 20.0 mm/s and laser power of 1000 W), gave the best microhardness

improvement of 99.3% of all the Al-Si-Sn-Cu coatings. While samples A (deposited at 16.7 mm/s and 1000 W) and X (deposited at 20.0 mm/s and 900 W) quaternary coatings showed 87.1% and 65.2% surface hardness improvement respectively. In addition, the improved hardness performance of sample M (deposited at 16.7 mm/s and laser power of 900 W) is about 49.7% which is the least improved hardness amongst all the quaternary coatings fabricated. The highest microhardness (602.23 HV, sample D) was found to be approximately 2.0 times the microhardness of the substrate (302 HV). The formation of hard intermetallic compounds by the temperature gradient and solidification process accounts for these results. On the other hand, hardness enhancement may be attributed to homogeneous dispersion of particles, as well as increasing reinforcement particle content, which eventually lockup with the matrix at the grain boundary. 5 weight percent in copper and 12 weight percent in silicon gave hardness that is 1.65-times greater than that of the base metal (302 $HV_{0.1}$). On the contrary, with a 10 weight percent in copper and 15 weight percent in silicon, the hardness enhancement is greater 2.0-times the base metal.

Excellent wear resistance and hardness performance has pointed to homogenous dispersion of silicon in the matrix while the friction coefficient goes down as indicated by the research of Alma Martinez-Hernández et al. [128]. Increase in weight percent of silicon leads to better hardness property. Shuar et al. [129] showed the relationship between decreased scanning speed and increased grain size average. But when the grain size is otherwise, there is an increase in the scanning speed. This mechanism was thoroughly explained in the work of some researchers [109-111, 130, 131] as a form of

heat treatment which is determined by an increase in the number of scan changes, which in turn reduced the grain size with improved microstructures. This is as a result of strain hardening generated in material. The concentration of the laser beam exposed onto the base metal controls the input power when it comes to material processing. A greater input power comes from a higher laser beam and inversely. Tables 4.1 and 4.2 show the effect of different process factors on the hardness performance of Al-Si-Sn-Cu/Ti-6Al-4V coatings. Calculation of the energy input in J/mm^2 as shown in Table 4.1 is given by equation 1 [132].

$$Q = \frac{2T}{UW} \quad (1)$$

Where T is laser power (W), U is beam radius (mm), and W is the scanning speed (mm/s). Morphology of the surface was modified by the mechanism of the laser energy density during cladding process which in also depend on scanning speed and laser power.

Table 4.1: Process Parameters L4 Orthogonal Array Values of Al-Si-Sn-Cu/Ti-6Al-4V

Sample	Power (W)	Speed (mm/s)	Energy Input (J/mm^2)	Vickers Hardness ($HV_{0.1}$)
1	900	16.7	26.95	451.80
2	900	20.0	22.50	498.66
3	1000	16.7	29.94	564.93
4	1000	20.0	25.0	602.23

Table 4.2: Hardness Values of Al-Si-Sn-Cu/Ti-6Al-4V Coatings.

Sample number	Description	Laser Power (W)	Scanning speed (mm/s)	Vickers Hardness ($HV_{0.1}$)
Substrate	Ti-6Al-4V alloy	-	-	302.40
1 (M)	Al-12Si-10Sn-5Cu	900	16.7	451.80
2 (X)	Al-12Si-10Sn-5Cu	900	20.0	498.66
3 (A)	Al-15Si-10Sn-10Cu	1000	16.7	564.93
4 (D)	Al-15Si-10Sn-10Cu	1000	20.0	602.23

Table 4.3 and Figure 4.18 present the coefficients of friction table of Al-Si-Sn-Cu/Ti-6Al-4V quaternary coatings and variation of friction coefficient against sliding time of reinforced Al-Si-Sn-Cu quaternary coatings under dry sliding situation at a load of 15 N. With the incorporation of the Al-Si-Sn-Cu coatings, friction coefficients were observed to be reduced. Like hardness property, several hard intermetallic contributed to the enhanced wear resistance performance and microstructures of the Al-Si-Sn-Cu quaternary coatings such as SiTi, $CuTi_2$, Ti_3Al, $AlSi_3Ti_2$, $Al_{0.25}Sn_{0.75}V_3$ and $AlTi_{0.6}V_{0.4}$,. This gives reinforcement effect and higher loadbearing to the intermetallic formed. Sinusoidal waves were witnessed in the coefficient of friction of coatings with 5 weight percent of

copper at scanning speed of 20.0 mm/s (below 0.52 μ). Whereas a wavy graph with decreased scanning speed of 16.7 mm/s gave coefficient of friction about 0.43 to 0.56 μ. Grooves pull-out made the difference between silicon and copper with 10 weight percent and 5 weight percent of copper. This also influence the yield and tensile strengths properties of the quaternary coatings. The reduction of the wear resistance of the coatings is a result of many inclusions. Coefficient of friction of 0.43 of Al-15Si-10Sn-10Cu at scanning speed of 20.0 mm/s and laser power of 1000 W influence the wear resistance performance reduced the wear rate. Though the weight percent of copper was increased to 10 while that of silicon was increased to 15. Due to increased weight percent of silicon and copper with high melting points, higher laser power is required to melt the quaternary composition. Cooling rate can be rapid if the scanning speed is increased during the cladding process and this can lead to improved microstructures as a result of the fast cooling rate.

As a result of excellent wear resistance performance with low friction coefficient at load of 15 N as indicated from the wear results, Samples M (16.7 mm/s, 900 W), X (20.0 mm/s, 900 W), A (16.7 mm/s, 1000 W), and D (20.0 mm/s, 1000 W) coatings displayed 10.70%, 19.20%, 29.2%, and 44.18 reduction in friction coefficient respectively. Al-15Si-10Sn-10Cu (sample D) quaternary coating revealed the best wear resistance performance amongst all the coated samples. The enhanced wear resistance was as a result of intermetallic (Ti_3Al, CuTi, Al_3Ti, $CuTi_2$, $Ti(Fe_{0.76}Al_{0.74})_2$) compounds, homogeneous distribution and refined grain sizes. A soft strengthening in the aluminum-based matrix is Sn as used in bearing alloys. By adding Sn to aluminium matrix, alloy anti-friction features such as compatibility, conformability, and embed ability are enriched. Silicon as hard

phase in aluminium matrix microstructures boosted the wear performance of the quaternary coatings. Entrenched particles of silicon in the aluminium matrix reduced the wear rate of the Al-Si-Sn-Cu quaternary coatings as shown in Figure 4.19 in the SEM of the wear tracks. Addition of copper reinforced the quaternary coatings to withstand delamination and wear degradation. The addition of silicon in the aluminium matrix caused Tin particles to diffuse uniformly as a result of eutectic silicon phases with which they are formed.

It is showed that an increase in silicon content results in decreased wear loss in all the quaternary coatings except control. This high wear resistance of Al-Si-Sn-Cu/Ti6Al4V composite is due to the presence of silicon which acts as load-supporting element. It is also observed that the dispersion of silicon, a hard face in the matrix tends to reduce the wear loss of the Al-Si-Sn-Cu/Ti6Al4V quaternary coatings. Interfacial bond between the matrix and the silicon particle perform a major role in wear mechanisms.

Table 4.3: Friction Coefficient of Al-Si-Sn-Cu Quaternary Coatings.

SAMPLE	SCAN SPEED (mm/s)	FRICTION COEFFICIENT (μ)
CONTROL (Ti6Al4V)		0.62
Al-12Si-10Sn-5Cu-900	16.7	0.56
Al-12Si-10Sn-5Cu-900	20.0	0.52

Al-15Si-10Sn-10Cu-1000	16.7	0.48
Al-15Si-10Sn-10Cu-1000	20.0	0.43

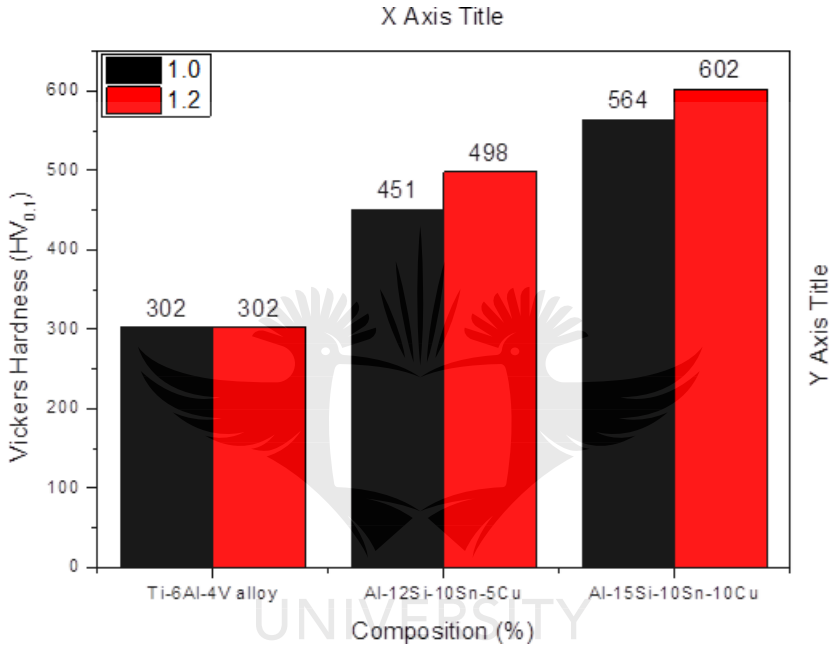

Figure 4.17: Variation of Vickers Hardness of Al-Si-Sn-Cu coatings against Composition

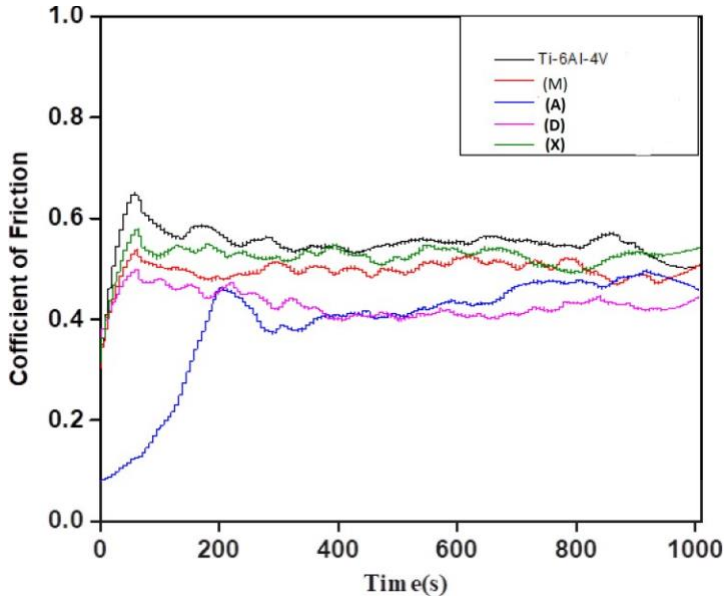

Figure 4.18: Variation of coefficients of friction of Al-Si-Sn-Cu/Ti-6Al-4V coatings against Time

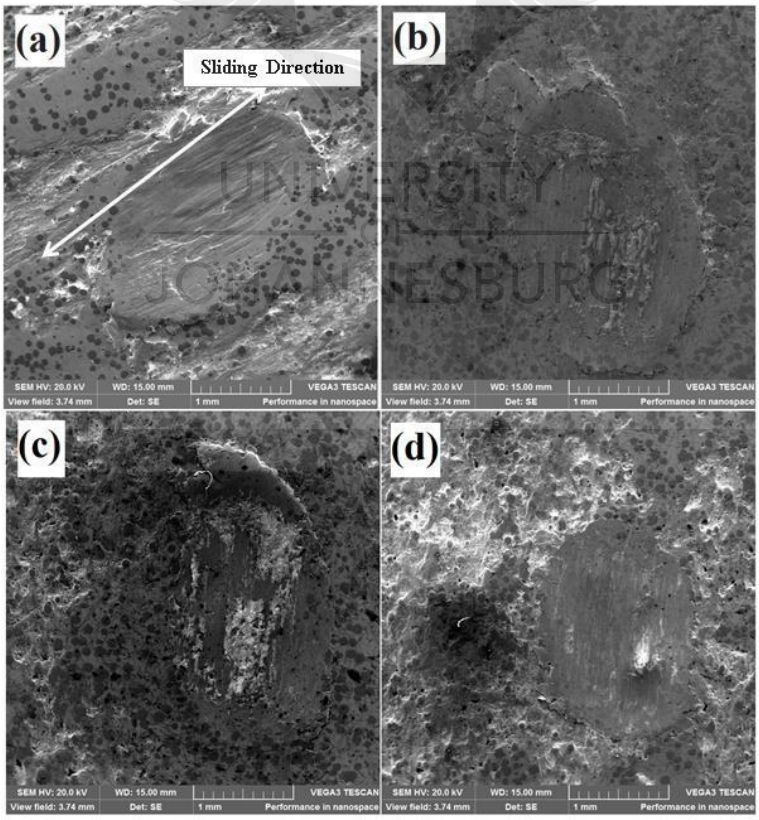

Figure 4.19: SEM Images of the Wear Tracks of (a) M (b) X (c) A and (d) D Quaternary Coatings

The improvement degree depends on the coating quality, refinement of the microstructures, and the metallurgical adhesion between the coating and the substrate as revealed by each property studied. The vast development in the hardness and wear property of titanium alloy was because of the optimized process parameters used in this research. The well-optimized laser process factors and suitable selection of reinforced powders enabled the achievement of improved surface hardness and wear resistance properties. Optimization of key process parameters is one of the key factors in avoiding delamination of quaternary coatings from the base metal. Strong and sturdy bond exists between the reinforcements coatings and the base metal.

4.7. Mechanical Properties of Al-Sn-Si-Cu Composite Coatings

The advent of indentation testing has led to measurement of bulk hardness thereby revealing the mechanical properties of materials such as yield strength and tensile strengths as stated by several researchers [133]. Several equations have been stated by some researchers to link yield and tensile strengths to hardness indention. Al-Si-Sn-Cu coatings mechanical properties were determined from these equations (2) and (3) [133]. These values are shown in Table 4.4.

$$J = \left(\frac{G}{2.9}\right)\left(\frac{k}{0.217}\right)^{k} \tag{2}$$

$$L = \left(\frac{G}{3}\right)_{k}(0.1) \tag{3}$$

G is the hardness values in Vickers, and strain hardening coefficient is denoted by k, with value of 0.15 [133]. J is the tensile strengths while L signifies yield strengths. Enhancement in the values of both the tensile and yield strengths can be seen in Table 4.4 compared to the base metal, titanium alloy. Some researchers [134] also indicated other linear equations 4 and 5 linking Vickers hardness indentations to both the yield and ultimate tensile strengths.

$$J = -99.8 + 3.734G \quad (4)$$

$$L = -90.7 + 2.876G \quad (5)$$

Asides the Vickers hardness values, no other parameters are needed to compute the tensile and yield strengths of materials. Increased in silicon content impacts on the values of tensile and yield strengths to the maximum values of 1.93 and 1.39 GPa respectively at 10 wt. % of Silicon. The results show that both the yield and tensile strengths for the coatings are enhanced as compared to the substrate (Ti-6Al-4V alloy).

The mechanical properties of the quaternary coatings like yield strength and tensile strength showed improvement in their values. Samples M (16.7 mm/s, 900 W), X (20.0 mm/s, 900 W), A (16.7 mm/s, 1000 W), and D (20.0 mm/s, 1000 W) coatings displayed tensile strengths of 1.45 GPa, 1.69 GPa, 1.81 GPa, and 1.93 GPa respectively. It shows an enhancement of 49.48%, 74.23%, 86.6%, and 98.97% in tensile strengths of quaternary coatings compared to titanium alloy substrate. Moreover, Samples M (16.7 mm/s, 900 W), X (20.0 mm/s, 900 W), A (16.7 mm/s, 1000 W), and D (20.0 mm/s, 1000 W) coatings displayed yield strengths of 1.05 GPa, 1.15 GPa, 1.31 GPa, and 1.39 GPa respectively. It shows an enhancement of 50%, 64.29%, 87.14%, and 98.57% in yield strengths of the quaternary coatings compared to titanium alloy substrate. There is

significant impact of refined grains on the hardness values and microstructures of the coatings as seen in Table 4.2. The enriched hardness of the quaternary coatings is a result of combined strengthening effects within the coatings, as produced by the presence of theses hard intermetallic phases. This in turn were as a results of optimized process parameters during the experimental work. Addition of silicon to the matrix of aluminium-tin impact on the mechanical properties. These can be further enhanced by addition of small weight percent of copper into the matrix by cautiously controlling the ratio and distribution of the ingredients of a composite as well as the processing conditions. As revealed by the results, Table 4.4 clearly show the influence silicon, weight percent of copper, weight percent of tin and carefully selected processing conditions on both the tensile and yield strengths of the quaternary coatings.

Table 4.4: Properties of Al-Si-Sn-Cu/Ti-6Al-4V Composite Coatings

Samples	Laser Power (W)	Average Hardness ($HV_{0.1}$)	Tensile strength (GPa)	Yield strength (GPa)
Ti-6Al-4V alloy	-	302 ± 1.09	0.97	0.70
Al-12Si-10Sn-5Cu-16.7	900	452 ± 3.16	1.45	1.05
Al-12Si-10Sn-5Cu-20.0	900	498± 4.58	1.69	1.15
Al-15Si-10Sn-10Cu-16.7	1000	564± 3.64	1.81	1.31
Al-15Si-10Sn-10Cu-20.0	1000	602± 2.59	1.93	1.39

4.8. Numerical Modelling

The system geometry used COMSOL multiphysics to validate this experiment. The geometry was established on 3D boundaries (k_1, k_2, h) to generate the design. The tangential components are denoted by k_1 and k_2 and h as normal component. In order to identify the normal and tangential components, selection of deformed configuration was necessary in the frame section of boundary system.

Assumptions used in this model are stated below:

- Direction Z is used for the movement of laser beam and vertical to the base metal. This occurs at steady velocity.
- The materials for the base metal and reinforcements are The substrate and deposition material are stated as isotropic and homogeneous.
- The thermos-physical properties of the materials are dependent on temperature.
- The flow of the reinforcement powders is taken to be Laminar, incompressible and Newtonian.
- Convection, heal losses and radiation are not considered in this model.

From the domain menu, the initial temperature (293K) and time-dependent heat equations were determined by the values of the initial and solid domains. Equations 6-8 were used for the heat transfer in solid according to Fourier's law.

$$\rho C_p \frac{\partial T}{\partial t} + \rho C_p \, u \,.\nabla T + \nabla . q = Q \qquad (6)$$

or

$$\frac{\partial p}{\partial t} + \nabla . (\rho \mathbf{v}) = 0 \qquad (7)$$

The integrand $\nabla . (\rho \mathbf{v})$ is expressed in cartesian coordinates **v** = (u, v, w)

$$\nabla.(\rho\mathbf{v}) = \frac{\partial(\rho u)}{\partial x} + \frac{\partial(\rho v)}{\partial y} + \frac{\partial(\rho w)}{\partial z} \quad (8)$$

where: ρ is the solid density [kg/m^3], C_p is the solid heat capacity at constant pressure, u is the velocity field defined by translation motion sub-node when model parts move in the frame of material [m/s], Q is the heat source [W/m^3] and q is the heat flux [W/m^2] which is determined using equation 9:

$$q = -k\nabla T \quad (9)$$

where: k is the thermal conductivity [$W/m.K$] and ∇T is the change in temperature [K]. Material selected determines the default thermal conductivity. For the heat transfer interface, default boundary condition used thermal insulation. This in turn indicates that the insulation of the domain has no heat flux and well protected. A deposited beam powder node was used to model the heat source brought by narrow laser metal deposited beam to a selected boundary.

Analysis of the mesh used different size of mesh to define the base metal and the laser track. The section of laser track used 0.06 cm for the minimal size of element and 0.15 cm for maximal size of element. 0.18 cm was used for the minimal size of element for the base metal and 0.38 cm for the maximal size of element. This is shown in Figure 4. 20. The mesh analysis contains 25118 elements and 5683 nodes in order to simulate the real experiment.

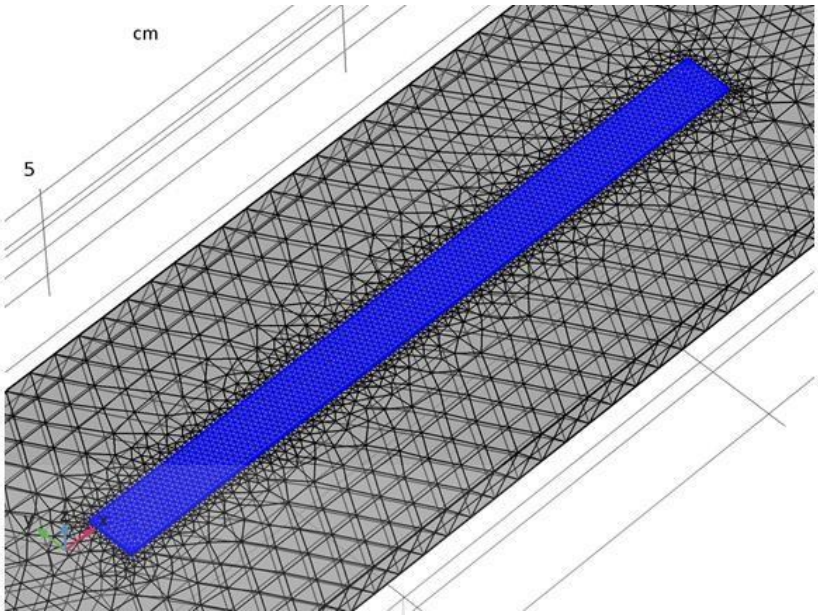

Figure 4.20: The Mesh System

The increased speed of the reinforcement particles that displays a proper flow of molten liquid is brought about by the increase in laser power; also noting that an increased laser power causes improvement, standardized distribution, and spheroidization as shown in Figures 4.21-4.23.

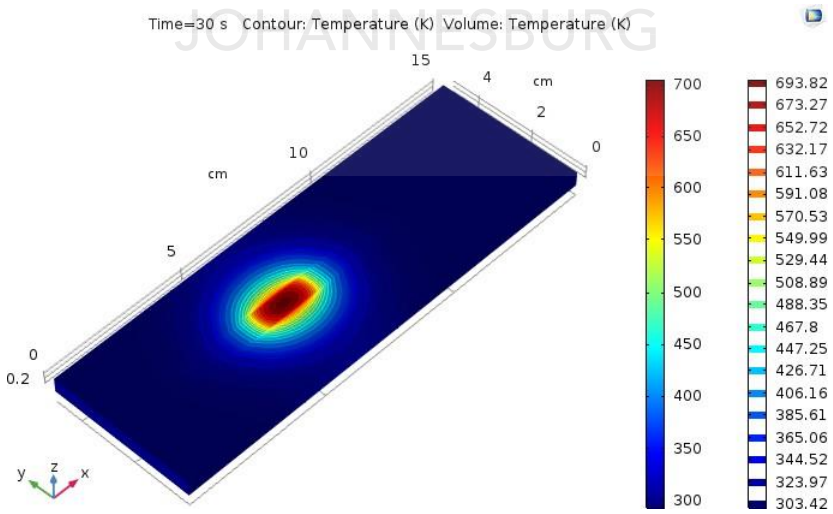

Figure 4.21: Contour Plot of Temperature Distribution Results at Various Points

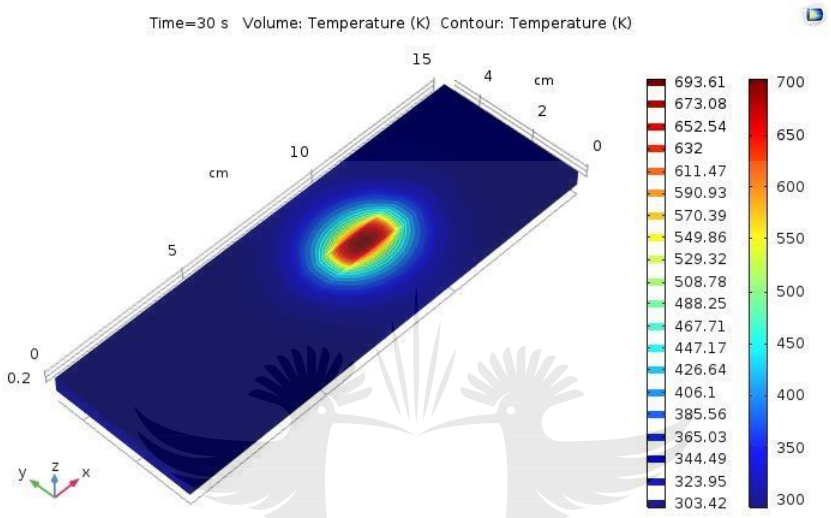

Figure 4.22: Contour Plot of Temperature Distribution Results at Various Points

As the laser beam moves from one point to another as shown in Figures 4.21-4.23, the temperature changes and the microstructures are determined by the laser input, scanning speed and fast cooling rate. High cooling rates form dendritic structures within the coatings. The major factors that determine the formation of the dendritic structure are the thermal gradients within the substrate during cooling and the cooling rates as shown in Figures 4.9 and 4.10. The faster and slower cooling rate causes the spacing of the dendritic arm.

The distance from the Ti-6AI-4V alloy substrate determines the peak temperature distribution in the molten pool. There is a notable affiliation between the powder feed rate

and laser scanning speed. The turbulent Marangoni convection current is the momentum and turbulence that occurs in the melt pool, which in fact is brought about by the blowing of the powders into the melt pool through the argon gas which carries the powders during laser metal deposition. A decrease in the aspect ratio of columnar grains comes into effect by the increase in equiaxed grains as the build height increases. Processing conditions on grain structure with its influence was also noted. The microstructural development can also be affected by other processing parameters such as the powder flow rate as suggested by the results. Therefore, the microstructural development may have been conclusively determined by the input energy density, which could be defined by laser power, scanning speed, powder flow rate, and thermal history.

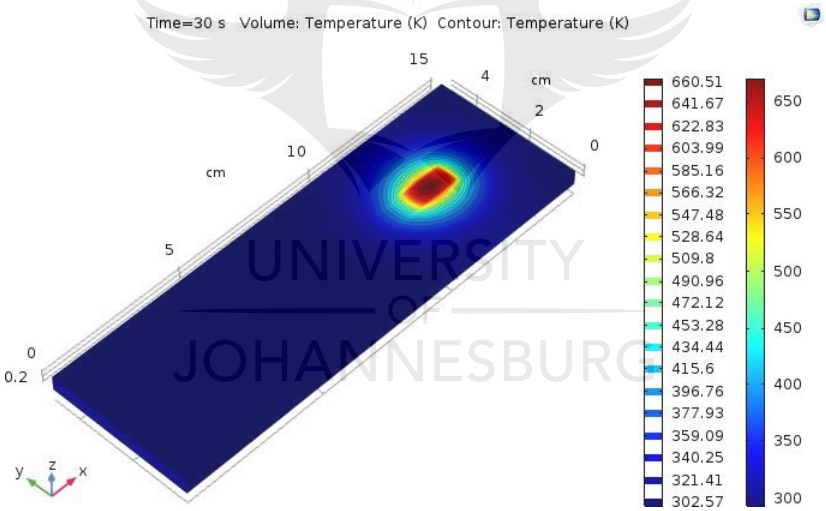

Figure 4.23: Contour Plot of Temperature Distribution Results at Various Points

Hence, there is influence on microstructure when any processing parameter affects the energy density and thermal history. The increase in line energies reduces its influence on the molten pool width, as confirmed by the simulations results. Only for various process

parameter combinations was the molten pool depth determined by simulations; with constant line energy resulting in near constant melt pool depth. Higher line energies increased the molten pool depth. The temperature history within the material is prevailed by the process, which influences the mechanical properties of the fabricated coatings.

4.9. Summary

The optimum control of the lase intensity and scan speed has a significant influence on the resulting morphology and properties of the material, such as the hardness and wear resistance performance and mechanical properties. The observations in the study indicated that raising the laser power promoted more grain growth, and allowed the merging of the structures, because the increased laser intensity introduces more heat into the process which produces more molten and the material interaction time is increased. Analysis of the mechanical properties showed that increasing the scan speed at a fixed laser power, increases the hardness and increases the wear resistance performance. The mechanical properties of the quaternary coatings like yield strength and tensile strength showed improvement in their values. Homogeneous and dense microstructures was accountable for the micro-hardness performance measured.

The chemical reactions that occurred during DLMD of titanium, aluminium, silicon, tin and copper produced few compounds like Ti_3Al, CuTi, Al_3Ti, $CuTi_2$, and $Ti(Fe_{0.76}Al_{0.74})_2$. These are the results of partial melting of the substrate with combinations of reactions of the various reinforcements in the melt pool. Rapid cooling and solidification had impacts on the types of compound formed in the coatings. Finally, the numerical model corresponds with the experimental results.

CHAPTER FIVE: CONCLUSIONS AND RECOMMENDATION

5.1 Introduction

During the recent employment of engineering materials, deterioration is bound to happen. Consequently, the revision of materials or new process designs has become the major assignment of material engineers in order to achieve gratifying properties, reduced expenditure, magnified performance, including the efficacy in the operation of the materials through a duration of time. The process of coating with different metallic or ceramic powders using a laser-based modification technique in order to modify the surfaces of the materials is an approach that material engineers have taken up as a way to intensify the properties of existing materials. The simplicity of this technique makes it very effective as it upgrades the metallic surface by changing the microstructure without changing the aggregate properties of the substrate.

The major impediments of titanium alloy are low hardness and poor tribological, which occur in many industrial applications. However, this study wanted to bring solutions that would prevent these constraints by improving the mechanical and wear behaviour of titanium and its alloy (Ti-6Al-4V), and synthesizing Al-Si-Sn-Cu reinforcements using the laser cladding technique. Therefore, to prevent the various forms of surface deterioration connected with titanium alloy grade 5, an assuring possibility is the application of novel metal matrix composite coatings through the laser cladding technique.

5.2 Final conclusion

The inference deduced from these investigations can be found below:

- ➲ The improvement degree depends on the coating quality, refinement of the microstructures, and the metallurgical adhesion between the coating and the substrate as revealed by each property studied. The vast development in the hardness and wear property of titanium alloy was because of the optimized process parameters used in this research.
- ➲ The microhardness results indicated that sample D, Al-15Si-10Sn-10Cu (deposited at 20.0 mm/s and laser power of 1000 W), gave the best microhardness improvement of 99.3% of all the Al-Si-Sn-Cu coatings. While samples A (deposited at 16.7 mm/s and 1000 W) and X (deposited at 20.0 mm/s and 900 W) quaternary coatings showed 87.1% and 65.2% surface hardness improvement respectively. In addition, the improved hardness performance of sample M (deposited at 16.7 mm/s and laser power of 900 W) is about 49.7% which is the least improved hardness amongst all the quaternary coatings fabricated. The highest microhardness (602.23 HV, sample D) was found to be approximately 2.0 times the microhardness of the substrate (302 HV). The formation of hard intermetallic compounds by the temperature gradient and solidification process accounts for these results.

- ➲ As a result of excellent wear resistance performance with low friction coefficient at load of 15 N as indicated from the wear results, Samples M (16.7 mm/s, 900 W), X (20.0 mm/s, 900 W), A (16.7 mm/s, 1000 W), and

(20.0 mm/s, 1000 W) coatings displayed 10.70%, 19.20%, 29.2%, and 44.18% reduction in friction coefficient respectively. Al-15Si-10Sn-10Cu (sample D) quaternary coating revealed the best wear resistance performance amongst all the coated samples. The enhanced wear resistance was as a result of intermetallic (Ti_3Al, CuTi, Al_3Ti, $CuTi_2$, $Ti(Fe_{0.76}Al_{0.74})_2$) compounds, homogeneous distribution and refined grain sizes.

➲ The mechanical properties of the quaternary coatings like yield strength and tensile strength showed improvement in their values. Samples M (16.7 mm/s, 900 W), X (20.0 mm/s, 900 W), A (16.7 mm/s, 1000 W), and D (20.0 mm/s, 1000 W) coatings displayed tensile strengths of 1.45 GPa, 1.69 GPa, 1.81 GPa, and 1.93 GPa respectively. It shows an enhancement of 49.48%, 74.23%, 86.6%, and 98.97% in tensile strengths of quaternary coatings compared to titanium alloy substrate. Moreover, Samples M (16.7 mm/s, 900 W), X (20.0 mm/s, 900 W), A (16.7 mm/s, 1000 W), and D (20.0 mm/s, 1000 W) coatings displayed yield strengths of 1.05 GPa, 1.15 GPa, 1.31 GPa, and 1.39 GPa respectively. It shows an enhancement of 50%, 64.29%, 87.14%, and 98.57% in yield strengths of the quaternary coatings compared to titanium alloy substrate.

5.3 Recommendations

It is recommended that further work should be carried out in the following areas:

- ➲ Alkaline salt and chloride (acid) as forms of diverse environments should be considered in studying the electrochemical behavior of the coatings.
- ➲ During laser processing, the effect of two powder feeders and gas rates should be compared to admixed powders.
- ➲ Stress-strain analysis of the melt pool geometry should be carried out in order to understand the impact of laser processing parameters on the geometry and dynamics of solidification.

REFERENCES

[1] Akinlabi, S.A., Mashinnini, M.P., Ajayi, O.O., Abioye, A.A., Fatoba, O.S., Akinlabi, E.T. (2018). Characterisation of laser metal deposited titanium and Molybdenum composite. IOP Conf. Series: Materials Science and Engineering **413** (2018) 012067 doi:10.1088/1757-899X/413/1/012067

[2] Fatoba O.S; Akinlabi, S.A**.,** Akinlabi, E.T**.,** Erinosho, M.F. (2018). Influence of Process Parameters on the Mechanical Properties of Laser Deposited Ti-6Al-4V Alloy: Taguchi and Response Surface Model Approach. Materials Today: Proceedings. Vol. 5, issue 9, part 3. Pp. 19181-19190

[3] Dutta Majumdar, J. & Manna, I. (2015). 21 - Laser Surface Engineering of Titanium and Its Alloys for Improved Wear, Corrosion and High-Temperature Oxidation Resistance. In: Waugh, J.L.G. (Ed.). Laser Surface Engineering. Woodhead Publishing:483-521.

[4] Katta, S. and Chaitanya, G., (2017). Key Improvements In: Machining Of Ti6Al4V Alloy: A Review. In AIP Conference Proceedings (Vol. 1859, No. 1, P. 020048). AIP Publishing.

[5] Adesina, O., Popoola, P. & Fatoba, O. (2016). Laser Surface Modification: A Focus on the Wear Degradation of Titanium Alloy, Fiber Laser, Mukul Chandra Paul, Intech Open, DOI: 10.5772/61737.

[6] Fatoba O.S., Adesina O.S. Popoola A.P.I. (2018). Evaluation of microstructure, microhardness, and electrochemical properties of laser-deposited Ti-Co coatings on Ti-6Al-4V Alloy. The International Journal of Advanced Manufacturing Technology. 97(5), 2341-2350. http://dx.doi.org/10.1007/s00170-018-2106-7.

[7] Gharehbaghi, R., Fatoba, O.S., Akinlabi, E.T. (2018). Experimental Investigation of Laser Metal Deposited Icosahedral Al-Cu-Fe Coatings on Grade Five Titanium Alloy. 2018 IEEE 9th International Conference on Mechanical and Intelligent Manufacturing Technologies (ICMIMT 2018), Cape town, South Africa, pp. 31-36. doi: 10.1109/ICMIMT.2018.8340416.

[8] Fu, Y., Zhang, X.-C., Sui, J.-F., Tu, S.-T., Xuan, F.-Z. & Wang, Z.-D. (2015). Microstructure and wear resistance of one-step in-situ synthesized TiN/Al composite

coatings on Ti6Al4V alloy by a laser nitriding process. *Optics & Laser Technology,* 67(0), 4//:78-85.

[9] Weng, F., Chen, C. & Yu, H. (2014a). Research status of laser cladding on titanium and its alloys: a review. *Materials & Design,* 58:412-425.

[10] Obiegbu M.C., Akinlabi, E.T., Fatoba O.S. Akinlabi, S.A. (2019). The Effects of Silicon and Copper on the Microstructure and Wear Resistance Performance of Al-Si-Sn-Cu/Ti-6Al-4V Composite Coatings. 2019 IEEE 10th International Conference on Mechanical and Intelligent Manufacturing Technologies (ICMIMT 2019), Cape town, South Africa, pp. 20-25. doi: 10.1109/ICMIMT.2019.8712023.

[11] Fatoba O.S., Popoola A.P.I., Aigbodion V.S., Rambau T.G. (2017). The Influence of Laser Parameters on the Hardness Studies and Surface Analyses of Laser Alloyed Stellite-6 Coatings on AA 1200 Alloy: A response Surface Model Approach. International Journal of Microstructure and Materials Properties, 12(5-6), 319-331.

[12] Adebiyi D.I., Fatoba O.S., Pityana S.L., Popoola A.P.I (2016): Parameters Optimization, Microstructure and Microhardness of Silicon Carbide Laser Deposited on Titanium Alloy. In Proceedings of International Conference on Surface Modification Technologies, 29th June-1st July, 2016, Milan, Italy, pp.1-6

[13] Moorhouse, B. (2013). Controlling the interstitial element concentration in Ti-6Al- 4V using calciothermic reduction.

[14] Veiga, C., Davim, J. & Loureiro, A. (2012). Properties and applications of titanium alloys: a brief review. *Rev. Adv. Mater. Sci,* 32(2):133-148.

[15] Fatoba O.S; Akinlabi, E.T., Makhatha, M.E. (2018). Effects of Cooling Rate and Silicon Content on Microstructure and Mechanical Properties of Laser Deposited Ti-6Al-4V Alloy. Materials Today: Proceedings. Vol. 5, issue 9, part 3. Pp. 18368-18375. https://doi.org/10.1016/j.matpr.2018.06.176.

[16] Bloyce, A., Qi, P.Y., Dong, H. & Bell, T. (1998). Surface modification of titanium alloys for combined improvements in corrosion and wear resistance. *Surface and Coatings Technology,* 107(2–3), 9/10/:125-132.

[17] Chikarakara, E., Naher, S. & Brabazon, D. (2012). High speed laser surface modification of Ti–6Al–4V. *Surface and Coatings Technology,* 206(14), 3/15/:3223-3229.

[18] Fatoba, O.S., Akinlabi, E.T. Akinlabi, S.A. (2018). Effects of Fe addition and Process Parameters on the Wear and Corrosion Properties of Laser Deposited Al-Cu-Fe Coatings Ti-6Al-4V Alloy. 2018 IEEE 9th International Conference on Mechanical and Intelligent Manufacturing Technologies (ICMIMT 2018), Cape town, South Africa, pp. 74-79. doi: 10.1109/ICMIMT.2018.8340424.

[19] Bansal, D.G., Eryilmaz, O.L. & Blau, P.J. (2011). Surface engineering to improve the durability and lubricity of Ti–6Al–4V alloy. *Wear,* 271(9–10), 7/29/:2006-2015.

[20] Dutta Majumdar, J. & Manna, I. (2015). Laser surface engineering of titanium and its alloys for improved wear, corrosion and high-temperature oxidation resistance. In: Waugh, J.L.G. (ed.). *Laser Surface Engineering*. Woodhead Publishing:483- 521.

[21] Fatoba O.S., Akinlabi S.A., Gharehbaghi R., Akinlabi E.T (2018). Microstructural Analysis, Microhardness and Wear Resistance Properties of Quasicrystalline Al-Cu-Fe Coatings on Ti-6Al-4V Alloy. Materials Express Research. 5(6), 1-14. https://doi.org/10.1088/2053-1591/aaca70.

[22] Gong X. Lydon J. Cooper K. Chou K. (2014b). Beam Speed Effects on Ti-6Al-4V Microstructures in Electron Beam Additive Manufacturing, *J. Mater. Res*. **29**, 1951-1959.

[23] Fatoba O.S., Adesina O.S. Popoola A.P.I. (2018). Evaluation of microstructure, microhardness, and electrochemical properties of laser-deposited Ti-Co coatings on Ti-6Al-4V Alloy. The International Journal of Advanced Manufacturing Technology. 97(5), 2341-2350. http://dx.doi.org/10.1007/s00170-018-2106-7.

[24] M.C. Obiegbu; O.S. Fatoba; E.T. Akinlabi., S.A. Akinlabi (2019). Experimental Study on Characteristics of Laser Metal Deposited Al-Si-Sn-Cu/Ti-6Al-4V composite coatings. Materials Express Research. Volume 6, number 4, 1-11**.** https://doi.org/10.1088/2053-1591/aafe4d.

[25] Fu, Y., Zhang, X.C., Sui, J.F., Tu, S.T., Xuan, F.Z. & Wang, Z.-D. (2015). Microstructure and wear resistance of one-step in-situ synthesized TiN/Al composite coatings on Ti6Al4V alloy by a laser nitriding process. *Optics & Laser Technology,* 67(0), 4//:78-85.

[26] Weng, F., Chen, C. & Yu, H. (2014a). Research status of laser cladding on titanium

and its alloys: a review. *Materials & Design,* 58:412-425.

[27] Dai J, Zhang F, Wang A, Yu H and Chen C, “Microstructure and Properties of Ti-Al coating and Ti-Al-Si system coatings on Ti-6Al-4V fabricated by laser surface alloying,” *Surface & Coatings Technology,* vol. 309, pp. 805-813, 2017.

[28] Cheng Y, Wu X, Xue Z, M. E, Skeldon P and Thompson G.E, “Microstructure corrosion and wear performance of plasma electrolytic oxidation coatings formed on Ti-6Al-4V alloy in silicate-hexametaphosphate electrolyte,” *Surface and Coatings Technology,* vol. 217, pp. 129-139, 2013.

[29] El-labban H.F, Al-wadai H and Mahmoud E.R.I, “Laser cladding of Ti-6Al-4V alloy with vanadium carbide particles,” *Advances in Production Engineering & Management,* vol. 9, pp. 805-813, 2014.

[30] Popoola A.P.I, Phume L, Pityana S & Aigbodion V.S, 2016, In-situ Formation of Laser Ti6Al4V-TiB Composite coatings on Ti6Al4V Alloy, *Surface & Coating Technology*, Vol. 161-170.

[31] Gu D, “Classification of Laser AM processes metallurgical mechanisms,” in *Laser Additive Manufacturing of High-Performance Materials*, Heidelberg, Springer-Verlag, 2015, pp. 15-18.

[32] Kief H.B and Roschiwal H.A, “Additive Manufacturing Processes,” in *CNC Handbook*, McGraw-Hill Professional, 2012.

[33] Swift K.G and Booker J.D, Manufacturing Process Selection Handbook- From Design to Manufacture, Elsevier, 2013.

[34] Bian L, Shamsaei N and Usher J.M, Laser-Based Additive Manufacturing of Metal Parts, New York: CRC Press Taylor & Francis Group, 2018.

[35] Gillespie L.K, “Design for Advanced Manufacturing: Technologies and Processes,” in *Design for Laser Cladding*, New York, McGraw-Hill Education Holdings, 2017, pp. 1-3.

[36] Weng F, Chen C and Yu H, “Research status of laser cladding on titanium and its alloy:Review,” *Materials & Design,* vol. 58, pp. 412-425, 2014.

[37] Toyserkani E, Khajepour A and Corbin S.F, Laser Cladding, New York: CRC Press, 2004.

[38] Shan K, Hag I, Khan A, Shan S.A, Khan M and Pinkerton A.J, “Parameter study of

Development of Inconel-Steel Functionally Graded Materials," *Material & Design,* vol. 54, pp. 531-538, 2014

[39] Goodarzi D.M, Pekkarinen J and Salminem A, "Effect of process parameters in laser cladding on substrate melted areas and the substrate melted shape," *Laser Applications,* vol. 27, 2015.

[40] Meboldt M and Klahn C, "Analysis of the influence of shielding and carrier gas," in *Industrializing Additive Manufacturing*, Springer, 2017, p. 67.

[41] Farayibi P.K, Laser Cladding of Ti-6Al-4V with Carbide and Boride Reinforcements using Wire and Powder Feedstock, University of Nottingham, 2014.

[42] Yilbas B.S and Shuja S.Z, Laser Surface Processing and Model Studies, Springer Science & Business Media, 2013.

[43] Jeffus L, "Gas shielding welding," in *Welding: Principles and Applications*, Cengage learning, 2016, p. 274.

[44] Arcam EBM system, "Ti-6Al-4V Titanium alloy," Arcam AB, [Online]. Available: http://www.arcam.com/wp-content/uploads/Arcam-Ti6Al4V-Titanium-Alloy.pdf. . [Accessed 22 February 2018].

[45] Lu, Junxia, Ling Chang, Jin Wang, Lijun Sang, Shikai Wu, and Yuefei Zhang. 2018. "In-situ investigation of the anisotropic mechanical properties of laser direct metal deposition Ti6Al4V alloy." *Materials Science & Engineering A 712:* 199–205.

[46] Rousseau, Jean Nicolas, Alexandre Bois-Brochu, and Carl Blais. 2018. "Effect of oxygen content in new and reused powder on microstructural and mechanical properties of Ti6Al4V parts produced by directed energy deposition." *Additive Manufacturing 23:* 197–205.

[47] Vilardell, A.M, P Krakhmalev, G Fredriksson, F Cabanettes, A Sova, D Valentin, and P Bertrand. 2018. "Influence of surface topography on fatigue behavior of Ti6Al4V alloy by laser powder bed fusion." *Procedia CIRP 74:* 49–52.

[48] Turichin, G.A, O.G Klimova-Korsmik, M.O Gushchina, S.A Shalnova, R.S Korsmik, V.V Cheverikin, and A.S Tataru. 2018. "Features Of Structure Formation In α+β Titanium Alloys." *Procedia CIRP 74:* 188–191.

[49] Mahamood, Rasheedat M, and Esther T Akinlabi. 2017. "Scanning Speed Influence on the Microstructure and Micro hardness Properties of Titanium Alloy Produced by

Laser Metal Deposition Process." *6th International Conference of Materials Processing and Characterization.* Johannesburg: Materials Today: Proceedings 4:. 5206-5214.

[50] Brusa, Eugenio, Raffaella Sesana, and Enrico Ossola. 2017. "Numerical modeling and testing of mehcanical behaviour of AM TItanium alloy bracket for aerospace applications." *2nd International Conferrence on Structural Integrity, ICSI 2017.* Funchal, Madeira, Portugal: Procedia Structural Integrity 5:. 753-760.

[51] Krzyzanowski, Michal, Szymon Bajda, Yijun Liu, Andrew Triantaphyllou, W.Mark Rainforth, and Malcolm Glendenning. 2016. "3D analysis of thermal and stress evolution during laser cladding bioactive glass coatings." *Journal of the Mechanical Behaviour of Biomedical Materials 59:* 404-417.

[52] Zhang, Jingwei, Frank Liou, William Seufzer, and Karen Taminger. 2016. "A coupled finite element cellular automaton model to predict thermal history and grain morphology of Ti-6Al-4V during direct metal deposition (DMD)." *Additive Manufacturing 11:* 32–39.

[53] Ahmadi, S.M., R. Kumar, E.V. Borisov, R. Petrov, S. Leeflang, Y. Li, N. Tümer, R. Huizenga, A.A. Zadpoor, and V.A. Popovich. 2019. "From microstructural design to surface engineering: A tailored approach for improving fatigue life of additively manufactured meta-biomaterials." *Acta Biomaterialia 83:* 153–166.

[54] Oyelola, Olusola, Peter Crawforth, Rachid M'Saoubi, and Adam T. Clare. 2016. "Machining of Additively Manufactured Parts: Implications for Surface Integrity." *3rd CIRP Conference on Surface Integrity (CIRP CSI).* Nottingham: Procedia CIRP 45:. 119 – 122.

[55] Xu, H., H. Xing, and A. Dong. 2019. "Investigation of gum metal coating on Ti6Al4V plate by direct laser deposition." *Surface & Coatings Technology* 1-29.

[56] Mishra, SK, S Ghosh, and S Aravindan. 2019. "Performance of laser processed carbide tools for machining of Ti6Al4V alloys: A combined study on experimental and finite element analysis." *Precision Engineering* 1-38.

[57] Seo, Ja-Ye, and Do-Sik Shim. 2018. "Effect of track spacing on porosity of metallic foam fabricated by laser melting deposition of Ti6Al4V/TiH2 powder mixture." *Vacuum 154:* 200–207.

[58] Tan, Adrian Wei-Yee, Wen Sun, Ayan Bhowmik, Jun Yan Lek, Iulian Marinescu, Feng Li, Nay Win Khun, Zhili Dong, and Erjia Liu. 2018. "Effect of coating thickness on microstructure, mechanical properties and fracture behaviour of cold sprayed Ti6Al4V coatings on Ti6Al4V substrates." *Surface & Coatings Technology 349:* 303–317.

[59] Rotella, Giovanna, Stano Imbrogno, Sebastiano Candamano, and Domenico Umbrello. 2018. "Surface integrity of machined additively manufactured Ti alloys." *Journal of Materials Processing Tech. 259:* 180–185.

[60] Mahamood, Rasheedat M., and Esther T. Akinlabi. 2018. "Processing Parameters Influence on Microhardness in Laser Metal Deposited Titanium Alloy using Design of Experiment." *Materials Today: Proceedings 5:* 20437–20442.

[61] Oliveira, V.M.C.A., C. Aguiar, A.M. Vazquez, A. Robin, and M.J.R. Barboza. 2014. "Improving corrosion resistance of Ti–6Al–4V alloy through plasma-assisted PVD deposited nitride coatings." *Corrosion Science 88:* 317–327.

[62] Dzugan, J., M. Seifi, R. Prochazka, M. Rund, P. Podany, P. Konopik, and J.J. Lewandowski. 2018. "Effects of thickness and orientation on the small scale fracture behaviour of additively manufactured Ti-6Al-4V." *Materials Characterization 143:* 94–109.

[63] Farayibi, P.K, T.E Abioye, J.W Murray, P.K Kinnell, and A.T Clare. 2015. "Surface Improvement of Laser Clad Ti-6Al-4V Using Plain Waterjet and Pulser Electron Beam Irradiation." *Journals of Materials Processing Technology 218:* 1-11.

[64] Molaei, Reza, Ali Fatemi, and Nam Phan. 2018. "Significance of hot isostatic pressing (HIP) on multiaxial deformation and fatigue behaviors of additive manufactured Ti-6Al-4V including build orientation and surface roughness effects." *International Journal of Fatigue 117:* 352–370.

[65] Yang, Qingcheng, Pu Zhang, Lin Cheng, Zheng Min, Minking Chyu, and Albert C. To. 2016. "Finite element modeling and validation of thermomechanical behavior of Ti-6Al-4V in directed energy deposition additive manufacturing." *Additive Manufacturing 12:* 169–177.

[66] Biswal, Romali, Abdul Khadar Syed, and Xiang Zhang. 2018. "Assessment of the effect of isolated porosity defects on the fatigue performance of additive

manufactured titanium alloy." *Additive Manufacturing 23:* 433–442.

[67] Khatri, Ashutosh, and Muhammd P. Jahan. 2018. "Investigating tool wear mechanisms in machining of Ti-6Al-4V in flood coolant, dry and MQL Conditions." *Procedia Manufacturing 26:* 434-445.

[68] Sun, Dongsheng, Dongdong Gu, Kaijie Lin, Ji Ma, Wenhua Chen, Jie Huang, Xiaofeng Sun, and Mingqiang Chu. 2019. "Selective laser melting of titanium parts: Influence of laser process parameters on macro- and microstructures and tensile property." *Powder Technology 342:* 371–379.

[69] Zhang, Dongyun, Weidong Wang, Yanwu Guo, Songtao Hu, Dongdong Dong, Reinhart Poprawe, Johannes Henrich Schleifenbaum, and Stephan Ziegler. 2019. "Numerical simulation in the absorption behavior of Ti6Al4V powder materials to laser energy during SLM." *Journal of Materials Processing Tech. 268:* 25–36.

[70] Tan, Pengfei, Fei Shen, Biao Li, and Kun Zhou. 2019. "A thermo-metallurgical-mechanical model for selective laser melting of Ti6Al4V." *Materials & Design 107642* 1-35.

[71] Mishra, Ashish Kumar , and Arvind Kumar. 2019. "Numerical and experimental analysis of the effect of volumetric energy absorption in powder layer on thermal-fluidic transport in selective laser melting of Ti6Al4V." *Optics and Laser Technology 111:* 227–239.

[72] Wang, M., H.Q. Li, D.J. Lou, C.X. Qin, J. Jiang, X.Y. Fang, and Y.B. Guo. 2019. "Microstructure anisotropy and its implication in mechanical properties of biomedical titanium alloy processed by electron beam melting." *Materials Science & Engineering A 743:* 123–137.

[73] Rubino, Felice, Fabio Scherillo, Stefania Franchitti, Antonino Squillace, Antonello Astarita, and Pierpaolo Carlone. 2019. "Microstructure and surface analysis of friction stir processed Ti-6Al-4V plates manufactured by electron beam melting." *Journal of Manufacturing Processes 37:* 392–401.

[74] Vrancken, B., Thijs, L., Kruth, J.P. and Van Humbeeck, J., 2012. Heat treatment of Ti6Al4V produced by Selective Laser Melting: Microstructure and mechanical properties. *Journal of Alloys and Compounds*, *541*, pp.177-185.

[75] Stoffregen, H.A., Butterweck, K. and Abele, E., 2014, August. Fatigue analysis in

selective laser melting: review and investigation of thin-walled actuator housings. In *25th Solid Freeform Fabrication Symposium* (pp. 635-650).

[76] Wu Y, Wang A.H, Zhang Z, Zheng R.R, Xia H.B and Wang Y.N. 2018. “Laser alloying of TiSi compound coating on Ti-6Al-4V alloy for the improvement of bioactivity,” *Applied Surface Science,* vol. 305, pp. 16-23.

[77] Zhang, J., Li, W., Yan, L. and Liou, F., 2018. A two-dimensional simulation of grain structure growth within the substrate and the fusion zone during direct metal deposition. *Comptes Rendus Mécanique*, *346*(11), pp.1072-1086.

[78] Tian, Y., Gora, W.S., Cabo, A.P., Parimi, L.L., Hand, D.P., Tammas-Williams, S. and Prangnell, P.B., 2018. Material interactions in laser polishing powder bed additive manufactured Ti6Al4V components. *Additive Manufacturing*, *20*, pp.11-22.

[79] Wu, B., Pan, Z., Ding, D., Cuiuri, D., Li, H., Xu, J. and Norrish, J., 2018. A review of the wire arc additive manufacturing of metals: properties, defects and quality improvement. *Journal of Manufacturing Processes*, *35*, pp.127-139.

[80] Dhanda, M., Haldar, B. and Saha, P., 2014. Development and characterization of hard and wear resistant MMC coating on Ti-6Al-4V substrate by laser cladding. *Procedia materials science*, *6*, pp.1226-1232.

[81] Riedlbauer, Daniel, Thorsten Scharowsky, Robert F. Singer, Paul Steinmann, Carolin Korner, and Julia Mergheim. 2017. "Macroscopic simulation and experimental measurement of melt pool characteristics in selective electron beam melting of Ti-6Al-4V." *Int J Adv Manuf Technol* 88: 1309–1317.

[82] Vajpai, Sanjay Kumar , Kei Ameyama, Mie Ota, Tomoyuki Watanabe, Ryo Maeda, Tatsuya Sekiguchi, Guy Dirras, and David Tingaud. 2014. "High performance Ti-6Al-4V alloy by creation of harmonic structure design." *IOP Conf. Series: Materials Science and Engineering* 63.

[83] Chastand, Victor, Astrid Tezenas, Yannick Cadoret, Phillipe Quaegebeur, Wilson Maia, and Eric Charkaluk. 2016. "Fatigue characterisation of Titanium Ti-6Al-4V samples produced by Additive Manufacturing." *Procedia Structural Integrity* 2: 3168-3176.

[84] Leicht, Alexander , and Elon Oskar Wennberg. 2015. *Analyzing the Mechanical Behavior of Additive Manufactured Ti-6Al-4V Using Digital Image Correlation.*

Diploma work in the Master programme Materials Engineering, Gothenburg, Sweden: Chalmers.

[85] Turichin, Gleb, Zemlyakov Evgeniy, Babkin Konstantin, Ivanov Sergei, and Vildanov Artur. 2018. "Laser metal deposition of Ti-6Al-4V alloy with beam oscillation." *Procedia CIRP 74:* 184–187.

[86] Mulay, R.P, J.A Moore, J.N Florando, N.R Barton, and M Kumar. 2016. "Microstructure and mechanical properties of Ti-6Al-4V: Mill-annealed versus direct metal laser melted alloys." *Materials Science & Engineering A 666:* 43-47.

[87] Waghmare, Dipak Tanaji, Chinmaya Kumar Padhee, Ritesh Prasad, and Manoj Masanta. 2018. "NiTi coating on Ti-6Al-4V alloy by TIG cladding process for improvement of wear resistance: Microstructure evolution and mechanical performances." *Journal of Materials Processing Tech. 262:* 551–561.

[88] Ali, Samar Reda Al-Sayed , Abdel Hamid Ahmed Hussein, Adel Abdel Menam Saleh Nofal, Salah Elden Ibrahim Hasseb Elnaby, Haytham Abdelrafea Elgazzar, and Hassan Abdel Sabour. 2017. "Laser Powder Cladding of Ti-6Al-4V α/β Alloy." *Materials 10:* 1178.

[89] Neikter , M., R. Woracek, T. Maimaitiyili, Ch. Scheffzük, M. Strobl, M.-L. Antti, P. Åkerfeldt, R. Pederson, and C. Bjerkén. 2018. "Alpha texture variations in additive manufactured Ti-6Al-4V investigated with neutron diffraction." *Additive Manufacturing 23:* 225–234.

[90] Muhammad, Muztahid , Mohammad Masoomi, Brian Torries, Nima Shamsaei, and Meysam Haghshenas. 2018. "Depth-sensing time-dependent response of additively manufactured Ti-6Al-4V alloy." *Additive Manufacturing 24:* 37–46.

[91] Buciumeanu, M., A. Bagheri, N. Shamsaei, S.M. Thompson, F.S. Silva, and B. Henriques. 2018. "Tribocorrosion behavior of additive manufactured Ti-6Al-4V biomedical alloy." *Tribology International 119:* 381–388.

[92] Promoppatum, Patcharapit, Recep Onler, and Shi-Chune Yao. 2017. "Numerical and experimental investigations of micro and macrocharacteristics of direct metal laser sintered Ti-6Al-4V products." *Journal of Materials Processing Technology 240:* 262–273.

[93] Pratap, T., and K. Patra. 2018. "Mechanical micro-texturing of Ti-6Al-4V surfaces for

improved wettability and bio-tribological performances." *Surface & Coatings Technology 349:* 71–81.

[94] Book, Todd, and Michael D. Sangid. 2016. "Strain localization in Ti-6Al-4VWidmanstätten microstructures produced by additive manufacturing." *Materials Characterization 122:* 104–112.

[95] Vora H.D, Rajamure R.S, Dahotre S.N, Ho Y, Banerjee R and Dahotre N.B, "Integrated experimental and theoretical approach for corrosion and wear evaluation of laser surface nitride Ti-6Al-4V biomaterial in physiological solution," *Mechanical behaviour of Biomedical Materials,* vol. 97, pp. 153-164, 2014.

[96] Guo S, Lu Y, Wu S, Liu L, He M, Zhao C, Gan Y, Lin J, Luo J and Xu X, "Preliminary study on the corrosion resistance, antibacterial activity and cytotoxicity of selective-lasermelted Ti-6Al-4V-xCu alloys," *Materials Science and Engineering,* vol. 72, pp. 631-640, 2016.

[97] Zhao B, Wang H, Qiao N and Wang C and Hu M, "Corrosin resistance characteristics of a Ti-6Al-4V alloy scaffold that is fabricated by electron beam melting and selective laser melting for implantation in vivo," *Materials Science and Engineering,* vol. 70, pp. 832-841, 2017.

[98] Chikarakara E, Naher S and Brabazon D, "High speed laser surface modification of Ti-6Al-4V," *Surface & Coatings Technology,* vol. 206, pp. 3223-3229.

[99] ASTM International, "Standard Guide for Preparation of Metallographic Specimens," ASTM E3-11, 2017. [Online]. Available: https://www.astm.org/Standards/E3.htm. [Accessed 12 August 2018].

[100] ASTM International, "Standard Practice for Preparing an Optical Microscope for Dimensional Measurements," ASTM F728-81, 2003. [Online]. Available: https://www.astm.org/Standards/F728.htm. [Accessed 12 August 2018].

[101] ASTM International, "Standard Practice for Calculation of Corrosion Rates and Related Information from Electrochemical Measurements," ASTM G102-89, 2010. [Online]. Available: https://www.astm.org/DATABASE.CART/HISTORICAL/G102-89R10.htm. [Accessed 12 August 2018].

[102] ASTM International, "Standard test method for Wear Testing with a Pin-on Disk Apparatus," ASTM G99-17, [Online]. Available:

https://www.astm.org/Standards/G99. [Accessed 12 August 2018].

[103]Fatoba, O.S., Akinlabi, E.T., Akinlabi, S.A. (2018). Numerical Investigation of Laser Deposited Al-Based Coatings on Ti-6Al-4V Alloy. 2018 IEEE 9th International Conference on Mechanical and Intelligent Manufacturing Technologies (ICMIMT 2018), Cape town, South Africa, pp. 85-90. doi: 10.1109/ICMIMT.2018.8340426.

[104]Durejko T., Zietala M., Łazińska M. Structure and properties of the Fe_3Al-type intermetallic alloy fabricated by laser engineered net shaping (LENS) Mater. Sci. Eng. A. 2016;650:374-381. doi: 10.1016/j.msea.2015.10.076

[105]Popoola, A.P.I., Fatoba, O.S., Aigbodion, V.S. And Popoola, O.M. 2017. Tribological Evaluation of Mild Steel with Ternary Alloy of Zn-Al-Sn by Laser Deposition, International Journal of Advanced Manufacturing Technology, 89(5-8), 1443-1449. DOI 10.1007/s00170-016-9170-7.

[106]Banerjee, D. & Williams, J.C. 2015. Materials and engineering: An evolving landscape. *MRS Bulletin,* 40(12):999-1008.

[107]Akinlabi S.A; M.P. Mashinini; Fatoba O.S; Akinlabi E.T. (2018). Characterization of corrosion behaviour of laser beam formed titanium alloy. IOP Conference Series Materials Science and Engineering 423(1):012174. DOI: 10.1088/1757-899X/423/1/012174.

[108]Liu, X.-B., Meng, X.-J., Liu, H.-Q., Shi, G.-L., Wu, S.-H., Sun, C.-F., Wang, M.-D. & Qi, L.-H. 2014b. Development and characterization of laser clad high temperature self-lubricating wear resistant composite coatings on Ti–6Al–4V alloy. *Materials & Design,* 55(0), 3//:404-409.

[109]Gong, X., Lydon, J., Cooper, K. & Chou, K. 2014. Beam speed effects on Ti–6Al–4V microstructures in electron beam additive manufacturing. *Journal of Materials Research,* 29(17):1951-1959.

[110]Makhatha, M.E., Fatoba, O.S. & Akinlabi, E.T. (2018). Effects of rapid solidification on the microstructure and surface analyses of laser-deposited Al-Sn coatings on AISI 1015 steel. Int J Adv Manuf Technol. 94 (1-4), 773-787. https://doi.org/10.1007/s00170-017-0876-y.

[111]Fatoba, O.S; Popoola, A.P.I; Aigbodion, V.S (2016). Experimental study of Hardness values and Corrosion Behaviour of Laser Alloyed Zn-Sn-Ti Coatings of UNS

G10150 Mild Steel, Journal of Alloys and Compounds, 658, 248-254.

[112]Weng, F., Yu, H., Chen, C. & Dai, J. 2015. Microstructures and Wear Properties of Laser Cladding Co-based Composite Coatings on Ti-6Al-4V. *Materials and Design,* 80:174-181.

[113]Fatoba O.S., Akinlabi S.A; Akinlabi E.T. (2018): The Effects of Sn Addition on the Microstructure and Surface Properties of Laser Deposited Al-Si-Sn Coatings on ASTM A29 Steel. IOP Conference Series: Materials Science and Engineering, 328, pp. 1-11. doi:10.1088/1757-899X/328/1/012016.

[114]O.S. Fatoba; A.P.I Popoola; V.S. Aigbodion (2018). Electrochemical Studies and Surface Analysis of Laser Deposited Zn-Al-Sn Coatings on AISI 1015 Steel. International Journal of Surface Science and Engineering. 12 (1), 40-59. DOI: 10.1504/IJSURFSE.2017.10009146

[115] Fatoba, O.S; Popoola, A.P.I. Aigbodion, V.S. (2018) Laser Alloying of Al-Sn Binary Alloy onto Mild Steel: InSitu Formation. Hardness and Anti-Corrosion Properties. Lasers in Engineering, 39(3-6), 292-312.

[116] Aigbodion, V.S; Popoola, A.P.I; Fatoba, O.S (2016). Evaluation of Hardness values and Corrosion Behaviour of Laser Alloyed 20Al-20Sn-60Ti Coatings of UNS G10150 Mild Steel. International Journal of Advanced Manufacturing Technology, 86(1-4), 291-301 1-11. Doi 10.1007/s00170-015-8111-1.

[117]A. Shah, A. Kumar, J. Ramkumar. Analysis of transient thermo-fluidic behavior of melt pool during spot laser welding of 304 stainless-steel**.** J. Mater. Process. Technol., 256 (2018), pp. 109-120

[118]W. Tan, N.S. Bailey, Y.C. Shin. Numerical modeling of transport phenomena and dendritic growth in laser conduction welding of 304 stainless steel**.** International Manufacturing Science and Engineering Conference, Vol. 1, ASME (2011), pp. 243-251.

[119]C. Zhou, S. Zhao, Y. Wang, F. Liu, W. Gao, X. Lin Mitigation of pores generation at overlapping zone during laser cladding**.** J. Mater. Process. Technol., 216 (2015), pp. 369-374.

[120]D. Triantafyllidis, L. Li, F.H. Stott Mechanisms of porosity formation along the solid/liquid interface during laser melting of ceramics**.** Appl. Surf. Sci., 208–

209 (2003), pp. 458-462

[121] Wang T, Zhu Y.Y, Zhang S.Q, Tang H.B and Wang H.M, “Grain morphology evolution behaviour of titanium alloy components during laser melting deposition additive manufacturing,” *Alloys and Compounds,* vol. 632, pp. 505-513, 2015.

[122] Zhu Y, Liu D, Tian X.J, Li J and Wang H, “Microstructure evolution and layer bands of laser melting deposition Ti-6.5Al-3.5Mo-1.5Zr-0.3Si titanium alloy,” *Alloys and Compounds,* vol. 616, pp. 468-474, 2014.

[123] Porter D.A, Easterling K.E and Sherif M, Phase Transformations in Metals and Alloys, CRC press, 2009.

[124] Gharehbaghi R., Fatoba O.S. and Akinlabi E.T. (2018). Influence of Scanning Speed on the Microstructure of Deposited Al-Cu-Fe Coatings on a Titanium Alloy Substrate by Laser Metal Deposition Process. Proceedings at the 2018 IEEE 9th International Conference on Mechanical and Intelligent Manufacturing Technologies (ICMIMT 2018), Cape Town, South Africa, Pp. 44-49. Doi: 10.1109/Icmimt.2018.8340418.

[125] Shuai, C., Feng, P., Zhang, L., Gao, C., Hu, H., Peng, S. & Min, A. (2013). Correlation between Properties and Microstructure of Laser Sintered Porous β-TriCalcium Phosphate Bone Scaffolds, *Science and Technology of Advanced Materials*, 14, 1-10.

[126] M. Shunmugavel, A. Polishetty and G. Littlefair, “Microstructure and Mechanical Properties of Wrought and Additive Manufactured Ti-6Al-4 V Cylindrical Bars,” *Procedia Technology,* vol. 20, pp. 231-236, 2015

[127] A. Azarniya, X. Colera, M. Mirzaali, S. Sovizi, F. Bartolomeu, M. St Weglowski, W. Wits, C. Yap, J. Ahn, G. Miranda, F. Silva, H. Madaah Hosseini, S. Ramakrishna and A. Zadpoor, “Additive manufacturing of Ti–6Al–4V parts through laser metal deposition (LMD): Process, microstructure, and mechanical properties,” *Journal of Alloys and Compounds,* 2019.

[128] Martínez-Hernández, Alma & Federico, Manriquez & Torres, Julieta & Ortega, Raúl & Perez Bueno, Jose & Meas, Yunny & Trejo, Gabriel & Méndez-Albores, Alia. (2016). Electrodeposition of Ni-P/SiC Composite Films with High Hardness. 10.5772/61858.

[129] Shuai C. Feng, P. Zhang L. Gao C. Hu H. Peng S. and Min A. (2013). Correlation

between Properties and Microstructure of Laser Sintered Porous β-TriCalcium Phosphate Bone Scaffolds, *Sci. Technol. Adv. Mater*. **14**, 1-10.

[130] Akinlabi E.T. and Akinlabi S.A. (2012). Effect of Heat Input on the Properties of Dissimilar Friction Stir Welds of Aluminium and Copper. *Amer. J. Mater. Sci*. **2,** 147-152.

[131] Fatoba O.S; Akinlabi, S.A., Akinlabi, E.T. (2018). Numerical Modelling and Performance Effects of Laser Deposited Ti-Al-Sn Coating on ASTM A29 Steel. Presented at the International Conference on Mechanical Stress Evaluation by Neutron and Synchrotron (MECASENS 2017, 19th -22nd September 2017, Kruger Park, South Africa. Materials Research Proceedings. 4, 135-140. doi: http://dx.doi.org/10.21741/9781945291678-21.

[132] Mahamood, R.M., Akinlabi, E.T. & Akinlabi, S. Lasers Manuf. Mater. Process. (2015) 2: 43. https://doi.org/10.1007/s40516-014-0003-y

[133]J. R. Cahoon, W. H. Broughton, and A. R. Kutzak, “The determination of yield strength from hardness measurements,” Metallurgical Transactions, vol. 2, no. 7, pp. 1979–1983, 1971.

[134]K.S. Chenna, G.N. Kumar, K. JhaAbhay, P. Bhanu, On the prediction of strength from hardness for copper alloys, J.Mater.(2013).